Aus dem Max von Pettenkofer-Institut für Hygiene und Medizinische Mikrobiologie

Institut der Ludwig-Maximilians-Universität München

Vorstand: Prof. Dr. med. Sebastian Suerbaum

Addressing the impact of phages on gut microbial ecology and functions using a synthetic bacterial community

Dissertation

Zum Erwerb des Doktorgrades der Naturwissenschaften an der Medizinischen Fakultät der Ludwig-Maximilians-Universität München

vorgelegt von

Alexandra Charlotte von Strempel

aus

Burgwedel

2023

Mit Genehmigung der Medizinischen Fakultät
der Ludwig-Maximilians-Universität München

Betreuerin:	Prof. Dr. rer. nat. Barbara Stecher-Letsch
Zweitgutachter(in):	PD Dr. rer. nat. Hanna-Mari Baldauf
Dekan:	Prof. Dr. med. Thomas Gudermann
Tag der mündlichen Prüfung:	06. August 2024

Affidavit

von Strempel, Alexandra

Surname, first name

I hereby declare, that the submitted thesis entitled:

Addressing the impact of phages on gut microbial ecology and functions using a synthetic bacterial community

is my own work. I have only used the sources indicated and have not made unauthorised use of services of a third party. Where the work of others has been quoted or reproduced, the source is always given.

I further declare that the dissertation presented here has not been submitted in the same or similar form to any other institution for the purpose of obtaining an academic degree.

München, 30.09.2024

Place, Date

Alexandra von Strempel

Signature doctoral candidate

Table of Contents

List of publications conducted during this thesis:

von Strempel A, Weiss AS, Wittman J, Salvado Silva M, Ring D, Wortmann E, Clavel T, Débarbieux L, Kleigrewe K, Stecher B (2023):

Phage-targeting of protective commensals impairs resistance against *Salmonella* Typhimurium infection in gnotobiotic mice.

PLoS Pathog. 2023 Aug 21;19(8):e1011600. doi: 10.1371/journal.ppat.1011600.

Weiss AS, Niedermeier L, Burrichter AG, **von Strempel A,** Ring D, Meng C, Kleigrewe K, Lincetto C, Hübner J, Stecher B (2023):

Nutritional and host environments determine community ecology and keystone species in a synthetic gut bacterial community.

Nat Commun. 2023 Aug 8;14(1):4780. doi: 10.1038/s41467-023-40372-0.

Lamy-Besnier Q, Bignaud A, Garneau JR, Titecat M, Conti DE, **von Strempel A**, Monot M, Stecher B, Koszul R, Debarbieux L, Marbouty M (2023):

Chromosome folding and prophage activation reveal specific genomic architecture for intestinal bacteria.

Microbiome. 2023 May 19;11(1):111. doi: 10.1186/s40168-023-01541-x.

Weiss AS, Burrichter AG, Durai Raj AC, **von Strempel A**, Meng C, Kleigrewe K, Münch PC, Rössler L, Huber C., Eisenreich W, Jochum LM, Göing S, Jung K, Lincetto C, Hübner J, Marinos G, Zimmermann J, Kaleta C, Sanchez A, Stecher B (2022):

In vitro interaction network of a synthetic gut bacterial community.

ISME J, 16: 1095–1109, doi.org/10.1038/s41396-021-01153-z

Afrizal A, Jennings SAV, Hitch TCA, Riedel T, Basic M, Panyot A, Treichel N, Hager FT, Wong EO, Wolter B, Viehof A, **von Strempel A**, Eberl C, Buhl EM, Abt B, Bleich A, Tolba R, Blank LM, Navarre WW, Kiessling F, Horz HP, Torow N, Cerovic V, Stecher B, Strowig T, Overmann J, Clavel T (2022):

Enhanced cultured diversity of the mouse gut microbiota enables custom-made synthetic communities.

Cell Host Microbe. 2022 Nov 9;30(11):1630-1645.e25. doi: 10.1016/j.chom.2022.09.011.

List of abbreviations

AF	Anaerobic FCS medium
ABTS	2,2'-Azinobis [3-Ethylbenzothiazolin-6-sulfonsäure]-Diammoniumsalz
avir	avirulent
BHQ1	Black whole quencher 1
bp	Base pairs
BSA	Bovine serum albumin
°C	Degree Celsius
CD	Crohn`s disease
CFU	Colony forming units
Cq	Quantification cycle
CR	Colonization resistance
ddH2O	Double-distilled water (Ampuwa)
dH2O	Distilled water
DNA	Deoxyribonucleic acid
ds	Double-stranded
DSMZ	Deutsche Sammlung von Mikroorganismen und Zellkulturen
DTL	Detectionlimit
EDTA	Ethylenediaminetetraacetic acid
ELISA	Enzyme-linked immunosorbent assay
EM	Electron microscopy
FAM	6-carboxyfluoresceine
FCS	Fetal calf serum
gDNA	Genomic DNA
GF	Germfree
H&E	Hematoxylin and eosin
HEX	6-carboxyhexafluoresceine
HRP	Horseradish peroxidase
IBD	Inflammatory bowel disease
LB	Luria-Bertani
LCN-2	Lipocalin-2

MLN	Mesenteric lymphnode
MOI	Multiplicity of infection
MvP	Max von Pettenkofer-Institut
NCBI	National Center for Biotechnology Information
n.s.	Not significant
OMM	Oligo-Mouse-Microbiota
OD600	Optical density of 600 nm
ORF	Open reading frame
p.a.	Pro analysi
PBS	Phosphate buffered saline
p.c.	post challenge
PCR	Polymerase chain reaction
PFU	Plaque forming unit
p. i.	post infection
qPCR	Quantitative real-time polymerase chain reaction
RNA	Ribonucleic acid
rRNA	ribosomal Ribonucleic acid
RT	Room temperature
SD	Standard deviation
SDS	Sodium dodecyl sulfate
SM	Saline-magnesium
SPF	Specific pathogen-free
spp.	Species
S. Tm	*Salmonella enterica* serovar Typhimurium
Strep	Streptomycin
TE	Tris-EDTA
T3SS	Type three secretion system
T6SS	Type six secretion system
UC	Ulcerative colitis
wt	Wildtype

Abstract

The human gut is a complex ecosystem, harboring eukaryotic cells, bacteria and viruses. Alterations of the intestinal microbial communities are associated with an increasing number of human diseases. On the other hand, the gut microbiota protects the host against a variety of major human gastrointestinal pathogens. Bacteriophages (phages), viruses that infect bacteria, are important effectors and indicators of human health and disease by managing specific bacterial population structures and by interacting with the mucosal immune system. They are ubiquitous in nature and frequently ingested via food and drinking water. Moreover, bacteriophages are an attractive tool for microbiome engineering due to their specificity and the lack of known serious adverse effects on the host. However, most of our knowledge on phages is based on metagenomic studies and the functional role of virulent phages within the gastrointestinal microbiome remain poorly understood.

To obtain functional insights on the effect of phages in the gastrointestinal microbiome and its function in health and disease, I established a model to investigate the interaction of bacteriophages and cognate host bacteria in the mammalian gut. Therefore, I isolated specific phages targeting members of a synthetic bacterial consortium, the Oligo-MM^{14}, which consists of 14 well-characterized bacterial strains that form a stable community in gnotobiotic mice and provide colonization resistance against the human enteric pathogen *Salmonella enterica* serovar Typhimurium (*S.* Tm).

First, I characterized the isolated phages *in vitro* with respect to plaque morphologies, genomic features, lysis behaviors and host ranges. Further, I developed methods for specific absolute quantification via qPCR for the single phages, which allowed me to track the abundance of phages and host bacteria in the OMM community *in vitro* and *in vivo,* revealing that the phages amplify at varying degrees while not disturbing the overall community composition.

Furthermore, I showed, that phages lead to initial depletion of the target population in the mouse gut and thereafter coexist with the bacteria for up to a week after phage challenge. Moreover, the addition of phages targeting *Escherichia coli* and *Enterococcus faecalis,* two bacteria previously identified to mediate colonization resistance, led to a significant decrease of colonization resistance against *S.* Tm. This demonstrates that phages can affect microbial community functions. Infection susceptibility to *S.* Tm was markedly increased at an early time point after challenge with both phage cocktails but surprisingly, OMM^{14} mice were also

susceptible to *S.* Tm infection 7 days after a single phage inoculation, when the targeted bacterial populations were back to pre-phage administration density. Since the abundance of the other bacteria in the gut is not affected by administration of the phage cocktails, this effect is specifically attributed to the impact of the phages on their bacterial hosts. This suggests, that phages targeting protective members of the microbiota may in general increase the risk for *S.* Tm infection.

In summary, this work yields insights into phage-bacterial interactions in the gut and the effect of phages on fundamental microbiome functions, which will be important for evaluating the future use of phages for targeted microbiome manipulation.

Zusammenfassung

Das menschliche Verdauungssystem ist ein komplexes Ökosystem, das aus eukaryotischen Zellen, Bakterien und Viren besteht. Eine Veränderung dieser Darmmikrobiota wird in Verbindung mit einer wachsenden Zahl an Krankheiten gebracht. Darüber hinaus schützt das Mikrobiom im Darm den Wirt vor einer Vielzahl von gastrointestinalen Krankheitserregern. Bakteriophagen (Phagen), Viren die Bakterien infizieren, sind wichtige Effektoren und Indikatoren im gesunden und im kranken Darm, indem sie spezifische bakterielle Populationen regulieren und mit dem mukosalen Immunsystem interagieren. Sie sind allgegenwärtig in der Umwelt und werden von Menschen häufig über Nahrung und Trinkwasser aufgenommen. Darüber hinaus sind sie ein attraktives Instrument für die Manipulation des Mikrobioms, da sie im Gegensatz zu Antibiotika sehr spezifisch für einzelne Bakterien sind und keine Nebenwirkungen für den menschlichen Wirt bekannt sind. Dennoch basiert der Großteil unseres Wissens über Phagen auf metagenomischen Studien, und die funktionelle Rolle von virulenten Phagen im gastrointestinalen Mikrobiom ist weiterhin zum Großteil unbekannt.

Um die Auswirkung von Phagen auf Funktionen des gastrointestinalen Mikrobioms zu untersuchen, habe ich ein Modell etabliert, welches die Interaktion von Bakteriophagen und ihren Wirtsbakterien im Darm von Säugetieren untersucht. Dafür habe ich spezifische Phagen gegen Bakterienstämme eines minimalen bakteriellen Konsortiums, dem Oligo-MM^{14}, isoliert. Die Oligo-MM^{14} besteht aus 14 gut charakterisierten Bakterien, die gnotobiotische Mäuse stabil besiedeln und eine Kolonisierungsresistenz gegen den humanen Krankheitserreger *Salmonella* enterica Serovar Typhimurium (*S.* Tm) bieten.

Zunächst habe ich die isolierten Phagen *in vitro* charakterisiert und konnte zeigen, dass die Plaques, das Erbgut, das Lyse Verhalten und die Wirtsspektren der Phagen eine Vielzahl von Facetten aufweisen. Darüber hinaus entwickelte ich eine spezifische absolute Quantifizierung mittels qPCR für die einzelnen Phagen, was mir ermöglichte, die Abundanz der Phagen und der jeweiligen Wirtsbakterien in der OMM-Gemeinschaft zu verfolgen. Dabei stellte ich fest, dass die Phagen sich unterschiedlich stark vermehren, ohne die Gesamtzusammensetzung der Gemeinschaft zu stören.

Des Weiteren konnte ich zeigen, dass Phagen zu einer anfänglichen Reduktion der infizierten Bakterien im murinen Darm führen und danach bis zu einer Woche nach Gabe der Phagen mit den Bakterien koexistieren. Darüber hinaus führte die Zugabe von Phagen die *E. coli* oder

E. faecalis infizieren zu einer signifikanten Abnahme der Kolonisierungsresistenz gegen *Salmonella*, was darauf hindeutet, dass essentielle Funktionen des Mikrobioms durch Phagen beeinflusst werden können. Die Infektionsanfälligkeit für *S.* Tm war zu einem frühen Zeitpunkt nach Gabe der beiden Phagen-Cocktails deutlich erhöht, doch überraschenderweise waren OMM^{14}-Mäuse auch 7 Tage nach einer Inokulation der Phagen anfälliger für *S.* Tm-Infektion. Zu diesem Zeitpunkt hatten die von Phagen infizierten bakteriellen Populationen wieder die Dichte von vor Phagen-Verabreichung erreicht. Da die Abundanz der anderen Bakterien im Darm nicht von den Phagen beeinflusst wird, liegt es nahe, dass dieser Effekt spezifisch durch die Phagen erreicht wird. Dies weist darauf hin, dass Phagen, die schützende Mitglieder der Mikrobiota infizieren, das Risiko einer Salmonelleninfektion erhöhen können.

Zusammenfassend liefern diese Arbeit Einblicke in die Interaktionen zwischen Phagen und Bakterien im Darm und in die Auswirkungen von Phagen auf grundlegende Mikrobiom-Funktionen. Diese Ergebnisse sind von wichtiger Bedeutung für die Bewertung der zukünftigen Verwendung von Phagen zur gezielten Mikrobiom-Manipulation.

1. Introduction

1.1 The human gut microbiome

The human body is a complex ecosystem, hosting trillions of microorganisms that play a vital role in overall human health. Especially the gastrointestinal tract stands out as a fascinating and balanced environment that is colonized by of a vast array of bacteria, viruses, bacteriophages, fungi, and other microorganisms (Hoffmann et al., 2013; Human Microbiome Project, 2012) , all together engaging in dynamic and symbiotic relationship with its human host. The microbial density increases along the gastrointestinal tract, with only 10^3-10^4 microbial cells per gram content in the stomach and upper smaller intestine to up to 10^{12} cells per gram in the colon (Sender, Fuchs, & Milo, 2016). For centuries, the human gut was primarily seen as a site for digestion and absorption of nutrients (Turnbaugh et al., 2006). However, recent scientific advancements have revealed that the gut microbiome goes far beyond its digestive functions and is now recognized as an essential organ that affects various aspects of human physiology. Crucial functions of the microorganisms inhabiting the human gut are for example protection against enteric pathogens, breakdown of otherwise indigestible polysaccharides and synthesis of essential vitamins (Buffie & Pamer, 2013; Clavel, Lagkouvardos, Blaut, & Stecher, 2016; Stecher, 2015). This leads to a direct interplay between the microbiome and the host metabolism (Visconti et al., 2019). Also, it was already early realized that the microbiome has a direct influence on general mood and mental health (Goehler et al., 2005), termed gut-brain axis. This direct interaction has since been studied extensively and proven for many different aspects (Appleton, 2018), for example that the microbiome is able to regulate the motivation for exercise in mice (Dohnalova et al., 2022).

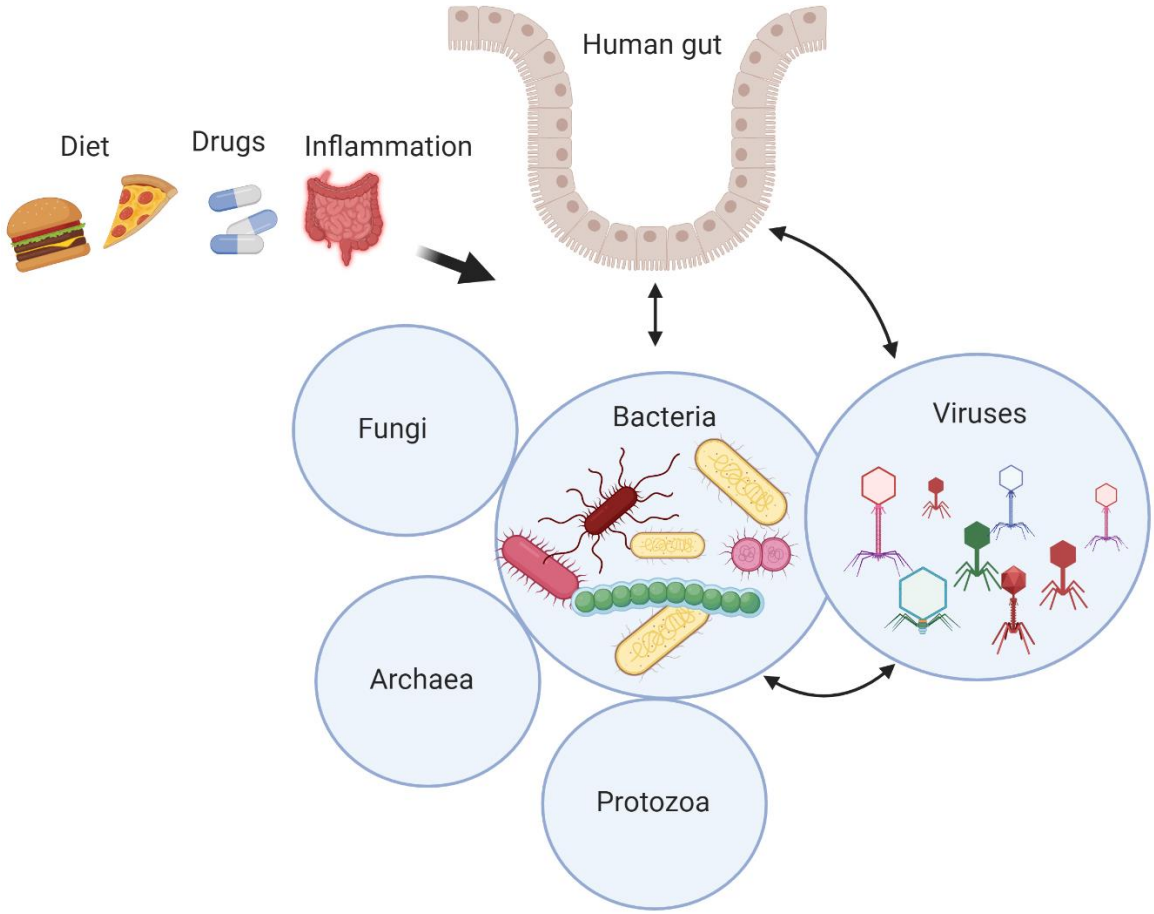

Fig 1: The human gut microbiome

Schematic depiction of the different microorganisms in the human gut. Bacteria, viruses (mostly bacteriophages), fungi, archaea and protozoa build the intestinal microbiome and form a stable community. External factors like diet, drugs and inflammation can influence the composition of the microbiota.

Figure created with Biorender.

Association studies using next generation sequencing, metagenomics, metatranscriptomics and metabolomics enable deep insights into the role of the microbiome in human health and diseases. It has been shown, that high species diversity, microbial gene richness, and stable core microbiota are considered properties of a health-promoting microbial community (Fan & Pedersen, 2021). However, relative distributions are unique between individuals (Hou et al., 2022; Osbelt et al., 2021) and may vary naturally by age (Guigoz, Dore, & Schiffrin, 2008) and environmental factors such as diet (David et al., 2014) or medication (Forslund et al., 2015; Freedberg et al., 2015). On the other hand, many gastrointestinal and metabolic diseases, for example inflammatory bowel disease, colon cancer or diabetes, are linked to changes in the gastrointestinal microbiome. As more is understood about the connection and functional

relevance of the microbiota in diseases, the more the potential treatment of diseases through microbiota manipulation has emerged as a field of interest (Pavel et al., 2021; Rashed, Valcheva, & Dieleman, 2022). Nevertheless, the majority of the interactions and the mechanisms of coexistence of the microorganisms in the gut remain unknown. Targeting specific bacteria that might enhance inflammation in the gut is not possible, since antibiotics and other drugs mostly have a broad host range, therefore also depleting beneficial bacteria. On the other hand, introducing bacteria with beneficial functions is also a challenge. The community dynamically evolves over time with their hosts and in such a complex environment, all nutrient niches are already filled, making it almost impossible for newly introduced bacteria to establish themselves (Mallott & Amato, 2021). Dynamic interactions of bacteria and their corresponding phages might influence abundance and metabolic levels in the gut, which might also impact important functions of the microbiome, like epithelial integrity or protection against invading pathogens. Functional studies are needed to shed light into these complex relationships and disentangle how the different members of the gut microbiome interact with each other.

1.2 Bacteriophages

Bacteriophages (phages) are viruses that specifically infect and replicate within bacteria. They are the most abundant biological entities on earth and can be found in various environments, including the mammalian gut (Dzunkova et al., 2019; Reyes, Semenkovich, Whiteson, Rohwer, & Gordon, 2012).

Phages can follow various life cycles. Most phages in the gut follow a lytic or lysogenic cycle which classifies them as virulent and lysogenic phages (Weinbauer, 2004). Virulent phages, also known as lytic phages, follow a lytic cycle within the host bacterium which consists of several stages. Upon attachment to a specific receptor on the bacterial cell surface, the phage injects its genetic material, usually DNA (dsDNA, ssDNA), but also sometimes RNA, into the host cell. The phage DNA takes over the bacterial cellular machinery, redirecting it to produce viral proteins and nucleic acid that are then assembled to form new phage particles. Ultimately, the host cell lyses, releasing numerous progeny phages, which can then go on to infect other bacterial cells (Rakhuba, Kolomiets, Dey, & Novik, 2010). This process results in the destruction of the host bacterium. Virulent phages are often characterized by their rapid replication and lysis of the host cells.

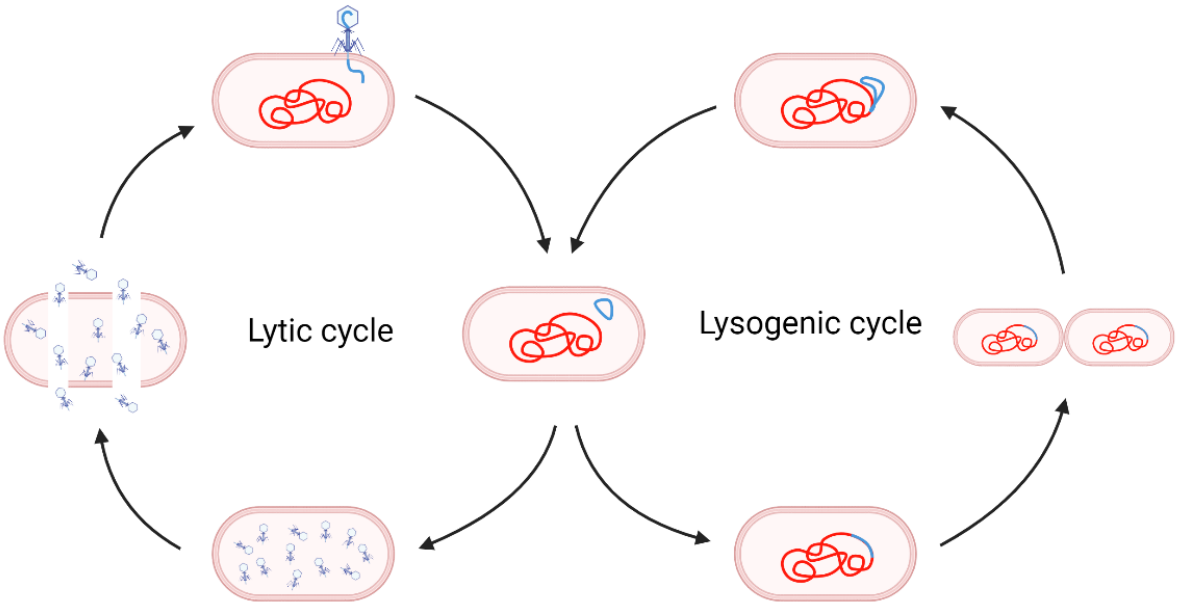

Fig 2: Phage replication cycle

Schematic depiction of the lytic and the lysogenic cycle of bacteriophages. In the lytic cycle, phages attach to a bacterial cell and insert their DNA. The cell then translates the DNA into virions, which get released by lysis of the cell. In the lysogenic cycle, the phage DNA gets incorporated into the host genome (prophage). Under certain conditions, the prophage excises itself and enters the lytic cycle.

Figure created with Biorender.

Lysogenic phages, also referred to as temperate phages, can adopt either a lytic or a lysogenic life cycle within the host bacterium. Unlike lytic phages, lysogenic phages do not immediately cause lysis of the host cell upon infection. Instead, they integrate their genetic material, called a prophage, into the bacterial chromosome. The prophage is replicated along with the bacterial DNA during cell division, resulting in the vertical transmission of the phage DNA to the host's daughter cells (Weinbauer, 2004). Under certain conditions, such as stress or environmental triggers (Boling et al., 2020; Oh et al., 2019), the prophage can become activated and switch to the lytic cycle. The prophage excises itself from the bacterial chromosome, initiates replication, and proceeds to produce progeny phages, leading to the lysis of the host cell. This mechanism not only provides advantages in phage propagation and survival, but the prophage can also confer additional properties to the host by carrying beneficial genes such as toxin production (Waldor & Mekalanos, 1996) or antibiotic resistance (Zhou, Liu, Song, & Chen, 2023). Understanding both mechanisms is crucial for developing phage-based therapies for microbiome manipulation.

Two more uncommon life cycles are known as pseudo-lysogenic, where the phage DNA stays inside the host cell in an inactive form, and carrier state, where phages cause a chronic infection to the bacteria host and phages are produced continuously without lysing the host cell (Naureen et al., 2020).

1.2.1 Phages in the gut microbiome

Phages have been shown to populate the human body where they make up the most numerous group in the human virome. Former 16s based approaches were blind for phages and only recently, large metagenomic studies have begun to shine light on the diversity of the human gut phageome (Camarillo-Guerrero, Almeida, Rangel-Pineros, Finn, & Lawley, 2021). Furthermore, metagenomic studies indicate that gut viral communities are unique to individuals and can persist for at least two and a half years (Minot et al., 2013; Shkoporov et al., 2019). By specifically targeting their bacterial hosts, they can influence bacterial functions, overall population structures and the metabolome in the gut (Hsu et al., 2019) which can lead to promotion or inhibition of inflammation. They are thought to be important regulators of bacterial populations (Chevallereau, Pons, van Houte, & Westra, 2022) and can even directly mediate preventive protection against pathogenic bacteria by adherence to the mucus in the gut (Almeida, Laanto, Ashrafi, & Sundberg, 2019). Metagenomic studies mostly identified largely temperate phages in the gut microbiota (Howe et al., 2016) and showed that their activation can be triggered by various environmental inducers including diet and drugs (Boling et al., 2020; Oh et al., 2019).

1.2.2 Mechanisms of coexistence of bacteria and virulent phages in the gut

Besides lysogenic phages, also virulent phages are found in the mammalian gut (Clooney et al., 2019) where they can target their bacterial hosts and thereby also functionally impact bacterial communities (Hsu et al., 2019). Although virulent phages are able to lyse and therefore kill their hosts in order to amplify themselves, they normally end up in a stable coexistence with their hosts in the gut (Guerrero et al., 2021; Lourenco et al., 2020). Mechanisms underlying this coexistence are still not fully understood but recent studies are aiming to investigate the interactions. Since coexistence is often not dependent on the development of phage resistant clones, one possible explanation is the spatial heterogeneity of the gut (Lourenco et al., 2020).

Phage inaccessible sites in the mucosa can serve as a spatial refuge for bacteria and therefore limit predation and foster coexistence. Further, the gut environment can regulate bacterial gene expression of *E. coli*, resulting in decreased susceptibility to phage infection (Lourenco et al., 2022). Also, biofilms can promote the development of bacterial communities harboring phage resistant and phage susceptible strains and therefore serve as a refuge for part of the bacterial population (Heilmann, Sneppen, & Krishna, 2012; Simmons et al., 2020).

Although recent metagenomic studies have addressed the diversity, abundance, individuality and stability over time of phages in the gut (Gregory et al., 2020) and recent studies also tackled the mechanisms behind predation and co-existence, little is known about the role of virulent phages in regulating intestinal microbiome functions and homeostasis. Ongoing research aims to uncover the complex interactions between phages and the gut microbiota, as well as their implications for human health and disease.

1.3 Phage therapy

Discovered at the beginning of the 20th century, it was early thought that phages could be used for the treatment of bacterial infections (D'Herelle, 2007). The widespread introduction of antibiotics however led to the neglection of phage research as a therapy option. With the rise of antibiotic resistance as a global health threat in recent years and the understanding of the importance of a balanced microbiota, the potential application of phages as strain specific antimicrobial agents has reemerged (Reardon, 2014).

One key advantage of phage therapy is its specificity, since each phage is highly specific to its bacterial host and is generally not targeting other bacteria or human cells. This specificity potentially reduces the risk of disrupting the microbiome and thus minimizing side effects (Loc-Carrillo & Abedon, 2011). Phage therapy already has shown promising results in treating a wide range of bacterial infections (Dedrick et al., 2019), including antibiotic-resistant strains such as MRSA (Methicillin-resistant *Staphylococcus aureus*) (Nasser et al., 2019) and multi-drug-resistant *Pseudomonas aeruginosa* (Kohler et al., 2023). Another study showed, that phages can be used to suppress IBD-associated bacteria in the gut and therefore might be used for the treatment of intestinal inflammation (Federici et al., 2022). It can be particularly beneficial in cases where traditional antibiotics have failed or when alternative treatment options are limited.

Despite its potential, there are still challenges associated with phage therapy, for example identifying the appropriate phages for a specific infection, phage specificity within the different isolates of the bacterial strain, and potential stimulation of the human immune system (Nilsson, 2014). Additionally, there is a growing need for more clinical trials and standardized protocols to establish the safety and efficacy of phage therapy but there are several obstacles that hinder the process. One being, that phage taxonomy has been in flux since its beginning. Historically, phages have been classified according to their morphology (Ackermann, 1992, 2001) but once molecular methods like sequencing have emerged, a much higher genomic diversity than previously thought has been revealed. Further, phages are polyphyletic, which makes a completely hierarchical virus classification impossible (Turner, Kropinski, & Adriaenssens, 2021). This leads to difficulties in predicting the characteristics of a certain phage by just looking at the closest relative. Also, phages are currently not clinically approved in Germany, leading to a very limited treatment volume of phage therapies. Besides that, there is no complete and common data collection to freely exchange phages and the corresponding information (Willy et al., 2023). Nevertheless, phage therapy is recognized as an important tool for the treatment of bacterial infections by offering a targeted and potentially effective alternative or addition to traditional antibiotics. Therefore, further research aims to investigate how phages affect, interact and coexist with their bacterial hosts within bacterial communities to get an idea on how to use them in a targeted and precise manner to manipulate bacteria.

1.4 Synthetic bacterial communities

Due to the high complexity and species richness of the intestinal microbiota, it is difficult to disentangle factors and mechanisms underlying host-microbiota interactions in health and disease. Therefore, working with a defined and less complex microbial community can help to perform experiments in a controlled manner. A synthetic bacterial community refers to an engineered community of microorganisms that is established in a germ-free environment. It contains a limited number of microorganisms, often representing key species that are necessary to perform specific functions or achieve desired outcomes (Bolsega, Bleich, & Basic, 2021; Clavel, Gomes-Neto, Lagkouvardos, & Ramer-Tait, 2017). These communities can easily be modified by adding or removing single bacteria. Germfree mice colonized with such a consortia, termed gnotobiotic mice, are valuable tools that allow researchers to control and manipulate the microbial composition, enabling a deeper understanding of how microorganisms

interact with each other and their hosts (Lagkouvardos et al., 2016; Schaedler, Dubs, & Costello, 1965; Weiss et al., 2022). Synthetic bacterial communities can be used *in vitro* and *in vivo* to study a vast variety of topics. One being to investigate the role of single microbes in health and disease by analyzing produced metabolites and their effect on community composition and inflammation levels. Also, it is possible to transplant microbial consortia from humans or animals to mice, resulting in a preclinical disease model (Dash et al., 2021). Further, one is able to study the influence of diet, diseases or other factors on the microbial community in a controlled way (Turnbaugh et al., 2009). Therefore, a possible way to study the influence of phages on their bacterial hosts and community function and composition is to work with synthetic microbial consortia *in vitro* and *in vivo*.

1.4.1 The Oligo-Mouse-Microbiota

One example for a genome based synthetic community is the Oligo-Mouse-Microbiota (OMM^{12}) (Brugiroux et al., 2016). The OMM^{12} consists of twelve mouse-derived bacterial strains (*Enterococcus faecalis* KB1, *Limosilactobacillus reuteri* I49, *Bifidobacterium animalis* YL2, *Clostridium innocuum* I46, *Blautia coccoides* YL58, *Enterocloster clostridioformis* YL32, *Flavonifractor plautii* YL31, *Acutalibacter muris* KB18, *Bacteroides caecimuris* I48, *Muribaculum intestinale* YL27, *Akkermansia muciniphila* YL44 and *Turicimonas muris* YL45) representing the five major phyla abundant in the murine gastrointestinal system, Bacillota, Bacteroidota, Verrucomicrobia, Actinomycetota and Pseudomonadota (Oren & Garrity, 2021). The consortium stably colonizes the mouse gut over several generations (Eberl et al., 2019) and the individual strains have been deposited at a public strain collection, are available for non-commercial use and are fully genome-sequenced (Garzetti et al., 2017; Lamy-Besnier, Koszul, Debarbieux, & Marbouty, 2021). Furthermore, the consortium can be extended by various bacterial strains to provide additive functions not present in the original community. For this work, the original consortium was amended with two bacteria, *E. coli* and *E. muris*, leading to the newly established OMM^{14} consortium. When *E. coli* Mt1B1 is added to the community *in vivo*, it enhances the colonization resistance against *S.* Tm significantly, providing a key function of a complex microbiome (Eberl et al., 2021). The OMM^{12} community has recently been extensively characterized *in vitro* and *in vivo* (Weiss et al., 2022; Weiss et al., 2023), making it a very practicable and reliable model for various research areas. It has been used worldwide to study infection of several pathogens like *Clostridium difficile* (Studer et al., 2016) as well as metabolic diseases as IBD (Fischer et al., 2020). Further, is has also been used to

answer questions in the fields of immunology (Feuerstein et al., 2020; Wyss et al., 2019) and microbial ecology (Afrizal Afrizal, 2022; Munch et al., 2023).

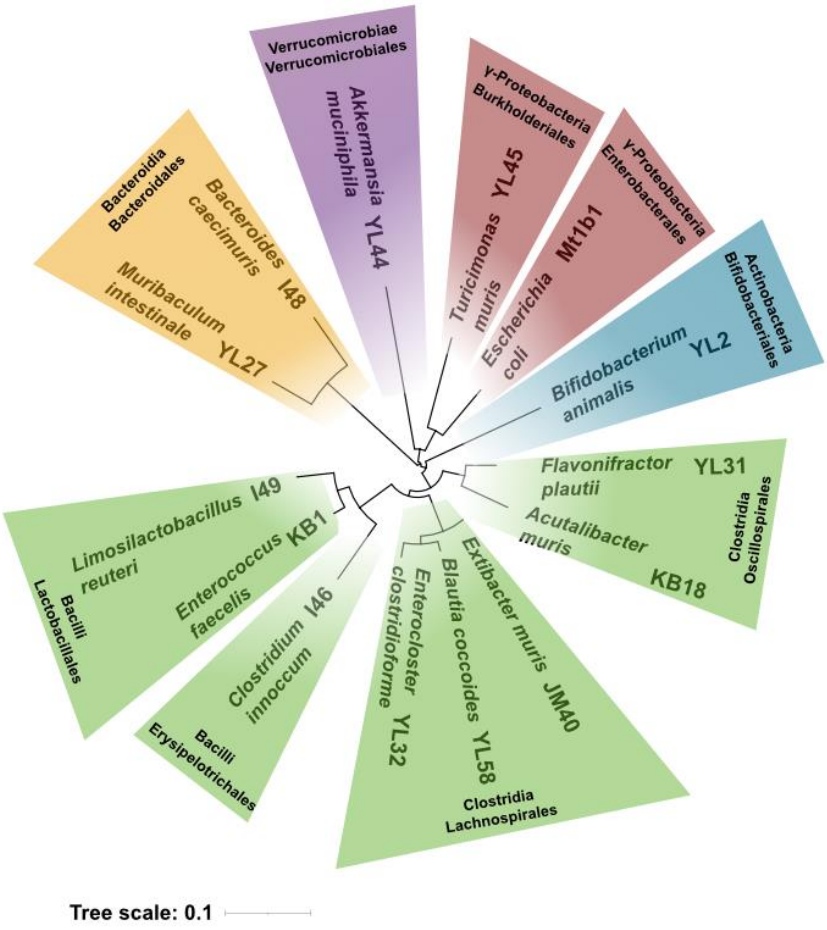

Fig 3: The OMM[14] bacterial model community

Phylogenetic tree of the OMM[14] based on 16s rRNA gene sequences.

Adapted from von Strempel et al., 2023

As phage research in the microbiome context gained more interest over the recent decades, the OMM model was also used in this field, for example to study prophage activation *in vitro* and *in vivo* (Lamy-Besnier et al., 2023) as well as infection and coexistence patterns (Lourenco et al., 2020). Overall, it is a useful and well establish model in microbiome research and can be amended with other bacteria to gain further functions (von Strempel et al., 2023).

1.4.2 The OMM[12] is a widely used model to study mechanisms of colonization resistance against *Salmonella*

Besides other important functions, the gut microbiome is known to form a protective barrier against human pathogens such as *Salmonella*, *Clostridioides difficile* or multi-resistant Gram-negative Bacteria (MRGN), which is termed colonization resistance (CR). Mechanisms underlying colonization resistance include substrate competition, production of bacteriocins or toxic metabolites or initiation of host immune responses (Buffie & Pamer, 2013). CR is higher in hosts with a complex microbiota and generally disrupted by drugs (Kim, Covington, & Pamer, 2017), dietary factors (Kreuzer & Hardt, 2020; Wotzka et al., 2019) and diseases (Rogers, Tsolis, & Baumler, 2021), but was also shown to be highly variable among healthy human individuals (Alavi et al., 2020; Osbelt et al., 2021). Other risk factors may exist, which are currently still unknown. There is also an increasing evidence that colonization resistance is not mediated by single bacterial species but rather by the interaction within a complex community. Protective bacteria may require a specific microbial context to counteract the invading pathogen.

S. Tm is a Gram-negative, facultative anaerobic, rod-shaped bacterium belonging to the family *Enterobacteriaceae*. *Salmonella enterica* serotypes (especially serovar Typhimurium, short *S.* Tm) cause infections worldwide, often transmitted via ingestion of contaminated food or water (Antimicrobial Resistance, 2022; Collaborators, 2022; European Food Safety, European Centre for Disease, & Control, 2022). The most common symptoms are diarrhea, abdominal cramps and fever. *S.* Tm induced gastroenteritis often does not need specific treatment, but can be severe in children, elderly and immunocompromised patients (Coburn, Grassl, & Finlay, 2007). Interestingly, only 1-5% of people that ingest *S.* Tm develop a symptomatic infection, and in the vast majority the onset of the infection is efficiently prohibited (Simonsen et al., 2009). This could be due to several genetic predispositions or differences in the immune system or disrupting events as discussed before (diet, drugs), but also to differences in the colonization resistance mediated by the gut microbiome (Stecher, 2021). Hence, disentangling the factors that strengthen or weaken the microbiome mediated colonization resistance is important to identify risk factors of *S.* Tm induced infections.

The OMM[12] mouse model has already been used to investigate different stages of *S.* Tm infection. In the Stecher lab, Brugiroux and colleagues could successfully show, that mice stably colonize with the OMM[12] consortium have an intermediate protection against *S.* Tm

compared to germfree mice and conventional laboratory mice harboring a complex microbiota. The addition of a mixture of 3 facultative anaerobic bacteria (*Escherichia coli, Staphylococcus xylosus, Streptococcus danieliae*) to mice colonized with the OMM^{12} enhanced the colonization resistance against *S.* Tm to a degree comparable to conventional mice (Brugiroux et al., 2016). Following up, Eberl and colleagues could show that this increase in colonization resistance in OMM^{12} mice is also mediated by *E. coli* alone, by competing for galactitol with *S.* Tm, which is the limiting carbon source in this microbial background. Interestingly, the protective context is dependent on the presence of other members of the OMM^{12}. If *E. faecalis* KB1 or the *Lachnospiraceae* strains *B. coccoides* YL58 and *E. clostridioformis* YL32 are dropped out from the consortium, *E. coli* does not mediate colonization resistance, showing that this important function of the microbiome is context dependent (**Fig4**, (Eberl et al., 2021).

These studies show, that colonization resistance is mediated by the microbiome but also dependent on multiple factors that can influence the abundance and interaction of single strains and that synthetic bacterial communities are a great tool to specifically identify these single factors to get a better understanding of this complex function.

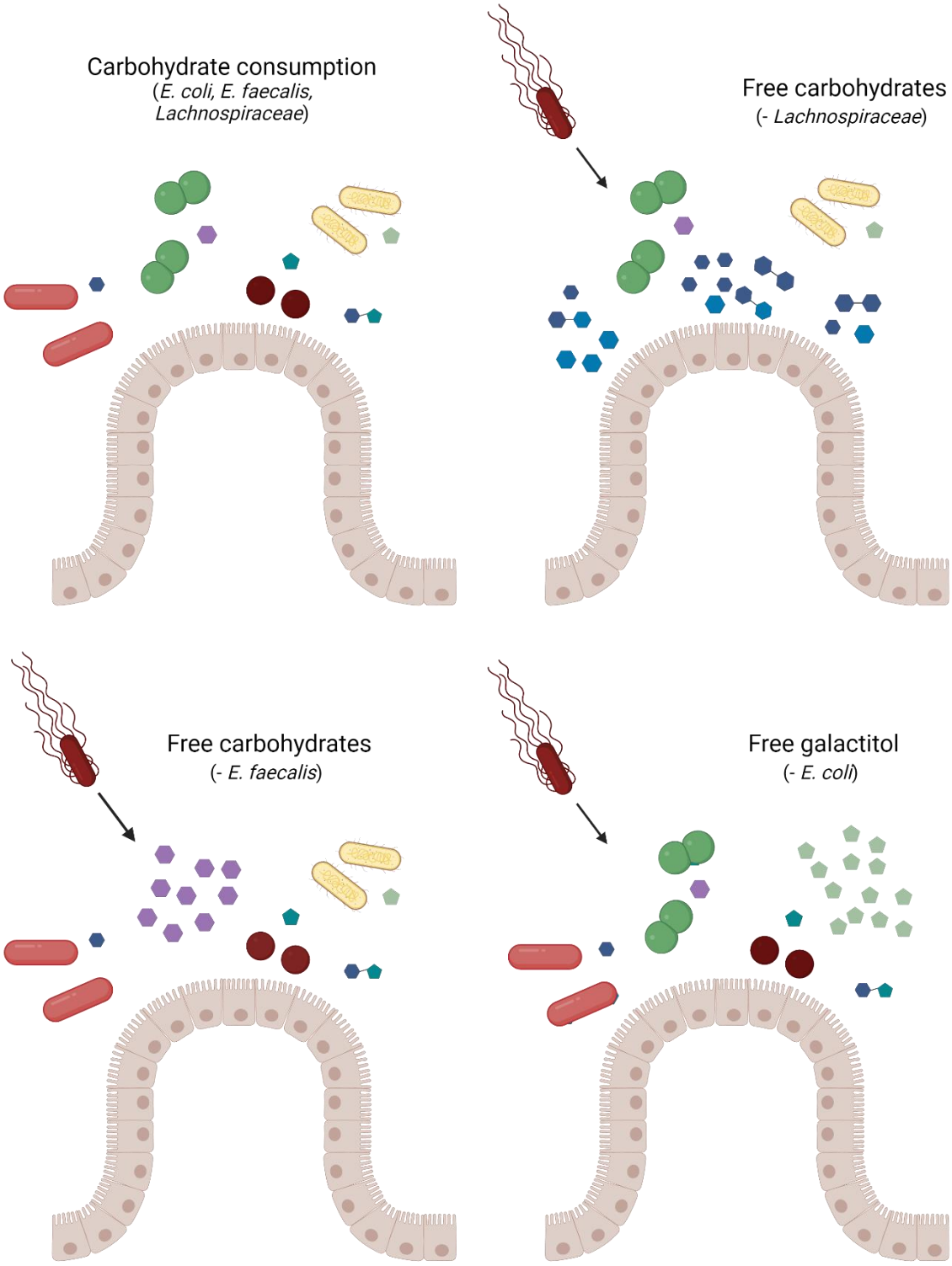

Fig 4: Colonization resistance against *Salmonella* is mediated by carbohydrate consumption of several bacteria in the OMM community

Full CR is only mediated when all members of the OMM[12] consortium and *E. coli* are present and consume carbohydrates in the gut. Free carbohydrates enable S. Tm to invade. For *E.coli*, this competition relies on the consumption of galactitol, for the other bacteria the exact mechanism is still unclear.

Figure created with Biorender.

2. Aims of this thesis

Although phages are an interesting and emerging field in microbiome research and are seen as potential agents for manipulation of bacterial communities and targeting of harmful bacteria, little is known about their influence on their hosts *in vivo* and on community functions and homeostasis. Since phages are able to decrease numbers of potential protective bacteria in the gut, they might be a potential risk factor for a *Salmonella* infection when taken up with food or water. Therefore, investigating the influence of phages on important community functions like colonization resistance is crucial to understand and provide a better knowledge base for further phage-based treatment approaches.

In this work, I aim to establish and characterize a phage collection for the OMM model. To gain more functions in the model, I amended the OMM^{12} with two additional members, *E. coli* Mt1B1 and *Extibacter muris* JM40, a secondary bile acid producer, to enhance CR against gastrointestinal pathogens (Eberl et al., 2021; Streidl et al., 2021). The new consortium consisting of 14 different bacterial strains will be referred to as OMM^{14} in the following study and will be used to establish a gnotobiotic mouse line. The isolated phages will then be characterized *in vitro* to gain more knowledge about genome features, lysis behavior and host range.

Secondly, I want to characterize the phages in the OMM^{14} consortia regarding their ability to amplify in a more complex environment and their long term effect on their host bacteria. For this, I established a specific absolute quantification for the isolated phages to test their influence on their host bacteria and the general community structure *in vitro* and *in vivo*.

As a third aim, I aim to investigate how phages that target protective bacteria in the gut have an influence on the colonization resistance against *S.* Tm. Therefore, I also plan to employ the OMM model since it was already shown to protect against *S.* Tm infection in the past when *E. coli* is present. I want to see how phages interact and coexist with their host bacteria and *in vivo* and if they are able to change structural outcomes of the community. Further, I want to test if phages are able to impair the colonization resistance against *S.* Tm by targeting *E. coli* Mt1B1 and *E. faecalis* KB1, two bacteria that confer colonization resistance in the community context.

This work aims to elucidate the role of phages on community functions and their influence on their host bacteria within a minimal bacterial model community.

3. Materials and Methods

3.1 Materials

Table 1: List of instrumentation used in this thesis

Devices	Supplier
Centrifuge 5430R; rotor: 5430R	Eppendorf, Hamburg Germany
Centrifuge Biofuge pico	Heraeus, Hanau Germany
Centrifuge Heraeus multifuge X3R Rotor: 75003603	Heraeus, Hanau Germany
Centrifuge: 4K15; Rotor: 12169	Sigma-Aldrich, St. Louis US
Crimper (diam. 11 mm)	Sigma-Aldrich, St. Louis US
Crimper (diam. 20 mm)	VWR, Darmstadt Germany
Decapper (diam. 11 mm)	Sigma-Aldrich Sigma-Aldrich, St. Louis US
Decrimper (diam. 20 mm)	VWR, Darmstadt Germany
Gel Imaging System: GelDoc Go	Bio-Rad, Feldkirchen Germany
Lightcycler	Roche, Mannheim
Leitz DM-RBE microscope	Leica Microsystems, Wetzlar Germany
Carl Zeiss 46-70-85 microscope	Carl Zeiss, Oberkochen Germany
Microplate Reader Epoch 2	BioTek, Santa Clara US
Microplate Stacker Biostack 4	BioTek, Santa Clara US
Nanodrop	Thermo Fischer Scientific, Karlsruhe Germany
ND-1000 spectrophotometer	Peqlab, Erlangen Germany
Safe 2020 Class II Biological Safety Cabinet	Thermo Fisher Scientific, Karlsruhe Germany
Thermocycler: peqstar 2X gradient	Peqlab, Erlangen Germany
Thermomixer C	Eppendorf, Hamburg Germany
Thermomixer comfort	Eppendorf, Hamburg Germany
Tissue Lyser LT	Qiagen, Hilden Germany
Vinyl Anaerobic Chamber with Vacuum Airlock	Coy Laboratory Products Inc., Grass Lake US

Table 2: List of chemicals, reagents and kits used in this thesis

Chemicals, Reagents, and Kits	Supplier
0.1 mm-diameter zirconia/silica beads	BioSpec Products, Bartlesville US
2x FastStart Essential DNA Probes Master	Roche, Mannheim
1 kb Gene Ruler DNA Ladder	Thermo Fisher Scientific, Karlsruhe Germany
ABTS	Calbiochem 194430
Agar (Bacto)	Becton, Dickinson & Company, Le Pont de Claix, France
Agarose	Bio & Sell, Feucht Germany

AMPure XP Reagent	Beckman Coulter, Brea US
Brain Heart Infusion	Thermo Fisher Scientific, Karlsruhe Germany
Cetrimonium bromide (CTAB)	Sigma-Aldrich, St. Louis US
CloneJet PCR Cloning Kit	Thermo Scientific, Karlsruhe Germany
Crystal violet	Sigma-Aldrich, St. Louis US
Cysteine hydrochloride	Sigma-Aldrich, St. Louis US
ddH_2O	Thermo Fisher Scientific, Karlsruhe Germany
Dream Taq Master Mix (2X)	Thermo Fisher Scientific, Karlsruhe Germany
Ethanol absolute	Sigma-Aldrich, St. Louis US
Ethidium bromide, 1 % solution	AppliChem, Darmstadt Germany
FastStart Essential DNA probes Master	Roche, Mannheim
Fecal bovine serum analog	NeoFroxx, Einhausen Germany
Glucose	Carl Roth, Karlsruhe Germany
Glycerol	Carl Roth, Karlsruhe Germany
Hemin	Sigma-Aldrich, St. Louis US
Iodine (for lugol solution)	Merck, Darmstadt Germany
Isopropanol	AppliChem, Darmstadt Germany
KCl	Carl Roth, Karlsruhe Germany
K_2HPO_4	Carl Roth, Karlsruhe Germany
Kaliumiodid (for lugol solution)	VWR, Darmstadt Germany
Loading Buffer	Thermo Fisher Scientific, Karlsruhe Germany
Menadione	Sigma-Aldrich, St. Louis US
Na_2CO_3	Merck, Darmstadt Germany
NaCl	Carl Roth, Karlsruhe Germany
NotI Fermentas	Thermo Fisher Scientific, Karlsruhe Germany
NotI reaction buffer Fermentas	Thermo Fisher Scientific, Karlsruhe Germany
NucleoSpin gDNA Clean-Up Kit	Macherey-Nagel, Düren Germany
NucleoSpin Gel and PCR Clean-Up Kit	Macherey-Nagel, Düren Germany
NucleoSpin Plasmid Mini Kit	Macherey-Nagel, Düren Germany
Phenol	Merck, Darmstadt Germany
Phenol/Chloroform/Isomylalcohol	Carl Roth, Karlsruhe Germany
Proteinase K	Carl Roth, Karlsruhe Germany
Safranin	Carl Roth, Karlsruhe Germany
SDS	Serva, Heidelberg Germany
Sodium Acetate	Honeywell, Offenbach Germany
Sterile water (Ampuwa)	Fresenius Kabi Deutschland GmbH
Trypticase Soy Broth	Thermo Fisher Scientific, Karlsruhe Germany
Tryptone	Carl Roth, Karlsruhe Germany
Tween	Carl Roth, Karlsruhe Germany
Qiagen Plasmid Plus Midi Kit	Qiagen, Hilden Germany
Q5 High-Fidelity DNA polymerase	New England Biolabs, Ipswich England
Virkon S	Du Pont, Neu-Isenburg Germany
Yeast extract	Carl Roth, Karlsruhe Germany
Yeast t_RNA solution	Roche, Mannheim

Table 3: Media composition used in this thesis

Media	Components	Gramm per liter
LB Agar	NaCl Yeast extract Tryptone Agar	5 g 5 g 10 g 15 g (3g for softagar)
LB 0.3 M NaCl	NaCl Yeast extract Tryptone	17.53 g 5 g 10 g
LB Medium	NaCl Yeast extract Tryptone	5 g 5 g 10 g
10x Phosphate Buffered Saline (PBS)	NaCl KCl Na_2HPO_4 KH_2PO_4	80 g 2g 6 .1 g 2.4 g
AF Medium	Brain Heart Infusion Trypticase soy broth Yeast extract K_2HPO_4 Hemin Glucose Autoclave and add: Na_2CO_3 Cysteine hydrochloride Menadione Complement inactivated FCS	18.5 g 15 g 5 g 2.5 g 1 mg 0.85 g 0.4 g 0.5 g 0.5 g 3 % of total volume

Table 4: Buffer composition

Buffer	Components	Concentration
TE buffer	Tris-Cl EDTA	10 mM 1 mM
Extraction buffer for DNA extraction	Tris NaCl EDTA Components were dissolved in ddH_2O	200 mM 200 mM 20 mM
SM buffer	NaCl $MgSO_4xH_2O$ Tris-HCl	100 mM 8.1 mM 50 mM
ELISA blocking buffer	1x PBS BSA	 2 %
ELISA wash buffer	1x PBS Tween-20	 0.05 %
ELISA substrate buffer	NaH_2PO_4, pH4	0.1 M
ELISA substrate	Substrate buffer ABTS H_2O_2	10 ml 1 mg 5µl

Table 5: Antibodies used in this thesis

Antibody, origin	**Supplier, dilution**
Lipocain-2 capture antibody, rat	R&D, Part 842440, 1:200
Lipocalin-2 detection antibody, rat	R&D, Part 842440, 1:200
Streptavidin-HRP, rat	Biolegend 405210

Table 6: Software used in this thesis

Software	**Developer**
Affinity Designer	Serif, Nottingham, Great Britian
Biorender	Biorender, Toronto Canada
Excel 2016	Microsoft, Redmond US
Gen 5 microplate reader and imager software	BioTek, Santa Clara US
GraphPad Prism 8	GraphPad Software, Boston US
Image J	Public Domain, BSD-2
Leica Application Suite X (V. 3.0.0.15697)	Cytek, Fremont, CA, United States
LightCycler 96	Roche, Mannheim
Word 2016	Microsoft, Redmond US

3.2 Methods

3.2.1 Bacterial strains and culture conditions

3.2.1.1 Bacterial strains used in this thesis

The following bacterial strains were used in this study to perform the *in vitro* and *in vivo* experiments: *Enterococcus faecalis* KB1 (DSM 32036), *Bifidobacterium animalis* YL2 (DSM 26074), *Acutalibacter muris* KB18 (DSM 26090), *Muribaculum intestinale* YL27 (DSM 28989), *Flavonifractor plautii* YL31 (DSM 26117), *Enterocloster clostridioformis* YL32 (DSM 26114), *Akkermansia muciniphila* YL44 (DSM 26127), *Turicimonas muris* YL45 (DSM 26109), *Clostridium innocuum* I46 (DSM 26113), *Bacteroides caecimuris* I48 (DSM 26085), *Limosilactobacillus reuteri* I49 (DSM 32035), *Blautia coccoides* YL58 (DSM 26115), *Escherichia coli* Mt1B1 (DSM 28618) (Eberl et al., 2019), *Extibacter muris* JM40 (DSM 28560) (Streidl et al., 2021), *S.* Tm^{wt} SL1344 (SB300) (Hoiseth & Stocker, 1981), *S.* Tm^{avir} M2707 (Maier et al., 2013), *Staphylococcus aureus* RG2 (DSM 104437).

3.2.1.2 Preparation of bacterial cryostocks

Bacterial stocks were prepared using a modified Hungate technique utilizing serum bottles as described before (von Strempel et al., 2023). Therefore, glass serum bottles were filled with 10 mL anaerobic medium (AF medium, : 18 $g.l^{-1}$ brain-heart infusion (Oxoid), 15 $g.l^{-1}$ trypticase soy broth (Oxoid), 5 $g.l^{-1}$ yeast extract, 2.5 $g.l^{-1}$ K_2HPO_4, 1 $mg.l^{-1}$ haemin, 0.5 $g.l^{-1}$ D-glucose, 0.5 $mg.l^{-1}$ menadione, 3% heat-inactivated fetal calf serum, 0.25 $g.l^{-1}$ cysteine-HCl x H_2O and closed with an airtight rubber plug and an aluminum crimp, anaerobically. For the stocks, small glass vials were filled with 500 µL of 20% glycerol + palladium and closed with crimp seals, anaerobically.

To start a primary culture, 1 ml frozen glycerol stock was added to serum bottle containing AF medium. To do so, all used serum bottles and cryostocks were first sterilized by burning a few drops of ethanol added to the rubber lid. Then, a sterile syringe was inserted into an oxygen-free gas serum bottle and flushed three times to remove oxygen inside. The needle was then inserted into the bacterial culture bottle through the rubber plug and 0.5 mL of culture was taken up and transferred into the third bottle containing fresh medium and incubated overnight at 37 °C. To generate cryostocks, using Hungate technique as described before, 500 µL of the subculture were filled into small glass vials containing 500 µL of 20 % glycerol + palladium, resulting in a final concentration of 10 % glycerol. The stocks were frozen and kept at -80 °C.

For quality control of the bacterial cryostocks Gram staining and 16S sequencing were performed.

3.2.1.3 Culture conditions

As described before (von Strempel et al., 2023), OMM[14] cultures used for *in vitro* experiments were prepared from individual frozen glycerol cryostocks (1 ml, 10 % glycerol + Palladium) in 10 ml AF medium in cell culture flasks and subcultured in another 10 ml of AF medium in cell culture flasks (flask T25, Sarstedt). Cultures were incubated at 37°C for 24 h without shaking under anaerobic conditions in an anaerobic chamber (gas atmosphere 7% H_2, 10% CO_2, 83% N_2). From the initial culture, subcultures were started in a 1:100 dilution and again incubated at 37°C for 24 h without shaking under anaerobic conditions.

For mouse infection experiments, *S.* Tm strains were streaked from frozen stocks on MacConkey agar plates (Oxoid) containing streptomycin (50 µg/ml) and incubated aerobically at 37 °C overnight. One colony was then re-suspended in 3 ml LB containing 0.3 M NaCl and incubated for 12 h at 37 °C on a wheel rotor under constant movement. A subculture (1:20 dilution) was prepared in LB with 0.3 M NaCl and incubated for another 4 h. Bacteria were washed in ice-cold sterile PBS by centrifugation for 2 min at 12000xg. The supernatant was removed and the pellet was re-suspended in PBS for gavage and distributed in aliquots (50 µl each).

3.2.2 Phage isolation and identification

3.2.2.1 Spot assays for phage plaque visualization on *E. coli* Mt1B1 and *E. faecalis* KB1

As described before, 1 ml of an exponentially growing bacterial culture, containing the phage host, was applied on an EBU agar plate, containing Evans Blue (1%) and Fluorescein sodium salt (1%) to visualize bacterial lysis (von Strempel et al., 2023). On EBU plates, lysis is indicated by a color change from light green to dark green. Excess liquid was carefully removed and the plate was dried under the laminar airflow cabinet for 15 minutes. Phage lysates were serially diluted in sterile PBS and 5 µl of each dilution was spotted on the bacterial lawn. The plate was then dried again to prevent mixing of the dilutions. The plate was incubated over night at 37°C. The next day, clear plaques (=dark color of the agar) were visible which indicated lysis of the bacteria on the plate. Plaques were counted to quantify plaque forming units (PFU).

3.2.2.2 Isolation of *E. faecalis* KB1 phages from sewage water

Isolation of phages targeting *E. faecalis* was done as described before (von Strempel et al., 2023). For isolation of specific phages, sewage water from different sources was filtered (0.22 µm) to get rid of bacteria and dirt, and mixed with an equal volume of 2 x LB media. Next, bacterial overnight culture in AF medium was added with a final dilution of 1/100 and incubated overnight at 37°C without shaking under aerobic conditions. The next day, the cultures were centrifuged at 6,000 x g for 10 min, filtered (0.22 µm) to remove the bacteria and spotted in serial dilution in PBS on a lawn of *E. faecalis* KB1 on EBU plates followed by another incubation at 37 °C overnight. Lysis appeared as a darker color on the plates. If plaques were visible, individual plaques were carefully picked with a pipet tip and diluted in 100 µl SM buffer (100 mM NaCl, 8.1 mM $MgSO_4$ x H_2O, 50 mM Tris-HCL (pH 7.5)), added to a fresh bacterial subculture in 10 ml AF medium and incubated overnight at 37°C without shaking under aerobic conditions. This was repeated three times to purify the phage. The phage suspension was again centrifuged and filtered which resulted in a sterile phage suspension which was stored at 4°C and used for the *in vitro* and *in vivo* experiments.

3.2.2.3 Isolation of phages targeting *E. clostridioformis* YL32 and *C. innocuum* I46 and from sewage water

For isolation of phages specific for strictly anaerobic members of the OMM^{14} consortium, the same protocol was used in a slightly modified way. Sewage water from different sources was centrifuged (6000 x g, 15 min) and mixed with an equal volume of 2 x AF media. Next, bacterial overnight culture was added with a final dilution of 1/10 and incubated overnight at 37°C without shaking under anaerobic conditions. The next day, the cultures were centrifuged (6,000 x g, 10 min), filtered (0.22 µm) and spotted in serial dilution on AF plates overlayed with LB softagar containing the respective bacterial host, followed by another incubation at 37 °C overnight under anaerobic conditions. If clear plaques were visible, individual plaques were picked and diluted in 100 µl SM buffer (100 mM NaCl, 8.1 mM $MgSO_4$ x H_2O, 50 mM Tris-HCL (pH 7.5)), added to a fresh bacterial subculture in 10 ml AF medium and incubated overnight. This was repeated three times to purify the phage. Centrifugation and filtration of the culture resulted in a sterile phage suspension which was stored at 4°C and used for the *in vitro* and *in vivo* experiments.

3.2.2.4 Spot assays for phage plaque visualization on *E. clostridioformis* YL32 and *C. innocuum* I46

For phages vB_cin and vB_ccl, spot assays were performed on AF agar plates overlayed with softagar, since bacterial growth of *E. clostridioformis* YL32 and *C. innocuum* I46 was not very good on plain agar plates and therefore plaques are not visible very well. 0.5 ml of an exponentially growing bacterial culture, containing the phage host, was mixed with 2.5 ml of LB softagar (5g/l agar concentration) and poured on an AF agar plate under anaerobic conditions. After the soft agar hardened (15-30 min), phage lysates were serially diluted in sterile PBS and 5 µl of each dilution was spotted on the soft agar. The plate was incubated over night at 37°C. The next day, clear plaques indicating lysis of the bacteria could be detected. Plaques were counted to quantify plaque forming units (PFU).

3.2.2.5 Generation of phage cocktails targeting *E. faecalis* KB1 and *E. coli* Mt1B1

Generation of phage cocktails was done as described previously (von Strempel et al., 2023). First, 100 µl of purified and sterile phage suspension (prepared as described in 3.2.2.1 and 3.2.2.2) was added to 10 ml of LB media and incubated with 100 µl of overnight culture of their respective bacterial host overnight at 37°C under aerobic conditions. The next day, the cultures were centrifuged at 6,000 x g for 10 min, filtered (0.22 µm) to remove the bacteria and spotted in serial dilution in PBS on a lawn of their respective bacterial host on EBU plates. This was followed by another incubation at 37°C overnight. The next day, plaques were counted and plaque forming units were calculated for the phage suspensions ($\frac{number\ of\ plaques * dilution}{used\ phage\ lysate\ (ml)}$) and the phages were mixed together in a concentration of $1x10^7$ PFU/100µl each. The following phages were used in this study: Mt1B1_P3, Mt1B1_P10, Mt1B1_P17 (Lourenco et al., 2020), vB_efaS_Str1 (vB_EfaS_Strempel1, DSM 110103), vB_efaP_Str2 (vB_EfaP_Strempel2, DSM 110104), vB_efaS_Str6 (vB_EfaS_Strempel6, DSM 110108), vB_SauP_EBHT (DSM 26856) (von Strempel et al., 2023).

3.2.2.6 Generation of phage lysates targeting *E. clostridioformis* YL32 and *C. innocuum* I46

For phages vB_cin and vB_ccl, phage lysates were created in a slightly modified way. First, 100 µl of purified and sterile phage suspension (prepared as described in 3.2.2.3) was added to

10 ml of AF media and incubated with 100 µl of overnight culture of their respective bacterial host overnight at 37°C under anaerobic conditions. The next day, the cultures were centrifuged at 6,000 x g for 10 min, filtered (0.22 µm) to remove the bacteria and spotted in serial dilution on AF plates overlayed with softagar containing the respective bacterial host, followed by another incubation at 37°C overnight. The next day, plaque forming units were calculated for the phage suspensions ($\frac{number\ of\ plaques * dilution}{used\ phage\ lysate\ (ml)}$) and the phages were diluted to a concentration of $1x10^7$ PFU/100µl each. The following phages were used in this study: vB_ccl_YL32 and vB_cin_I46.

3.2.3 Phage genome characterization

3.2.3.1 Genomic DNA extraction from phage lysates

DNA extraction was performed as described previously (Lourenco et al., 2020; von Strempel et al., 2023). Briefly, the phage lysate (6 ml with at least 10^7 PFU/ml) was filled into a 15ml falcon tube. 75 µl of MgCL2 (1 M), 120 µl DNAse (1000 U/ml) and 2.4 µl RNAse (100 mg/ml) were added. After vortexing carefully, the mixture was incubated at 37 °C for 30 minutes. To stop the DNAse and RNAse activity, 240 µl of EDTA 0.5 M was added, followed by 30 µl of ProteinaseK (20 mg/ml) and 300 µl of SDS 10%. Incubation was performed for 30 minutes at 55 °C.

The lysate was transferred into a DNA free 50 ml falcon (Eppendorf) and an identical volume of PCI (phenol:chloroform:isoamylalcohol 25:24:1) was added. The mixture was centrifuged at 13 000 x g for 5 min to separate the two phases. The upper phase was carefully transferred to a new DNA free 50 ml falcon and 6 ml of PCI was added, mixed and centrifuged again. The upper, aqueous phase was then transferred into a fresh 50 ml falcon and 620 µl of 3M Sodium Acetate (pH=5.2) and 12.4 ml of ethanol p.a. were added. After slow homogenization the mix was left on ice to precipitate for 15 minutes, followed by centrifugation at 15 0100 x g for 20 minutes at 4 °C. The supernatant was removed and the pellet was washed with ice cold 70% ethanol. After drying, the DNA was solubilized in 150 µl TE buffer. Subsequently, gDNA was purified using the NucleoSpin gDNA clean-up kit (Macherey-Nagel) and stored at -20°C.

3.2.3.2 DNA sequencing, assembly and annotation

The three phages targeting *E. coli* Mt1B1 were sequenced and analyzed as described previously (Lourenco et al., 2020). Shortly, sequencing was performed using Illumina MiSeq Nano. Assembly was performed using a workflow implemented in Galaxy-Institut Pasteur and phage termini were determined by PhageTerm. Genbank Accession numbers: MT496969 (Mt1B1_P3), MT496971 (Mt1B1_P10), MT496970 (Mt1B1_P17). Visualization was performed using pharokka (Bouras et al., 2023).

The three *E. faecalis* KB1 phages were also sequenced previously (von Strempel et al., 2023) using Illumina MiSeq Nano and assembled with SPAdes (3.12.0) (Bankevich et al., 2012), NCBI Accession Number: PRJNA972641. Annotation was performed using PROKKA (Seemann, 2014) and taxonomic classification was performed using VICTOR (Meier-Kolthoff & Goker, 2017) as previously described (Korf et al., 2019). Visualization was performed using pharokka (Bouras et al., 2023).

Phages vB_ccl_YL32 and vB_cin_I46 were sequenced using Illumina MiSeq Nano and the raw sequence data obtained from sequencing were pre-processed using Trimmomatic (v0.36) (Bolger, Lohse, & Usadel, 2014) for removing low-quality reads with the parameters of SLIDINGWINDOW:10:15 MINLEN:25. The quality-filtered sequence reads were assembled into contigs using de novo assembly using metaviralspades (v3.13) (Bankevich et al., 2012) with default parameters. Retrieved contigs were verified using viralVerify (v.1.1) (Bankevich et al., 2012) to identify and assess the quality of the viral contigs. viralVerify predicts genes using prodigal (Hyatt et al., 2010) in metagenomic mode, then performs hmmsearch (Johnson, Eddy, & Portugaly, 2010) on the predicted proteins and uses the Naive Bayes classifier (NBC) (Rosen, Reichenberger, & Rosenfeld, 2011) to classify the contig as viral or non-viral. In addition, checkV (Nayfach et al., 2021) was used to further assess the quality and completeness of phage genomes, only phage sequences estimated as high-quality (i.e., >90% genome completeness) were filtered and used for further analysis. Taxonomic assignment and clustering of the contigs (VirClusters) were conducted using vConTACT v.2.0 (Gregory et al., 2020) with "–db 'ProkaryoticViralRefSeq85-Merged'–pcs-mode MCL–vcs-mode ClusterONE" option and also taxonomic assignment was verified with Viptree (v1.1.3) (Nishimura et al., 2017). Blastn (Rosen et al., 2011) was performed to find the closest hit from NCBI. Gene prediction and visualization was performed using pharokka (Bouras et al., 2023) tool v1.5.

3.2.4 Growth assays

3.2.4.1 Phage lysis *in vitro*

Bacterial growth was measured in 96 well plates (Sarstedt TC-cellculture plate) using an Epoch2 plate reader (GenTech) under anaerobic conditions. Inocula were prepared from an overnight culture and subculture and diluted in AF medium (Weiss et al., 2022) to a density of 0.01 OD_{600}. To determine phage growth and the effect of bacterial lysis, 150 µl of bacterial culture was added to each well, followed by either 10 µl of PBS as a control or 10 µl of sterile phage lysate with a defined concentration of active phages (PFU/ml), resulting in a MOI of 0.01 for the phages targeting *E. coli* and *E. faecalis*. The other two phages were added in a serial dilution to the culture of *E. clostridioformis* and *C. innocuum*. For a duration of 20 hours in total, measurements took place every 15 min. The plate was heated inside the reader to 37°C and a 30 second double orbital shaking step was performed prior to every measurement. (von Strempel et al., 2023).

3.2.4.2 OMM^{14} community cultures in batch culture

OMM^{14} communities in batch culture were cultivated as previously described (Weiss et al., 2022). Shortly, monoculture inocula were derived from an initial culture, then subsequently subcultured and diluted to an OD_{600} 0.1 in AF medium. From this, a community inoculum comprising all 14 strains in equivalent proportions was generated. The inoculum was distributed to 24 well plates, thereby diluting the inoculum 1:10 with 0.9 ml AF medium, resulting in an initial OD_{600} of 0.01 (time = 0h). 24-well plates were incubated at 37°C without shaking under anaerobic conditions. Samples were collected every 24 hours for qPCR analysis and spot assays, while the cultures were diluted 1:100 in AF medium. Phages were introduced into the community 12 hours after the third dilution, at a concentration of $1*10^6$ PFU per phage in 10 µl PBS.

3.2.5 Animal experiments

3.2.5.1 Inoculation of germ-free mice and establishment of a gnotobiotic OMM^{14} mouse line

Germ-free mice bred in our in-house facility were inoculated with OMM^{12} cryostock mixtures as described previously (Eberl et al., 2019; von Strempel et al., 2023) and individual frozen stocks of *E. muris* JM40 and *E. coli* Mt1B1. Stocks were thawed in 1% Virkon S (V.P. Produkte) disinfectant solution to hinder contaminations and used for inoculation of germ-free C57Bl/6 mice in a flexible film isolator. Mice were inoculated twice with 72 h between the inoculations with the bacterial mixtures and the two single stocks by gavage (50 µl orally, 100 µl rectally). The dual administration should enhance colonization of the bacteria. Mice were housed and bred in flexible film isolators (North Kent Plastic Cages) under germfree conditions. For experiments, mice were transferred into isocages (IsoCage P system, Tecniplast) under sterile conditions. Mice were supplied with autoclaved ddH_2O and autoclaved Mouse-Breeding complete feed for mice (Ssniff) *ad libitum*. For the following experiments, only mice starting from generation F1 were used, to ensure stable colonization of the consortium.

3.2.5.2 Phage challenge *in vivo*

For all experiments, female and male mice between 6-20 weeks were used and animals were assigned to experimental groups to match sex and age. Mice were kept in groups of at least two mice and maximum five mice per cage during the experiment. All animals were scored twice daily for their health status. Phage cocktails or single phages (10^7 PFU per phage in 100 µl PBS) were carefully administered by oral gavage. All mice were sacrificed by cervical dislocation on the last day of the experiment. Feces and cecal content were immediately weighed and either dissolved in 500 µl sterile PBS for plating (CFUs, PFUs) or frozen for later DNA extraction used for qPCR (von Strempel et al., 2023).

3.2.5.3 *S*. Tm infection *in vivo*

Mice were infected with *S*. Tm by oral gavage with 50 µl of bacterial suspension (approximately $5x10^7$ CFU). All mice were sacrificed by cervical dislocation. Feces and cecal content were weighed and either frozen for later DNA extraction or dissolved in 500 µl sterile PBS. Bacterial loads were determined as previously described (von Strempel et al., 2023): "*S*. Tm and *E. coli* Mt1B1 loads were determined by plating in several dilutions on MacConkey agar (Oxoid)

supplemented with respective antibiotics (vancomycin 7.5 µg/ml for *E. coli*, streptomycin 50 µg/ml for *S.* Tm). *E. faecalis* KB1 loads were determined by plating in several dilutions on BHI agar (Oxoid), supplemented with polymycin B 50 µg/ml. 100 µl of dissolved intestinal content were sterile filtered using Centrifuge Tube Filter (0.22 µm, Costar Spin-X) and spotted in serial dilutions in PBS on a lawn of *E. coli* and *E. faecalis* on EBU agar plates to determine the phage loads. Lipocalin-2 was quantified from supernatant of frozen cecal content. For metabolomics, samples were directly snap frozen in liquid N_2 and stored at -80°C until further processing. Samples for DNA extraction were stored at -20°C after weighing."

3.2.5.4 DNA extraction from intestinal content

gDNA extraction was performed using a phenol-chloroform based protocol as described previously (Eberl et al., 2021; Herp et al., 2019; von Strempel et al., 2023). Briefly, the fecal pellet or cecal content was resuspended in 500 µl extraction buffer (consisting of: 200 mM Tris-HCl, 200 mM NaCl, 20 mM EDTA in ddH_2O, pH 8, autoclaved), 210 µl 20 % SDS and 500 µl phenol:chloroform:isoamylalcohol (25:24:1, pH 7.9). Furthermore, 500µl of autoclaved 0.1 mm-diameter zirconia/silica beads (Roth) were added to ensure lysis of the cells. Bacterial cells were then lysed utilizing a bead beater (TissueLyser LT, Qiagen) for 4 min at 50 Hz. After centrifugation (14,000 x g, 5 min, RT), the aqueous upper phase was transferred into a new tube and the lower phase was discarded. Then, 500 µl phenol:chloroform:isoamylalcohol (25:24:1, pH 7.9) were added again and centrifugation was repeated for 5 min at 14000 xg. The resulting upper aqueous phase was gently mixed with 1 ml 96 % ethanol (p. a.) and 50 µl of 3 M sodium acetate by inverting the tube carefully for 3-5 times. After centrifugation for 30 min at 14,000 x g at 4 °C, the supernatant was carefully discarded and the gDNA pellet was washed with 500 µl ice-cold 70 % ethanol and again centrifuged (14,000 x g, 4 °C; 15 min). The resulting gDNA pellet was briefly dried and then resuspended in 100 µl Tris-HCL pH 8.0. Subsequently, gDNA was purified using the NucleoSpin gDNA clean-up kit (Macherey-Nagel) following manufacturer's instructions and stored at -20°C.

All animal experiments were done following the approved grant (Versuchstierantrag) with the number **ROB-55.2-2532.Vet_02-17-120**

3.2.6 Quantitative PCR for bacteria and phages

3.2.6.1 qPCR for bacterial members of the OMM[14] consortium

Quantitative PCR was established and optimized previously and therefore performed as described before (for the OMM[12] strains and *E. coli* Mt1B1 see (Brugiroux et al., 2016), for *E. muris* JM40 see (Streidl et al., 2021)). Briefly, duplex-assays were conducted in a Roche LighCycler96® system. DNA extracted from feces (as described before in 3.2.5.4) was diluted in Gibco water to a final concentration of 2 ng/µl. 2.5 µl of the samples were added as duplicates in 96 well plates (Roche), mixed with 0.2 µl of respective primers (30 µM) and hydrolysis probe (25 µM), 10 µl 2x FastStart Essential DNA Probes Master (Roche) and 5.5 µl H2O (Gibco). The following cycler conditions were used: preincubation for 10 min at 95 °C, followed by 45 cycles of 15 s 95 °C and 60 s 60 °C. Fluorescence was recorded after each cycle. Standard curves using linearized plasmids containing the 16S rRNA gene sequence of the individual strains were used for absolute quantification of 16S rRNA gene copy numbers of individual strains. Data were analyzed with the LightCycler96® software package (Roche).

3.2.6.2 qPCR targeting phages

Establishment of the qPCR for the phages was established using a similar protocol as for the bacteria and was described previously (von Strempel et al., 2023). Probe and primer design for the phages was done using the software PrimerExpress. As a template, either the phage tail fiber gene (P3, P10, P17), the phage major capsid protein gene (Str1, Str2), the phage major tail protein gene (Str6), PhageMinTail protein gene (vB_ccl) or phage holing gene (vB_cin) was used instead of the bacterial 16S rRNA gene to design probes, primers and plasmids (**Table 7**).

Designation	Sequence (5´- 3´)	Specificity	Purpose	Reference
vB_efa_Str1_std_fwd	GGCAAGAACTTATGGAACA	vB_efa_Str1 (major capsid protein)	Amplification of gene	von Strempel et al., 2023
vB_efa_Str1_std_rev	CTGGGTGTCAAAGTGATAA			
vB_efa_Str2_std_fwd	AACTTACTGGCAACTGAC	vB_efa_Str2 (major capsid protein)	Amplification of gene	von Strempel et al., 2023
vB_efa_Str1_std_rev	TACCTTTTCTTCTGGCTCT			
vB_efa_Str6_std_fwd	TTTACCTCAATGTCCACC	vB_efa_Str6 (major tail protein)	Amplification of gene	von Strempel et al., 2023

vB_efa_Str6_std_rev	TCTAGCTACATTCGTGGT			
Mt1B1_P3_fwd	GTCTGGCTTCGATTCTTT	Mt1B1_P3 (phage tail fibers protein)	Amplification of gene	von Strempel et al., 2023
Mt1B1_P3_rev	GGCTTTTCTACTTCCCTG			
Mt1B1_P10_fwd	ATCCCACCTCCTTATGCT	Mt1B1_P10 (phage tail fibers protein)	Amplification of gene	von Strempel et al., 2023
Mt1B1_P10_rev	GTACGCAAGTAACCTATCCC			
Mt1B1_P17_fwd	CTCGGTAACGTCCACACTA	Mt1B1_P17 (phage tail fibers protein)	Amplification of gene	von Strempel et al., 2023
Mt1B1_P17_rev	TCGTTGTGGCTTACCTCT			
vB_efa_Str1_fwd_qPCR	AGAAACACGTGCATTACCAGAATC	vB_efa_Str1 (major capsid protein)	qPCR	von Strempel et al., 2023
vB_efa_Str1_rev_qPCR	TCTGGGATAATTGCTGATGCAT			
vB_efa_Str1_Probe	FAM-TTTGAAGGTGTTAAGTCTG-BHQ-1			
vB_efa_Str2_fwd_qPCR	GCCCTAAACAACTACAACCATGAA	vB_efa_Str2 (major capsid protein)	qPCR	von Strempel et al., 2023
vB_efa_Str2_rev_qPCR	CTGAAGACCAGTTCTCTCCCAAA			
vB_efa_Str2_Probe	HEX-TTGGTGCAGCTTGGA-BHQ1			
vB_efa_Str6_fwd_qPCR	CGCCTCGTTGTGCTGCTA	vB_efa_Str6 (major tail protein)	qPCR	von Strempel et al., 2023
vB_efa_Str6_rev_qPCR	CGTGGTACGGCAGTATTAATCG			
vB_efa_Str6_Probe	HEX-ATCCATTCGCCAAGGTCGTTCTGTACC-BHQ1			
P3_fwd_qPCR	GTAATCTGTGCGCCAGTCGTT	Mt1B1_P3 (phage tail fibers protein)	qPCR	von Strempel et al., 2023
P3_rev_qPCR	CAGGGCAGCGCACCAT			
P3_probe	FAM-AACTGGTGCCTTCACCTCCGCAAAA-BHQ1			
P10_fwd_qPCR	GCGATCGTGTACCAAGGGATA	Mt1B1_P10 (phage tail fibers protein)	qPCR	von Strempel et al., 2023
P10_rev_qPCR	GGATATTGAGATTGCTGGCCTTA			

P10_probe	HEX-TCTGTGCGCAATACCAGAAGTCATACCTGC_BHQ1			
P17_fwd_qPCR	GCGCAGACATGTGACTTGTAAAG	Mt1B1_P17 (phage tail fibers protein)	qPCR	von Strempel et al., 2023
P17_rev_qPCR	GATAACAACGAAGGAAGAACACCAA			
P17_probe	HEX-CGCAGCCACTTCTCCGTTGGGA_BHQ1			
vB_I46_STD_fwd	ACACTGAGCGCCATAATAA	vB_cin_I46 (holin)	Amplification of gene	This study
vB_I46_STD_rev	GGTGGACTTGACGGAATA			
vB_YL32_STD_fwd	TGTGATGCTAGATGAGTGGT	vB_ccl_YL32 (tail sheat protein)	Amplification of gene	This study
vB_YL32_STD_rev	AAATCTCCACACACGGAA			
vB_ccl_YL32_fwd_qPCR2	TTTGAATTCCCACACAACCC	vB_ccl_YL32 (tail sheat protein)	qPCR	This study
vB_ccl_YL32_rev_qPCR2	CCATAGAACAGCCCACTACC			
vB_ccl_YL32_Probe2	FAM-CGTATATTAAGCATAAATACCCAGAATTATCAGGTGCAGA_BHQ1			
vB_cin_I46_fwd_qPCR1	AGGTGTCGCTAAAAAGGTAATG	vB_cin_I46 (holin)	qPCR	This study
vB_cin_I46_rev_qPCR1	TTCCTCGCTTTCTTCGTTTC			
vB_cin_I46_Probe1	HEX-CTAAGATGGGACTACCTGTGCCGCAA_BHQ1			

Table 7: Primers and probes used for phage qPCR in this study

Primers used to generate a template were chosen to amplify approximately 1000-1500 bp of the chosen gene. PCR was conducted using a Q5 polymerase for proofreading and blunt ends. After visualization of the PCR product (with Q5 polymerase) on a 1% Agarose Gel, purification was performed using the NucleoSpin Gel and PCR Clean-Up Kit. The purified Products are then eluated in NE buffer and DNA concentration is determined with the Nanodrop. For the Ligation,

1-2 µl of PCR product (appr. 75ng), 2x Reaction Buffer, 1 µl pJET1.2/blunt Cloning vector (50 ng/µl). T4 DNA Ligase and nuclease-free water (to 20µl, all products from the CloneJet PCR Cloning Kit from Thermo Scientific) were gently mixed together and incubated at room temperature for 30 min. Next, 200µl of chemocompetent DH5α are thawed on ice and 5 µl of ligation product were added, followed by an incubation on ice for 30 min. Then, the cells were heat shocked (45 sec, 37°C) and immediately put on ice for 2 min. 800 µl of LB-media was added and incubated at 37 °C for 1h (650rpm). 50 µl of the mixture was plated on LB agar plates containing Ampicillin (100 µg/ml) and colonies were picked and re-streaked for purification the next day. Several colonies were then put in liquid culture (5 ml LB + Amp, 100 µg/ml), incubated over night at 37°C and pelleted (5000xg, 15 min, 4°C). The plasmid was extracted using the Nucleospin Plasmid Mini Kit (Machery Nagel) and send for Sanger Sequencing to check for the right insert. Once at least one clone is proven to contain the right insert, it is re-streaked and a 75 ml overnight culture (LB + Amp) was prepared. The plasmid was extracted using the Plasmid Plus Midi Kit (Quiagen) and linearized with the restriction enzyme NotI that cleaves the pJET1.2 backbone once (30 µg of plasmid, 2 µl NotI (Fermentas), 10µl buffer (Fermentas), Water up to 100 µl, overnight 37 °C). The linearized plasmids were cleaned up with the NucleoSpin Gel and PCR clean up kit and diluted to concentrations between 10^8-10^0 gene copies/ml. Absolute quantification was conducted as for the bacterial qPCR (Brugiroux et al., 2016).

3.2.7 Lipocalin-2 quantification

Lipocalin-2 levels in feces and cecal content were determined by an enzyme-linked immunosorbent assay (ELISA) kit and protocol from R&D Systems (DY1857, Minneapolis, US), following manufacturer's instructions as described before (von Strempel et al., 2023). Briefly, first the ELISA 96-well plates are coated with the capture antibody (rat α mouse lipocalin-2/NGAL capture mab) overnight at 4°C. The next day, the plates are washed with wash buffer (0.05% Tween-20 in PBS) three times followed by incubation with blocking buffer (2%BSA inPBS) for 1h at RT. Plates were washed again three times before the standards and samples were added. For this, a standard dilution in blocking buffer was prepared (40 ng/ml starting concentration) and 50µl was added per well. The feces were first dissolved in 500µl PBS and then added in several dilutions, also 50 µl per well. After the samples and the standards are added, the plate was incubated for 1 h at RT, followed by another washing step with wash

buffer, this time six times. Then, detection antibody was added (rat α mouse lipocalin-2/NGAL detection mab biotinylated), incubated for 1h at RT, washed six times, followed by addition of streptavidin-HRP. After another incubation for 1h at RT and another wash step, the samples were developed with substrate (1 mg ABTS + 10 ml substrate buffer and 5 µl H2O2) for 30-45 min at RT and the absorbance in E405 is measured using a plate reader.

3.2.8 Hematoxylin and eosin staining (HE staining) and histopathological scoring

HE staining was performed as described previously (Eberl et al., 2021; Herp et al., 2019; von Strempel et al., 2023). Cecal tissue, which was immediately frozen in O.C.T, was sliced into 5 µm sections using a cryotome (Leica) and positioned onto Superfrost Plus glass slides (Hartenstein). The sections were left to dry overnight and then treated with Wollman solution (95 % ethanol, 5 % acetic acid) for fixation for 30 seconds, followed by rinsing in running tap water (1 minute) and a final rinse in dH2O. Subsequently, the slides were exposed to Vectors's Hämalaun (Roth) for 20 minutes, washed in running tap water (5 minutes), immersed in de-staining solution (70 % ethanol with 1 % HCl) once, washed again in running tap water (5 minutes), and finally rinsed in dH2O with subsequent rinses in 70 % and 90 % ethanol. The slides were briefly dipped for 15 seconds in alcoholic eosin (90 % ethanol) with Phloxin (Sigma-Aldrich), rinsed in dH2O, and dehydrated successively in 90 % ethanol, 100 % ethanol, and xylene. The sections were directly mounted with Rotimount (Roth) and left to dry completely.

Histopathological scoring of cecal tissue was performed as described previously (Stecher et al., 2007; von Strempel et al., 2023). "Submucosal edema (0-3), infiltration of polymorphonuclear neutrophils (PMNs) (0-4), loss of goblet cells (0-3) and epithelial damage (0-3) was evaluated and all individual scores were summed up to give a final pathology score: 0-3 no inflammation; 4-8 mild inflammation; 9-13 profound inflammation."

3.2.9 Phylogenetic trees

3.2.9.1 Generation of a 16S rRNA gene-based phylogenetic tree for the OMM^{14} consortium

The genomes of the twelve strains of the OMM^{12} consortium (Garzetti et al., 2017) were accessed via DDBJ/ENA/GenBank using the following accession numbers: CP022712.1, NHMR02000001-NHMR02000002, CP021422.1, CP021421.1, NHMQ01000001-NHMQ01000005, NHTR01000001-NHTR01000016, CP021420.1, NHMP01000001-NHMP01000020, CP022722.1, NHMU01000001-NHMU01000019, NHMT01000001-NHMT01000003, CP022713.1, CP028714, KR364761.1 and annotated using Prokka (default settings) (Seeman, 2014). The 16S rRNA sequences of all strains were obtained. Using these sequences, the phylogenetic tree was prepared as followed (von Strempel et al., 2023): ”These rRNA FASTA sequences were uploaded to the SINA Aligner v1.2.11 (Pruesse, Peplies, & Glockner, 2012) to align these sequences with minimum 95% identity against the SILVA database. By this, a phylogenetic tree based on RAxML, GTR Model and Gamma rate model for likelihood was reconstructed. Sequences with less than 90% identity were rejected. The obtained tree was rooted using *midpoint.root()* in the phytools package (Revell, 2012) in R and visualized using iTOL online (Letunic & Bork, 2007).”

3.2.9.2 Generation of a genome-based tree for different *Enterococcus* strains

As described before (von Strempel et al., 2023), the genomes of all *Enterococcus* strains that were tested in this study regarding the host range of the phages and selected reference type strains of the family *Enterococcaceae*, were accessed via DDBJ/ENA/GenBank using the following accession numbers: PRJEB50452, GCA_002221625.2, JABAFU000000000, VUMK00000000, VUML00000000. A Maximum Likelihood tree was constructed with PhyloPhlAn 3.0 (Asnicar et al., 2020). The tree was exported in Newick tree format and annotation was done using iTOL online (Letunic & Bork, 2007).

3.2.10 Statistical analysis

Statistical details for each experiment are indicated in the figure legends and was performed as described before (von Strempel et al., 2023): “Mann-Whitney U test and Kruskal-Wallis test were performed using the software GraphPad Prism version 5.01 for Windows (GraphPad

Software, La Jolla California USA, www.graphpad.com). P values of less than 0.05 were considered as statistically significant and only those are indicated in the figures (*P<0.05, **P<0.01, ***P<0.001).”

3.2.11 Data analysis and Figures

The data generated in this thesis was analyzed and plotted using GraphPad Prism (Version 9.5.1). Or plotted with Microsoft Excel (Version 1808). Figures were partly generated using BioRender (https://biorender.com) if indicated in the figure legends. Affinity Designer (Version 1.10.4.1198). was used to build the final figures using the graphs made in GraphPad Prism (von Strempel et al., 2023).

4. Results

4.1 Workflow

The experimental setups used for isolation, characterization and functional studies of phages can be described as followed.

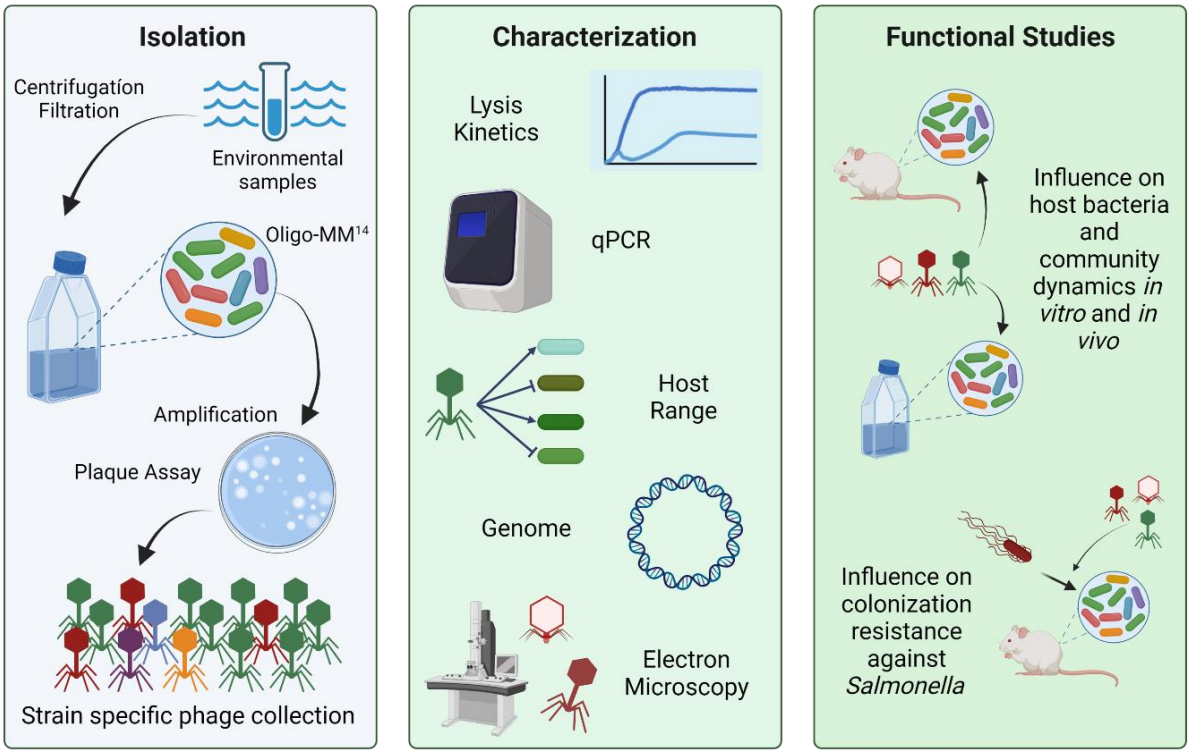

Fig 5: Workflow for isolating and characterizing bacteriophages targeting members of the OMM[14] community

The workflow can be separated into three different steps. First, the isolation of phages specifically targeting members of the OMM[14]. Second, characterization of the phages, followed by functional studies aiming to investigate the influence of phages on their hosts and the community *in vitro* and *in vivo*.

Figure created with Biorender.

First, isolation of phages was done as shown. Sewage water samples were centrifuged and filtered to get rid of dirt and bacteria and then mixed with a bacterial monoculture. If virulent phages specific for this bacterial strain were present in the sewage water sample, they amplified by lysis of the bacteria. After overnight incubation, this culture was filtered again to get rid of

any bacteria, and the presence of phages was checked by spot assays on a lawn of the respective bacteria. Phages would then be visible as clear plaques which indicates lysis of the bacteria. After isolation, phages were characterized regarding their lysis behavior in single culture, their host range and their morphology via electron microscopy. Further, genome analysis was done and a phage specific qPCR was established. Next, their impact on community structure, dynamics and function was evaluated in a more complex setup *in vitro* and in the mouse gut *in vivo*.

4.2 Isolation and characterization of virulent phages targeting bacteria of a synthetic bacterial community

4.2.1 Isolation and characterization of phages targeting *E. coli* Mt1B1

To target *E. coli* Mt1B1, I chose three virulent phages: Mt1B1_P3, Mt1B1_P10 and Mt1B1_P17 (short: P3, P10 and P17). These phages have been previously isolated from sewage water and characterized and found to target and coexist with their host strain in gnotobiotic OMM^{12} mice (Lourenco et al., 2020), which makes them great tools to use for this study. The phages exhibit different plaque morphologies when spotted on a lawn of their host. P3 forms big plaques with a light halo around, whilst phage P10 forms smaller plaques but with the same halo around. P17 however forms very small plaques which are almost not visible. This already shows how different the lysis behavior of the phages is (**Fig 6**).

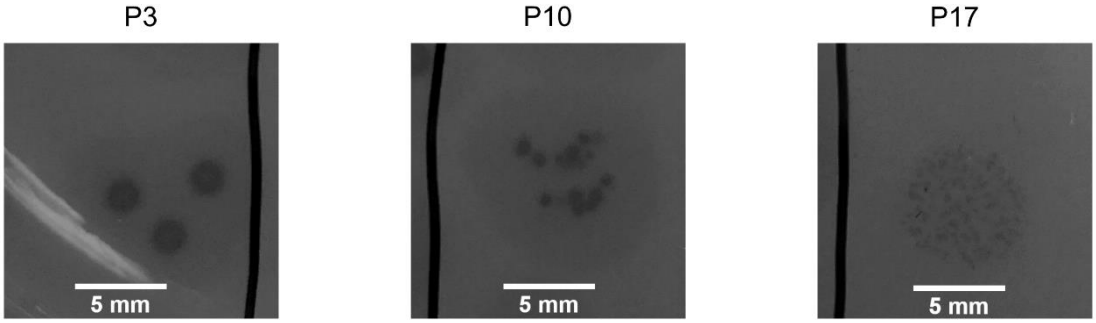

Fig 6: Plaque morphology of phages P3, P10 and P17

Plaque morphology of the three phages targeting *E. coli* Mt1B1. Phage lysates were spotted in serial dilutions on a lawn of *E. coli* and incubated overnight. Bacterial lysis by phages can be detected as clear spots in the bacterial lawn.

To get a better understanding of the genomic features, genome sequencing of all the isolated phages was performed. Taxonomic analysis by mapping the genome against existing datasets showed that P3 and P10 are podoviruses and belong to the genus *Teseptimavirus* and *Zindervirus*, respectively, whereas P17 shows characteristic features of a myovirus (**Table 8**, (Lourenco et al., 2020; von Strempel et al., 2023).

For P3, more than half of the genome is annotated with genes encoding proteins of known function. Most genes which encode proteins with known functions are classified to DNA and RNA metabolism, but also into structural proteins with head and packaging functions **(Fig 7A).** For P10, similar results can be seen (**Fig 7B**). P17 has the biggest genome of the *E. coli* phages, with over 150 kb, and has over 90% genes encoding proteins of unknown function (**Table 8**). The rest of the genes is mostly predicted to be involved in DNA and RNA metabolism and tail proteins (**Fig 7C**). All phages encode proteins related to lysis like holins or endolysins, which is consistent with their virulent behavior we observe.

Phage	**P3**	**P10**	**P17**	**Str1**	**Str2**	**Str6**
Host strain	*E. coli* Mt1B1	*E. coli* Mt1B1	*E. coli* Mt1B1	*E.faecalis* KB1	*E.faecalis* KB1	*E.faecalis* KB1
Family	*Podoviridae*	*Podoviridae*	*Myoviridae*	*Siphoviridae*	*Podoviridae*	*Siphoviridae*
Genus	*Teseptimavirus*	*Zindervirus*	unclassified	*Efquatrovirus*	*Saphexavirus*	*Copernicusvirus*
Genome size (kb)	40.3	45.4	151.2	41.6	18.1	57.7
Number of predicted OFRs	47	54	284	19	11	22
Genes unknown function (%)	40.4	64.3	94.7	72	59	74

Table 8: Characteristics of phages isolated in this study (modified from von Strempel et al., 2023)

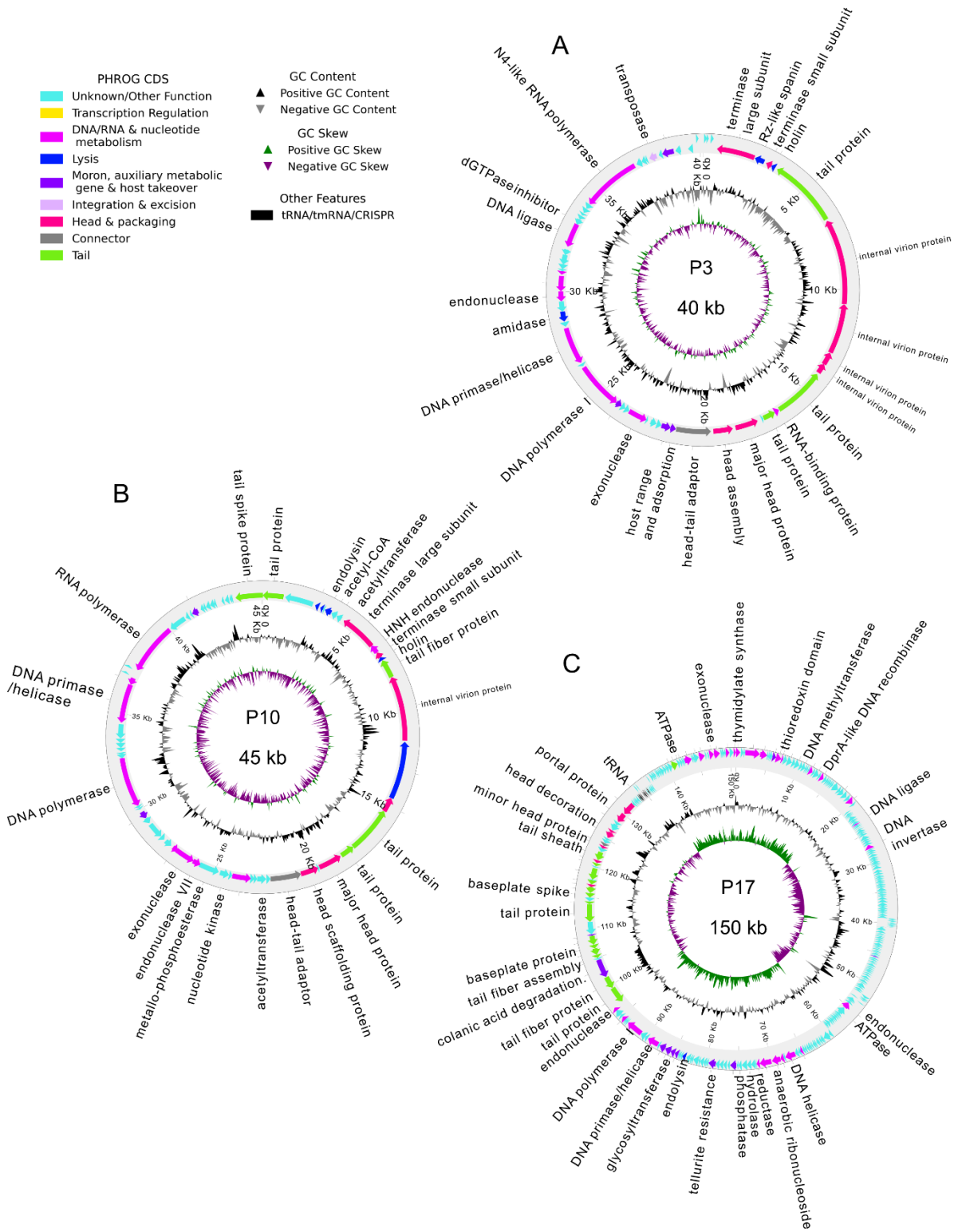

Fig 7: Genomes of phages P3, P10 and P17

Annotated genomes of phages targeting *E. coli* Mt1B1. (A) P3, (B) P10 and (C) P17. Turquoise color indicates genes encoding proteins with unknown functions, other colors indicate genes that encode proteins with known functions (see legend for further information).

To detect relationships to other phages that were already isolated, a contact analysis using vVonTACT v2.0 was conducted, which is using existing viral databases (NCBI) for taxonomic assignment and clustering. In the VirContact analysis, all *E. coli* phages isolated in this study (marked in pink) are part of big clusters of phages but don't cluster together in the same one (**Fig 8**) showing that their genomic features are not very similar. For P3, most phages that are in the same cluster target other *E. coli* strains, as well as *Pseudomonas* spp. (**Fig 8A**). For P10 this is also the case, but the overall cluster contains less phages (**Fig 8B**). P17 is almost only clustering together with other *E. coli* phages, as well as with some *Salmonella* and *Klebsiella* phages (**Fig 8C**).

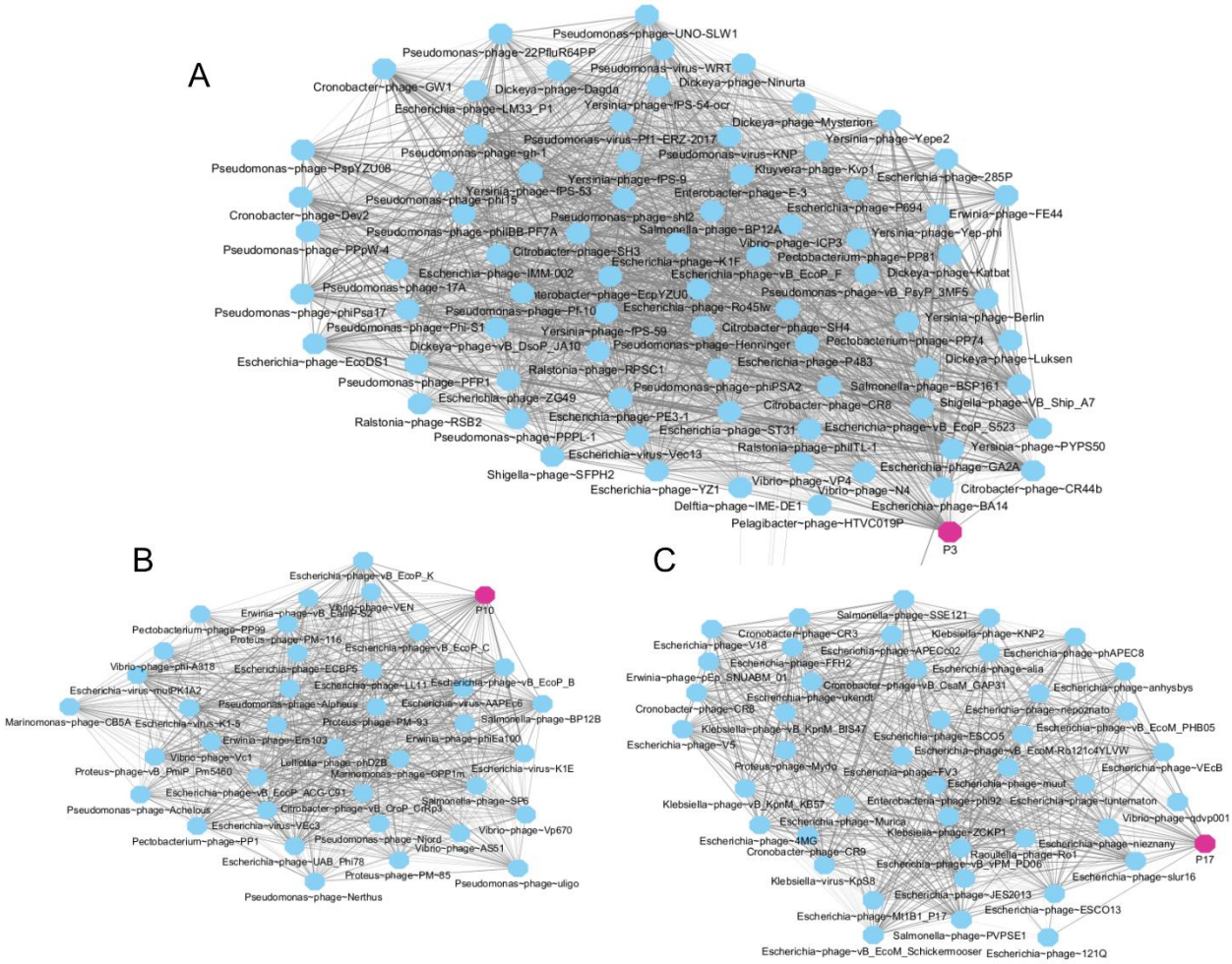

Fig 8: Clustering of phages P3, P10 and P17

VirCluster of phages targeting *E. coli* Mt1B1 (marked in pink). (A) P3, (B) P10 and (C) P17. Clusters were formed by a contact analysis using vConTACT v2.0. Phage genomes from NCBI marked in blue.

Next, phages were characterized regarding their impact on growth of *E. coli* in liquid culture. For this, phages were added to a liquid culture of *E. coli* in early stationary phase and growth was measured under anaerobic conditions in a plate reader. Consistent with Lourenco et al., I could show that each of the three phages individually reduced the growth of *E. coli* Mt1B1 in liquid culture *in vitro,* showing the strongest inhibition when added together (**Fig 9A**). For all phages, the lysis of bacteria became apparent within 30 minutes after treatment, resulting in a significant decrease in bacterial density. For P3 and P10, *E. coli* recovered after approximately one hour and shows an increase in growth which results in a lower OD than the control. For phage P17 and all three phages combined, the bacterial growth is strongly decreased for around 8 hours and only then followed by an up growth of *E. coli*. The phages added as a cocktail show the strongest initial growth inhibition, but after 10h the growth curve recapitulates the effect of phage P17 alone (von Strempel et al., 2023).

In a previous study, I tested the host range of the individual phages against several different *E. coli* strains (Afrizal Afrizal, 2022) (**Fig 9B**). For this, undiluted phage lysates of phages P3, P10 and P17 were added to a lawn of the respective strain and if a strain was susceptible, lysis was observed on plate. The results showed, that P17 exhibited the broadest host range, lysing 17 out of 19 tested strains, whereas the host range of P3 and P10 was narrow. Surprisingly, these two phages were only able to lyse the same strains. They exhibited a very similar lysis curve on *E. coli* Mt1B1 (**Fig 9A**), which might hint towards the same infection mechanisms and therefore the ability to infect the same strains. Furthermore, *E. coli* isolates that were susceptible to P3 and P10 clustered closely together in the phylogenetic analysis.

A

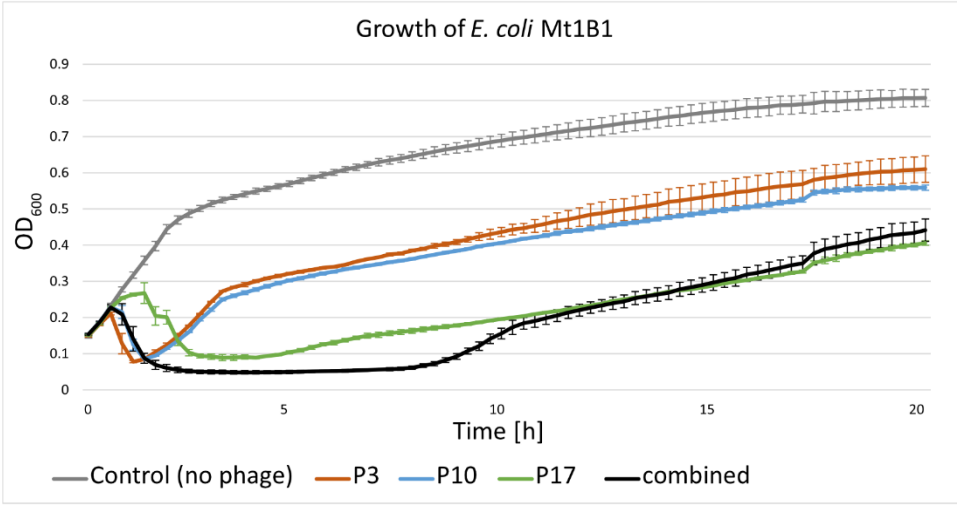

B

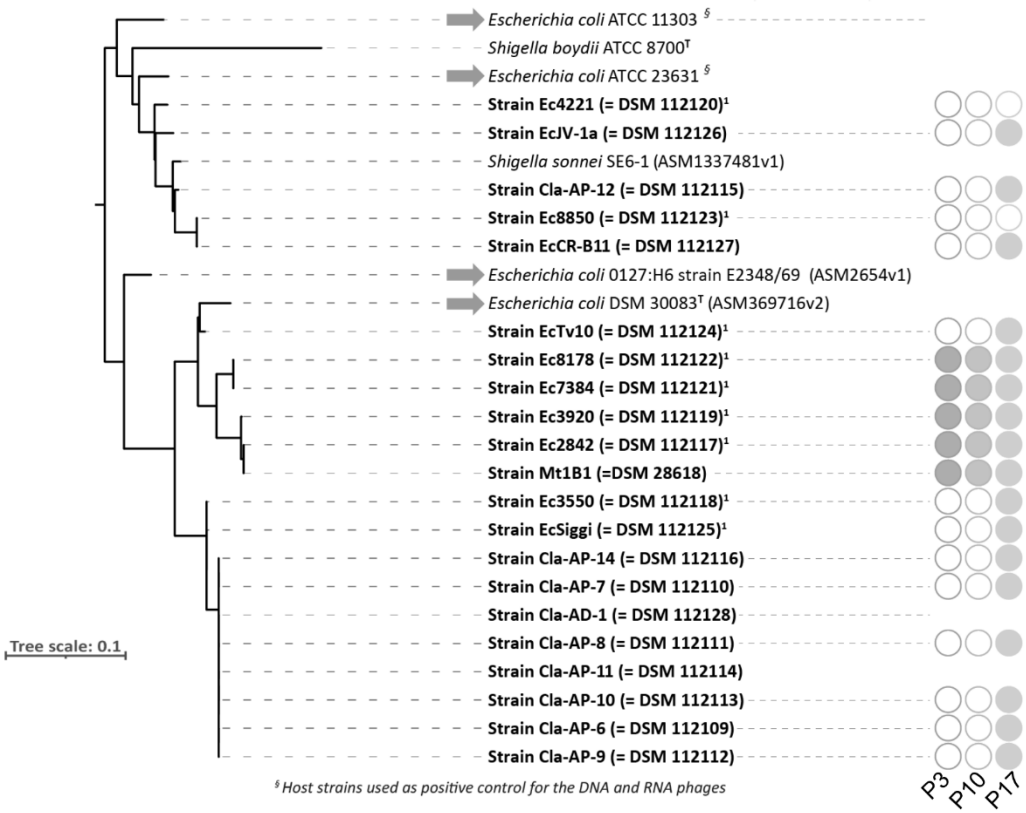

Fig 9: Growth effect and host range of phages P3, P10 and P17

(A) In grey: growth curve of *E. coli* Mt1B1 in LB medium measured under anaerobic conditions at 37°C, challenged with phage P3 (red), P10 (blue), P17 (green) and all three phages combined (black). Colored lines indicate median, error bars show standard deviation. (B) Host range of phage P3, P10 and P17 on different *E. coli* isolates, filled circle indicate observed lysis in spot assays, empty circles indicate resistance.

Figures and figure legend modified from von Strempel et al., 2023 (A) and Afrizal et al., 2023 (B).

4.2.2 Isolation and characterization of phages targeting *E. faecalis* KB1

Further, three phages targeting *E. faecalis* KB1 (DSM 32036) were isolated from different sewage water sources: vB_EfaS_Strempel1 (short: Str1, DSM 110103), vB_EfaP_Strempel2 (Str2, DSM 110104), vB_EfaS_Strempel6 (Str6, DSM 110108) (von Strempel et al., 2023). Spotted on a lawn of *E. faecalis*, different plaque morphologies can be detected (**Fig 10**). While Str1 and Str6 form clear plaques, phage Str2 exhibits bigger, turbid plaques. Further, Str1 and Str2 were successfully displayed using electron microscopy (EM), showing a long tail and a big capsule for Str1, which are characteristics of siphoviruses, whilst Str2 has no tail and a smaller head capsule, characteristic for podoviruses. Unfortunately, it was not possible to visualize Str6 in the EM.

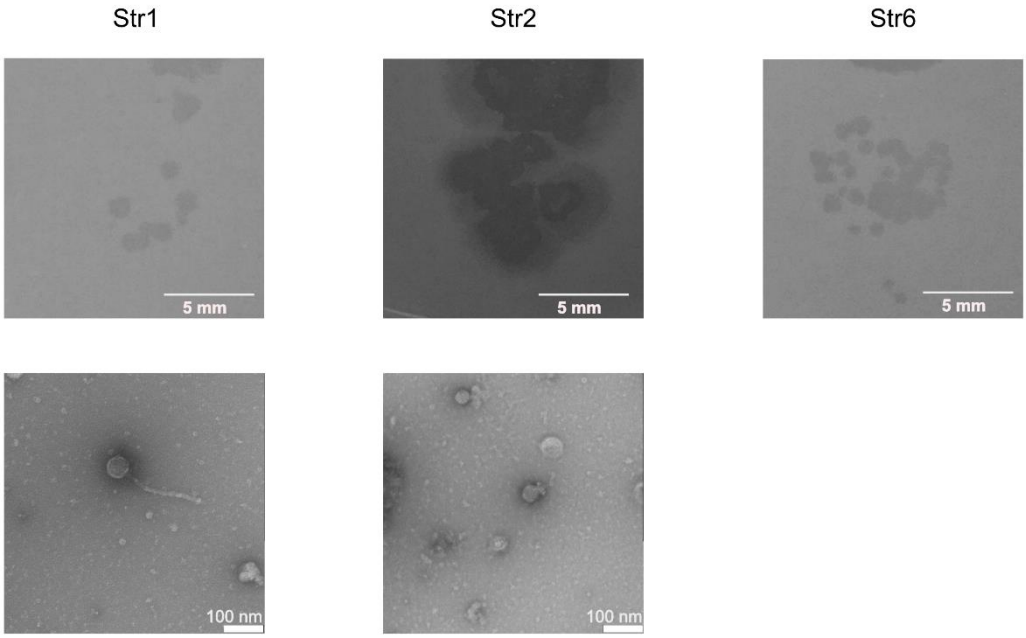

Fig 10: Plaque morphology and electron microscopy of phages Str1, Str2 and Str6

Plaque morphology of the three phages targeting *E. faecalis* KB1. Phage lysates were spotted on a lawn of *E. faecalis* and incubated overnight. Bacterial lysis by phages can be detected as clear spots in the bacterial lawn. Pictures below were done using electron microscopy.

As done with the phages targeting *E. coli*, these phages were also genome sequenced to understand their genomic features. By blasting to existing databases (NCBI), we could show that Str2 is a podovirus and belongs to the *Copernicusvirus* genus whilst Str1 and Str6 are members of the genus *Efquatrovirus* and *Saphexavirus*, respectively, and show characteristic features of siphoviruses (**Table 8**) (von Strempel et al., 2023). There are 68 putative ORFs predicted by PROKKA for Str1, with 72% of unknown function (genome size 42 kb) (**Table 8, Fig 11A**). For Str2, having the smallest genome of the three phages with 18 kb, 59% of the putative 27 genes encode for proteins of unknown function and Str6, the phage with the biggest genome of 58 kb, has 95 genes of which 74% encode for proteins of unknown function (**Table 8**). The genes which could be annotated to encode proteins with known functions can be categorized into several functional modules, including phage replication, DNA and RNA metabolism, lysis and phage structural protein (**Figure 11).** All three phages carry genes encoding for head and tail proteins and phage Str1 and Str2 carry a gene encoding for holin, a protein involved in degrading bacterial cell walls at the end of the lytic cycle. The genomes of Str2 and Str6 encode for a DNA polymerase, a function which is not annotated in the genome of Str1 **(Fig 11BC).**

Again, a VirCluster analysis was done to detect relations between the phages. This showed, that the clusters for all *E. faecalis* phages contained less phages then for the *E. coli* phages (**Fig 12**), indicating that there are less phages targeting *E. faecalis* in the existing data bases. Especially phage Str6 only clustered together with 16 other phages, of which 3 were also isolated in our lab on the same bacterial host (marked in orange, not published) (**Fig 12C**). The cluster of Str1 was larger but consists almost exclusively of other *Enterococcus* phages and three *Staphylococcus* phages (**Fig 12A**). Similar results were seen for phage Str2, which clustered in the biggest network but is also only connected to other *Enterococcu*s and *Staphylococcus* phages (**Fig 12B**). Of note, all three clusters include several phages that were isolated in our laboratory for a different study (marked also in orange) on the same host strain *E. faecalis* KB1, but almost 4 years apart from sewage water sources from different of Germany.

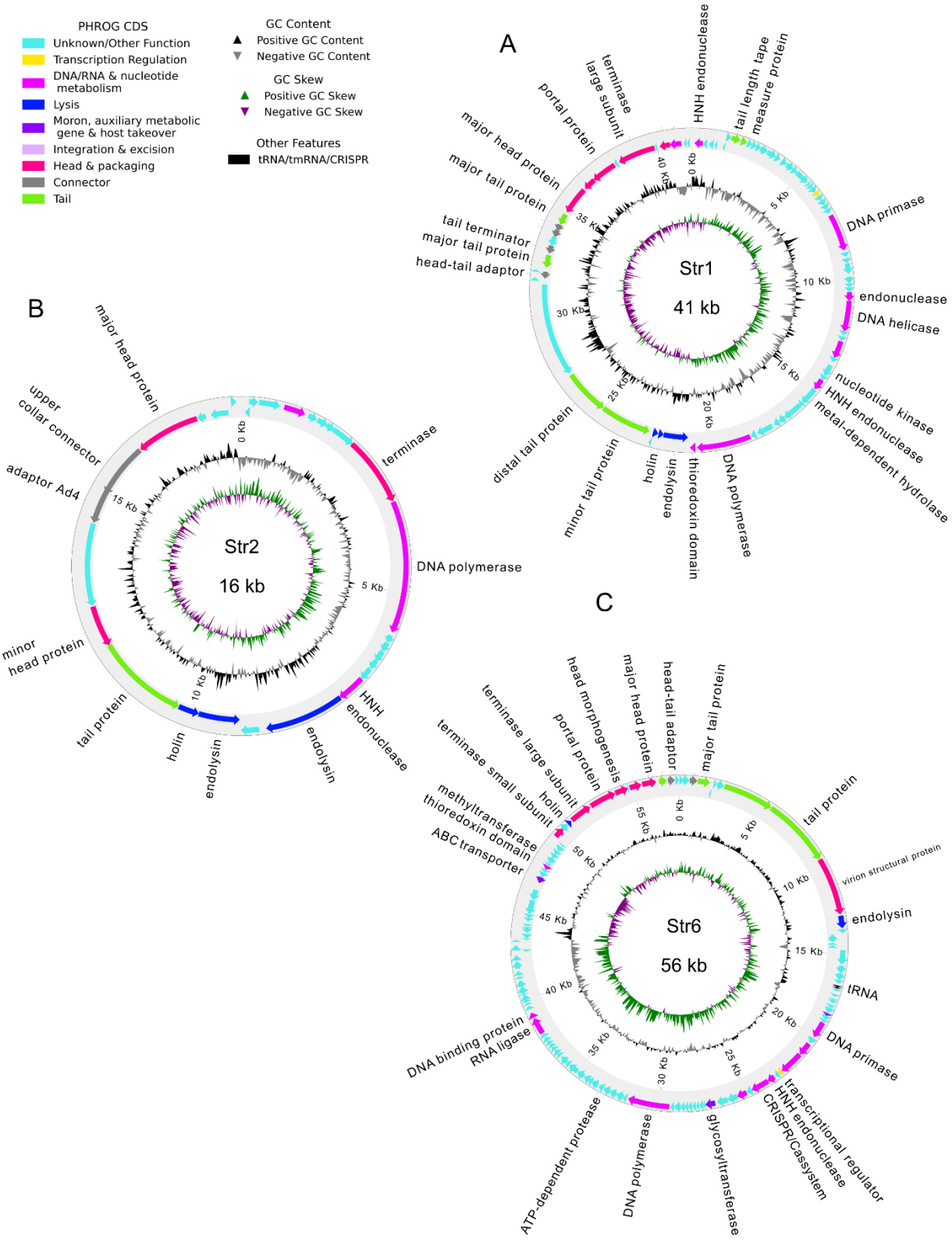

Fig 11: Genomes of phages Str1, Str2 and Str6

Annotated genomes of phages targeting *E. faecalis* KB1). (A) Str1, (B) Str2 and (C) Str6. Turquoise color indicates genes encoding proteins with unknown functions, other colors indicate genes that encode proteins with known functions (see legend for further information).

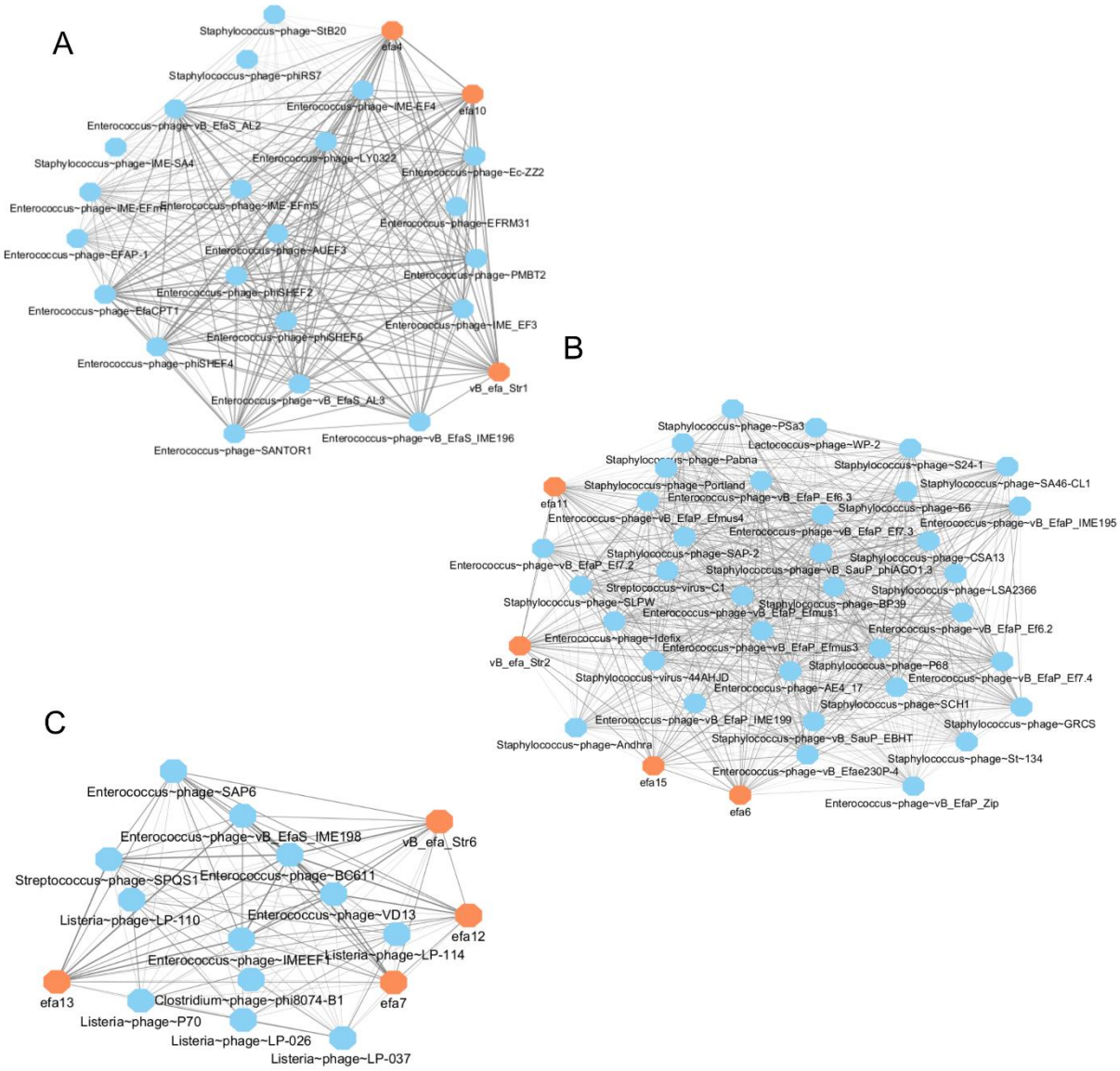

Fig 12: Clustering of phages Str1, Str2 and Str6

VirCluster of phages targeting *E. faecalis* KB1 (marked in orange). (A) Str1, (B) Str2 and (C) Str6. Clusters were formed by a contact analysis using vConTACT v2.0. Phage genomes from NCBI marked in blue, other phages isolated in our lab also marked in orange.

Next, theses phages were also characterized regarding their impact on the growth of *E. faecalis* KB1 in liquid culture. For this, phages were added to an early exponential culture of *E. faecalis* and growth was measured under anaerobic conditions using a plate reader. All three phages inhibited *E. faecalis* KB1 growth with different lysis profiles in liquid culture. Str1, Str2 and all three phages together showed a strong lysis after 30 min whereas phage Str6 exhibited lysis a bit later but was then depleting bacterial growth for almost 15 hours. In all treatments except for Str2 alone, the growth of *E. faecalis* is strongly reduced until 7 hours after phage treatment

or even longer for Str6, followed by an up growth of *E. faecalis* to different degrees. All three phages added together mostly recapitulate the lysis profile of Str1 (**Fig13B**). These results suggest, that in our case the phage cocktail might not be more efficient in reducing bacterial loads, but resemble the lysis patterns of the most efficient phage in the cocktail (von Strempel et al., 2023).

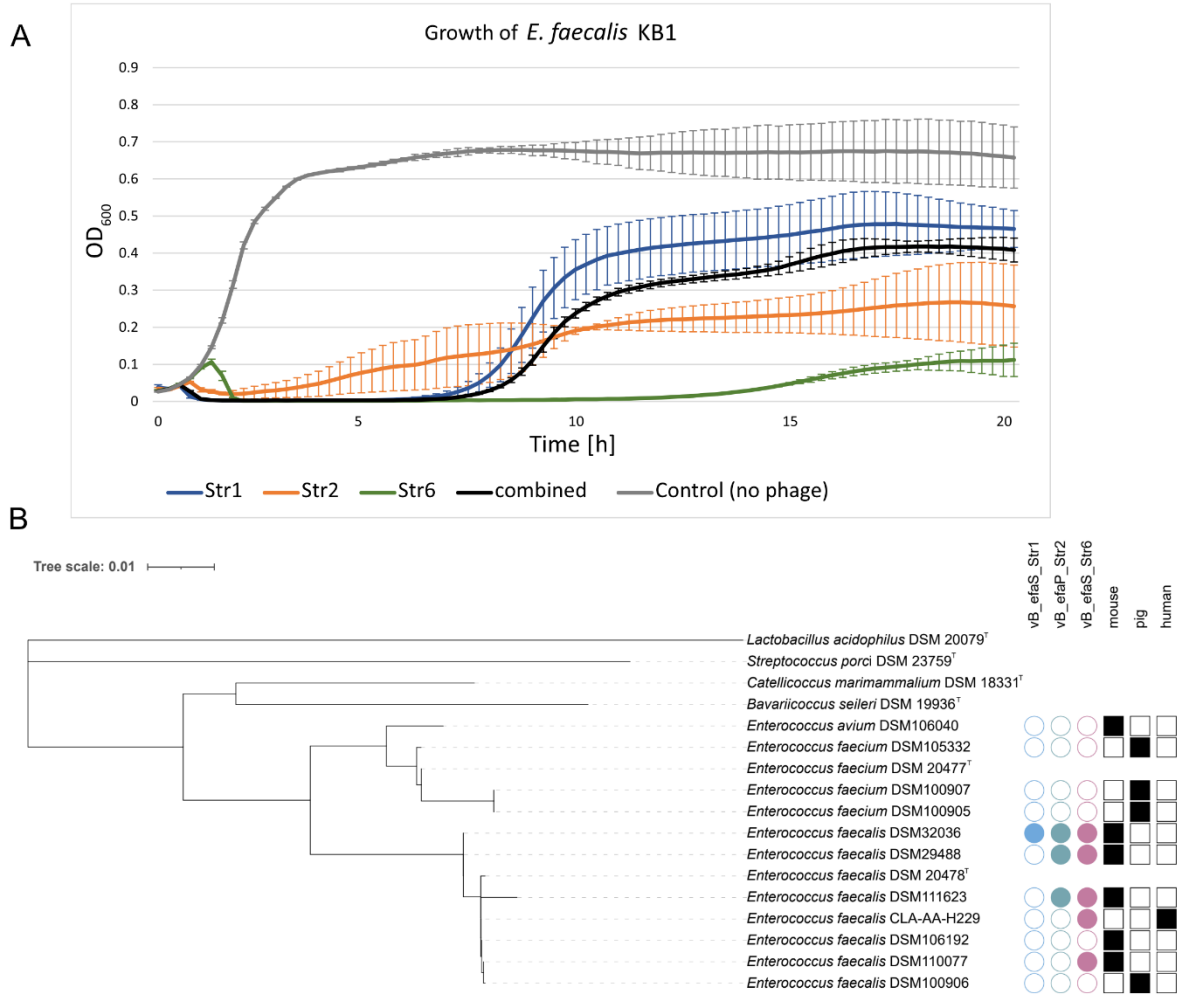

Fig 13: Growth effect and host range of phages Str1, Str2 and Str6

(A) Growth curve of *E. faecalis* KB1 in BHI medium (grey) measured under anaerobic conditions at 37°C, challenged with phage Str1 (blue), Str2 (orange), Str6 (green) and all three phages combined (black). Colored lines indicate median, error bars show standard deviation. (B) Host range of phages Str1, Str2 and Str6 on different *E. faecalis* and *E. faecium* isolates, displayed as a family tree of the bacteria. Filled circles stand for susceptibility on plate, empty circles stand for resistance. Boxes indicate origin of the respective isolate.

Figure and figure legend modified from von Strempel et al., 2023.

To display the host range of the phages, undiluted phage lysates were spotted on a variety of *Enterococcus faecalis* and *Enterococcus faecium* isolates and susceptibility was measured via visible lysis of the bacteria on plate. When tested against 12 *E. faecalis* and *E. faecium* strains isolated from different sources (mouse, pig and human), phage Str1 was highly strain-specific and only produced visible lysis on *E. faecalis* KB1 (**Fig13D**), the strain it was originally isolated on. In contrast, Str6 exhibited the broadest host range by targeting 5 out of 12 isolates, whereas Str2 was able to lyse 3 out of 12 isolates on plate (**Fig13D**). Further, only phage Str6 was able to inhibit growth of a bacterial isolate that was isolated from a human sample, whereas no phage was able to target the *E. faecalis* isolate originating from a pig sample (von Strempel et al., 2023). Since the three phages also exhibited different lysis patterns on *E. faecalis* KB1, this is matching with their different host ranges.

In addition, none of the six phages targeting *E. coli* and *E. faecalis* targeted the *Salmonella* strains used for the following experiments.

4.2.3 Isolation and characterization of phages targeting *E. clostridioformis* YL32 *and C. innocuum* I46

To target more bacterial members of the OMM^{14} consortium, I set out to isolate additional phages from environmental sewage samples. Two virulent phages were successfully isolated, targeting *E. clostridioformis* YL32 (vB_ccl_YL32, short vB_ccl) and *C. innocuum* I46 (vB_cin_I46, short: vB_cin). Both phages exhibited visible plaques on their bacterial hosts in spot assays on plate under anaerobic conditions (**Fig 14**). The plaque size and morphology differed between the phages. vB_ccl exhibited well visible, clear plaques on its host, whereas vB_cin produced very little plaques on plate with a slight halo around. Using electron microscopy, morphology of the phage vB_ccl revealed more about its taxonomy, showing characteristics of *Siphoviridae* by having a long tail (**Fig 14, Table 9**). For vB_cin however, no image could be obtained because of low quality of the sample.

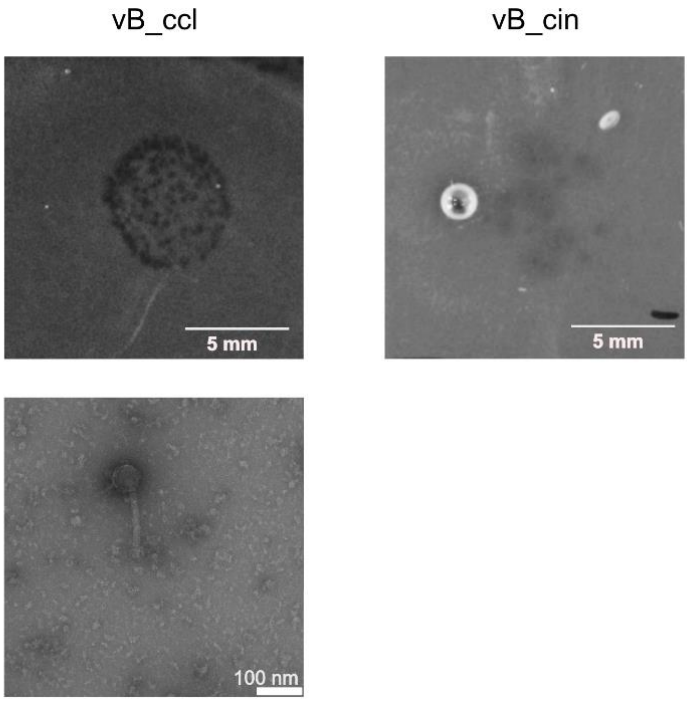

Fig 14: Plaque morphology and electron microscopy of phages vB_ccl and vB_ccl

Plaque morphology of phages targeting *E. clostridioformis* YL32 and *C. innocuum* I46. Phage lysates were spotted on a lawn of their bacterial hosts in soft agar and incubated overnight. Bacterial lysis by phages can be detected as clear spots in the bacterial lawn. Pictures below were done using electron microscopy.

Genome sequencing and assembly revealed genome sizes between 16 kb (vB_cin) and 64 kb (vB_ccl). Consequently, the number of predicted ORFs also varied, with vB_ccl having the most with 91, whilst vB_cin only had 23 predicted genes (**Table 9, Fig 15**). The number of genes encoding proteins with unknown function was high, which was to be expected from previous results from the phages targeting *E. coli* and *E. faecalis*. The annotations of the genome of vB_ccl revealed mostly phage related genes that encode for proteins like phage tail or phage capsid proteins, but also several genes that encode for DNA/RNA and nucleotide metabolism (**Fig 15A**). Further, two endolysins are encoded in the genome, which is expected for a virulent phage. For phage vB_cin, one gene encoding a DNA polymerase can be found, as well as a major head protein, one terminase and one endolysin (**Fig 15B**). Since the genome is quite small, only five genes could be annotated with known functions. Further taxonomic classification of the phages was done by blasting the genomes against existing databases (NCBI), showing that vB_ccl and vB_cin can be classified in the genus *Caudoviricetes*.

All in all, less genes than for the phages targeting *E. coli* and *E. faecalis* could be annotated with known functions, which could be due to the novelty of these phages targeting anaerobic gut bacteria.

Phage	**vB_ccl_YL32**	**vB_cin_I46**
Host strain	*E. clostridioformis* YL32	*C. innocuum* I46
Family	*Siphoviridae*	*unclassified*
Genus	*Caudoviricetes*	*Caudoviricetes*
Genome size (kb)	64	16.2
Number of predicted OFRs	91	26
Genes unknown function (%)	79	74

Table 9: Characteristics of phages targeting members of the OMM[14] isolated in this study

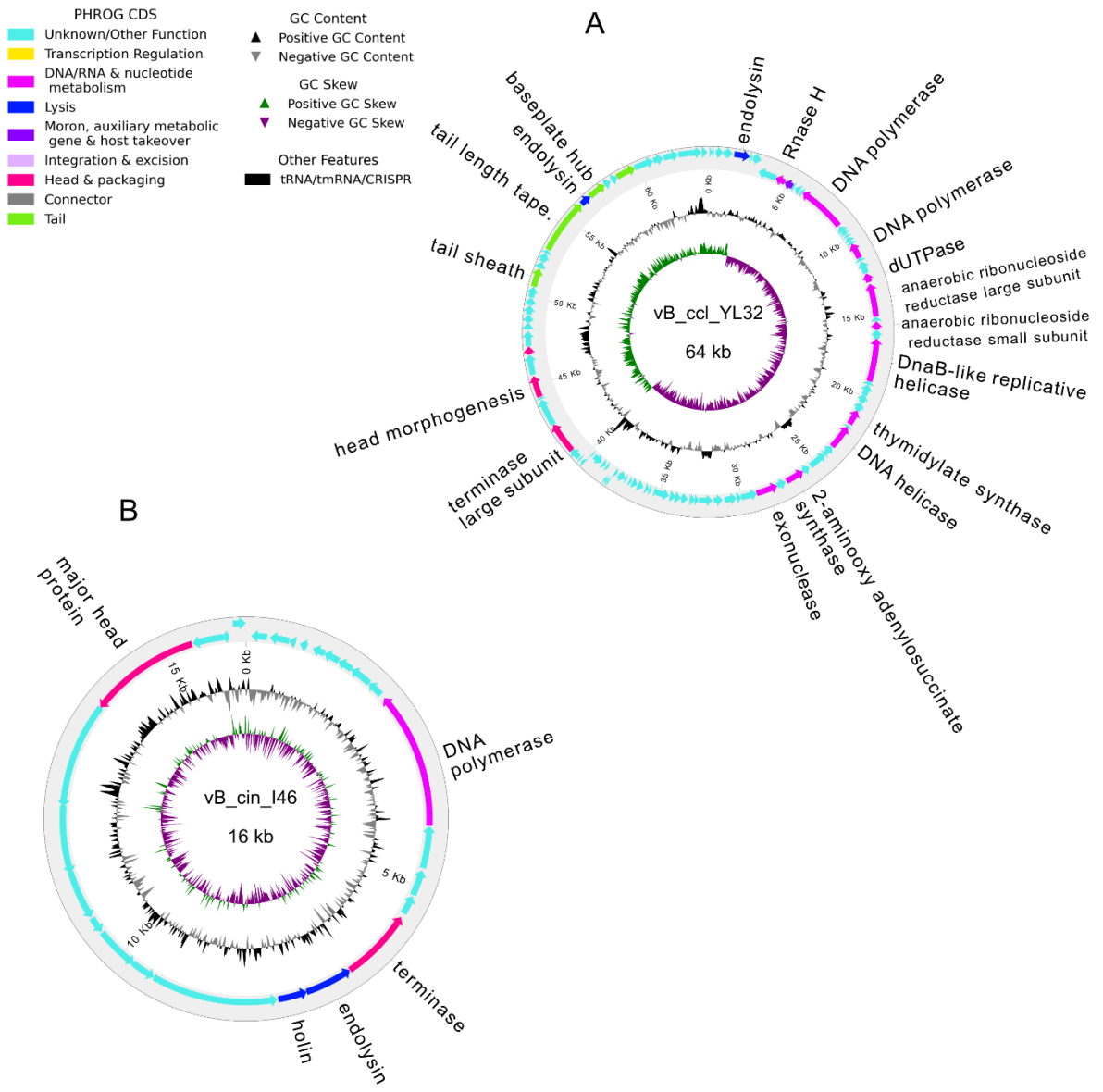

Fig 15: Genomes of phages vB_ccl and vB_cin

Annotated genomes of phages targeting (A) *E. clostridioformis* YL32 and (B) *C. innocuum* I46. Turquoise color indicates genes encoding proteins with unknown functions, other colors indicate genes that encode proteins with known functions (for further information see legend).

The VirCluster analysis could not identify any cluster for vB_ccl, hinting towards a lack of related phages in the used viral databases. Isolating phages targeting strictly anaerobic bacteria is more labor intensive and therefore the database for these phages is not as big as for aerobic lab strains like *E. coli*. Nevertheless, vB_cin is clustering in a large network, revealing the connection to mostly *Bacillus* phages (**Fig 16).**

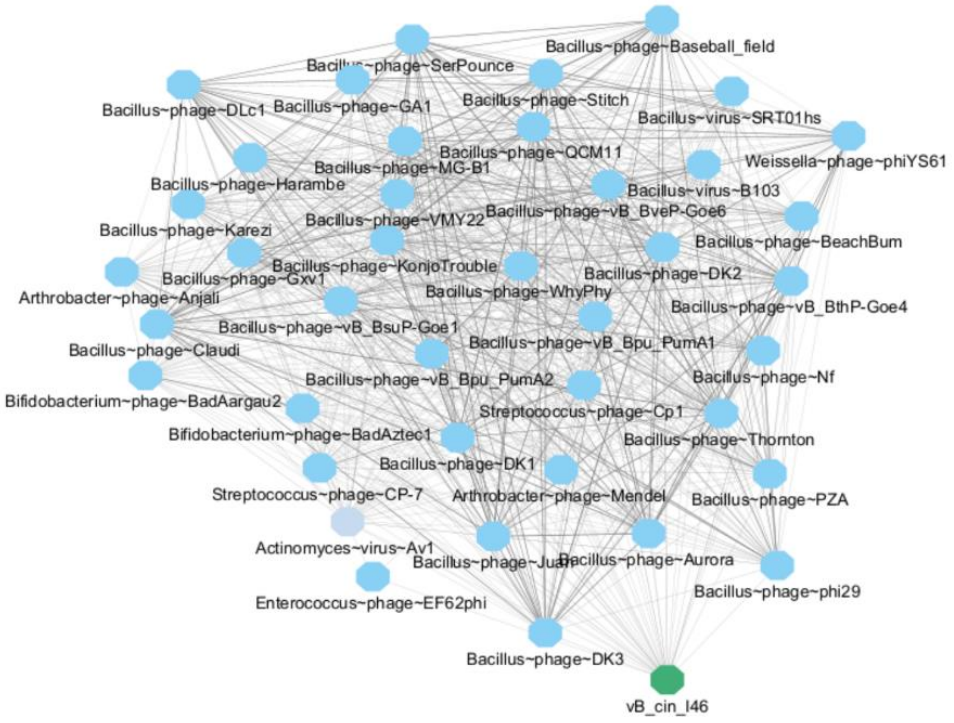

Fig 16: Clustering of phage vB_cin

VirCluster of phages targeting *C. innocuum* I46 (marked in green). Clusters were formed by a contact analysis using vConTACT v2.0. Phage genomes from NCBI marked in blue.

The effect of the phages on growth of their host bacteria was determined in liquid culture. Phage lysates were added in different concentrations to an early exponential culture of bacteria and growth was measured under anaerobic conditions using a plate reader. The phages did not exhibit a strong lysis on their bacterial hosts. *E. clostridioformis* YL32 is not affected in growth when the phage is added in low concentrations, but a slight decrease in late exponential growth can be detected when the phage is added in high numbers (**Fig 17A**). Phage vB_cin only showed an effect on its host *C. innocuum* I46 in high numbers in early stationary phase, where bacterial loads decreased in comparison to the control (**Fig 17B**), but this effect is not visible when the phage is added in lower numbers. In summary, the phages targeting the two *Clostridia* strains YL32 and I46 don't show strong lysis on their host bacteria in liquid culture, but form visible plaques on plate.

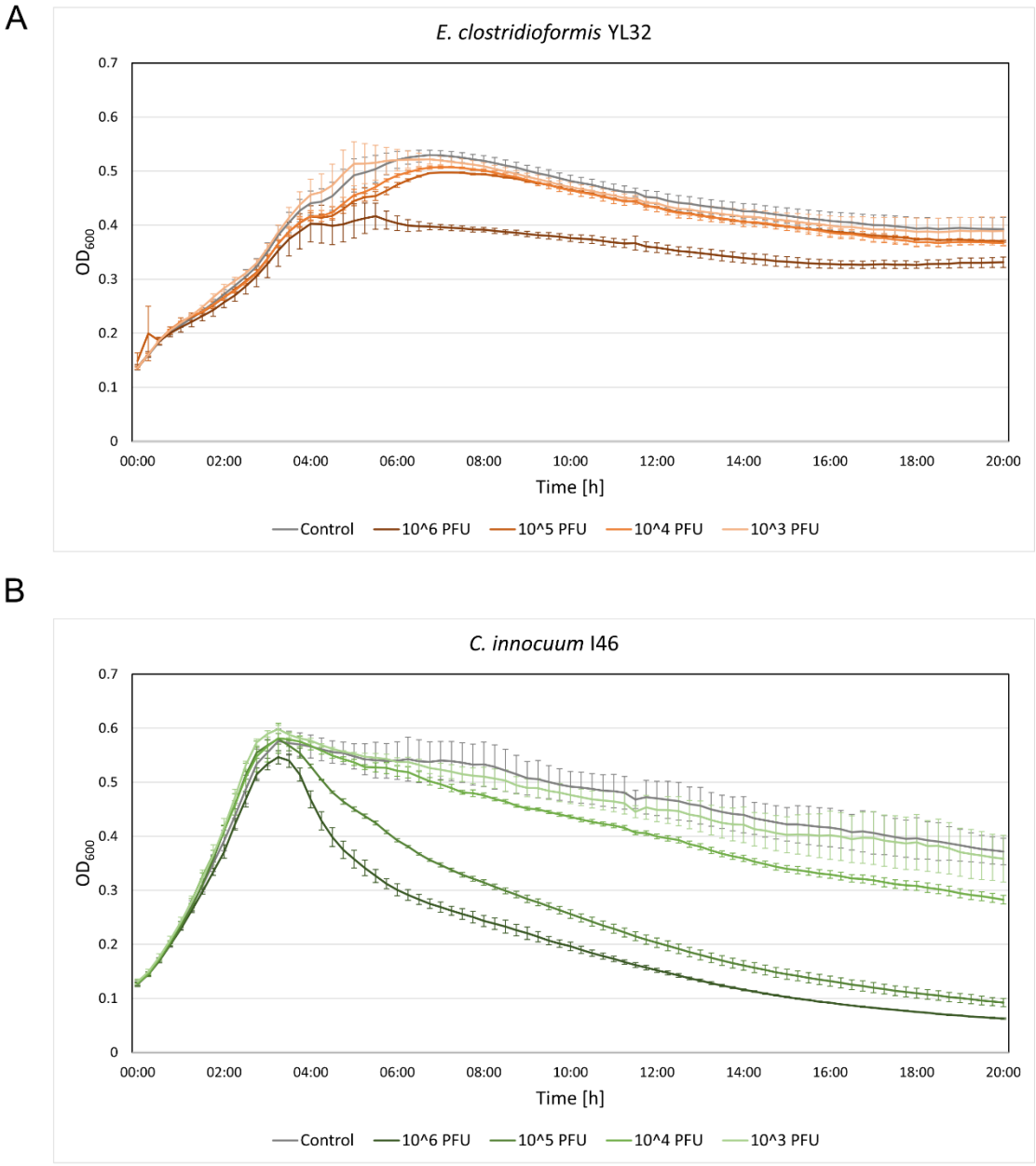

Fig 17: Growth curve of *E. clostridioformis* YL32 *and C. innocuum* I46 with phages

Growth curve of *E. clostridioformis* YL32 (A) in AF medium (grey) measured under anaerobic conditions at 37°C, challenged with phage vB_ccl in different concentrations (dark orange= highest concentration, light orange= lowest concentration). (B) Growth curve of *C. innocuum* I46 in AF medium (grey) measured under anaerobic conditions at 37°C, challenged with phage vB_cin in different concentrations (dark green= highest concentration, light green= lowest concentration). Colored lines indicate median, error bars show standard deviation.

4.2.4 Establishing a strain specific qPCR for 3Φ^{Mt1B1}, 3Φ^{KB1}, vB_ccl and vB_cin

After DNA sequencing, the annotated genomes of the phages were used to establish a strain specific qPCR to target each single phage during the experiments without the need to do spot assays. Further, distinguishing the phages by plaque morphology does not give reliable results.

The primer and probes for the bacterial qPCRs were designed using the 16s rRNA gene, since this is very conserved but still unique for each strain. Since there is no such gene for phages, other genes were used as templates which are thought to be preserved during phage infection but still unique to one phage. Annotation of the phages targeting *E. coli* revealed several phage specific genes **(Fig 7).** For all three phages, one phage tail protein was chosen, and primers were designed to amplify between 1000 and 1500 bp of the respective gene, since this is comparable to the size of a 16s rRNA gene. Primer and probes used for the qPCR were then designed on the chosen DNA fragment (**Table 7**). Phages targeting *E. faecalis* also had a few annotated phage specific genes, which were used as templates to design primer and probes (major head protein gene (Str1, Str2), tail protein gene (Str6), **Fig 11**). Although the two phages targeting *E. clostridioformis* and *C. innocuum* did not have a lot of known genes, there were still phage specific genes which were used for the qPCR. For vB_ccl, the tail sheath protein gene was chosen, and the holin gene for vB_cin (**Fig 15**). After establishing a standard dilution using pJET cloning (see methods), primer and probe combinations were tested on their efficiency and specificity. For this, a standard curve ranging between 10^8 copies/µl and 10^0 copies/µl of the respective gene was diluted in Gibco water containing yeast t-RNA (100 ng/µl) and measured in the Lightcycler (Roche). From three independent technical replicates, the efficiency was calculated using the equation $E=-1+10^{(-1/slope)}$. For the following measurements, only one standard dilution (10^3 copies/µl) was added to each plate and concentrations were calculated with the Lightcycler software using the respective efficiency for each primer/probe pair. Specificity and detection limit was tested by adding each primer and probe pair to a pool of 10^8 copies/µl standard dilutions containing all OMM^{14} members and all phages.

4.3 Impact of phages on their hosts in a synthetic bacterial community *in vitro*

4.3.1 Phages specifically target their host strains *E. coli* and *E. faecalis* without interfering the community composition

Next, we proceeded to investigate the effects of the isolated phages that target *E. coli* Mt1B1 and *E. faecalis* KB1 in the OMM^{14} community *in vitro*. To get the strongest effect on their bacterial host, the phages were not added single but together as a cocktail, with all phages present in equal numbers, resulting in two phage cocktails ($3\Phi^{Mt1B1}$ and $3\Phi^{KB1}$). The 14 community members (OMM^{14}) were added at equal ratios (OD_{600}) to anaerobic media (AF medium, (Weiss et al., 2022)) and diluted (1:100) every 24 h in batch culture for three days. 12 h after dilution, phages were added to the batch culture with a rough multiplicity of infection (MOI) of 0.01 and incubation was prolonged for three days while the batch culture was diluted every 24 h (**Fig 18A**).

A significant drop in *E. coli* CFUs was observed 36h after phage cocktails treatment, followed by an increase of *E. coli* density after 60 h almost up to levels in the control group (**Fig 18B**). The same was observed for *E. faecalis* levels after phage cocktail treatment, which dropped significantly by approximately two orders of magnitude below control levels after 36 h and resulting in a regrowth after 60 h (**Fig 18C**). All phage titers monitored by spot assays increased after 36 h, in accordance with the drop in their host bacterial populations (**Fig 18D**). Furthermore, phages were also tracked by specific qPCR since the different phages were hard to distinguish via plaque morphology. qPCR results revealed, that all three *E. coli* phages as well as *E. faecalis* phages Str1 and Str2 replicate in the batch culture environment in similar levels, whereas phage Str6 was undetectable after 60 h (**Fig 18EF**) (von Strempel et al., 2023).

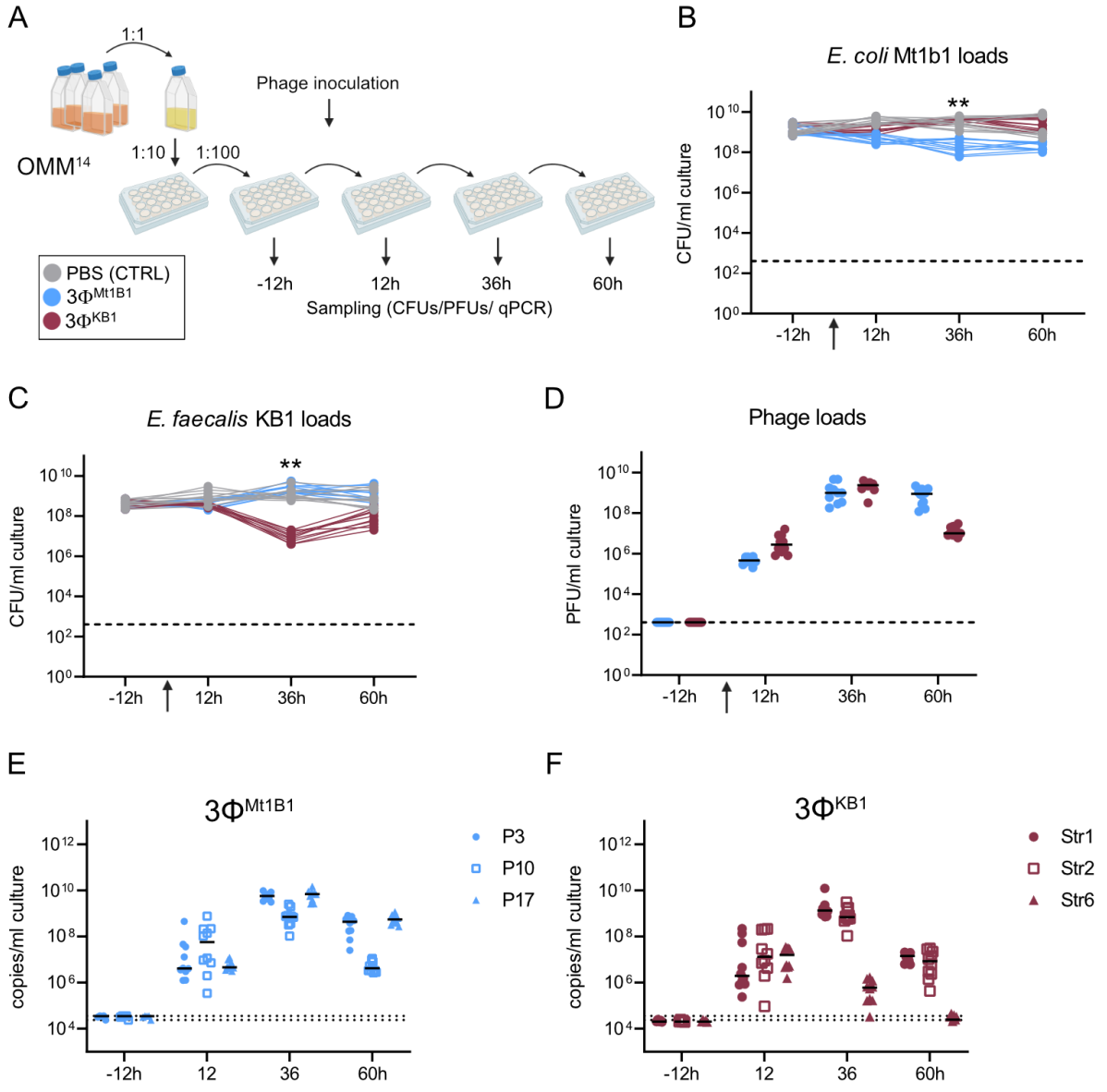

Fig. 18: Phages specifically target their hosts within a bacterial community *in vitro*

(A) Experimental setup for the batch culture. The OMM^{14} strains were first grown in monoculture, mixed at the same OD_{600} ratio and diluted every day 1:100 in AF medium. 12 hours after the third passage, phage cocktails 3Φ^{Mt1B1} or 3Φ^{KB1} were added to each well. Samples were taken for plating and qPCR before dilution. Scheme made with Biorender. (B) *E. coli* Mt1B1 and (C) *E. faecalis* KB1 loads determined by plating (Log10 CFU/ml) on agar plates containing selective antibiotics. (D) Phage loads determined via spot assays (E) Abundance of phages P3, P10 and P17 and (F) phages Str1, Str2 and Str6, determined by qPCR. Statistical analysis was performed using the Mann-Whitney Test comparing the treatment groups (N=10) against the control group (N=10) (* $p<0.05$, ** $p<0.01$, *** $p<0.001$). Each dot represents one well, black lines indicate median, dotted lines indicate detection limit (DTL). The experiment was conducted in two biological replicates with ten technical replicates in total.

Figure and figure legend modified from von Strempel et al., 2023.

The community composition was also monitored by strain specific qPCR on three time points and remained stable over three days and between the replicates (**Fig 19**). *E. coli* Mt1B1 and *Blautia coccoides* YL58 showed the highest absolute abundances as 16S rRNA copies per ml culture in the community as previously observed (Weiss et al., 2022). Three strains remained below the detection limit of the qPCR (*Bifidobacterium animalis* YL2, *Acutalibacter muris* KB18 and *Limosilactobacillus reuteri* I49) which was seen in previous experiments in our lab (Weiss et al., 2022) but all other strains were detected and showed minimal changes in their absolute abundance before and after phage treatment (**Fig19 A-C**). General fluctuations in all treatment groups are visible in the batch culture setup after 60h (**Fig19 C**), but addition of the two phage cocktails did not affect the overall composition of the OMM^{14} community members, suggesting that these phages can be used as strain-specific tools for community manipulation (von Strempel et al., 2023).

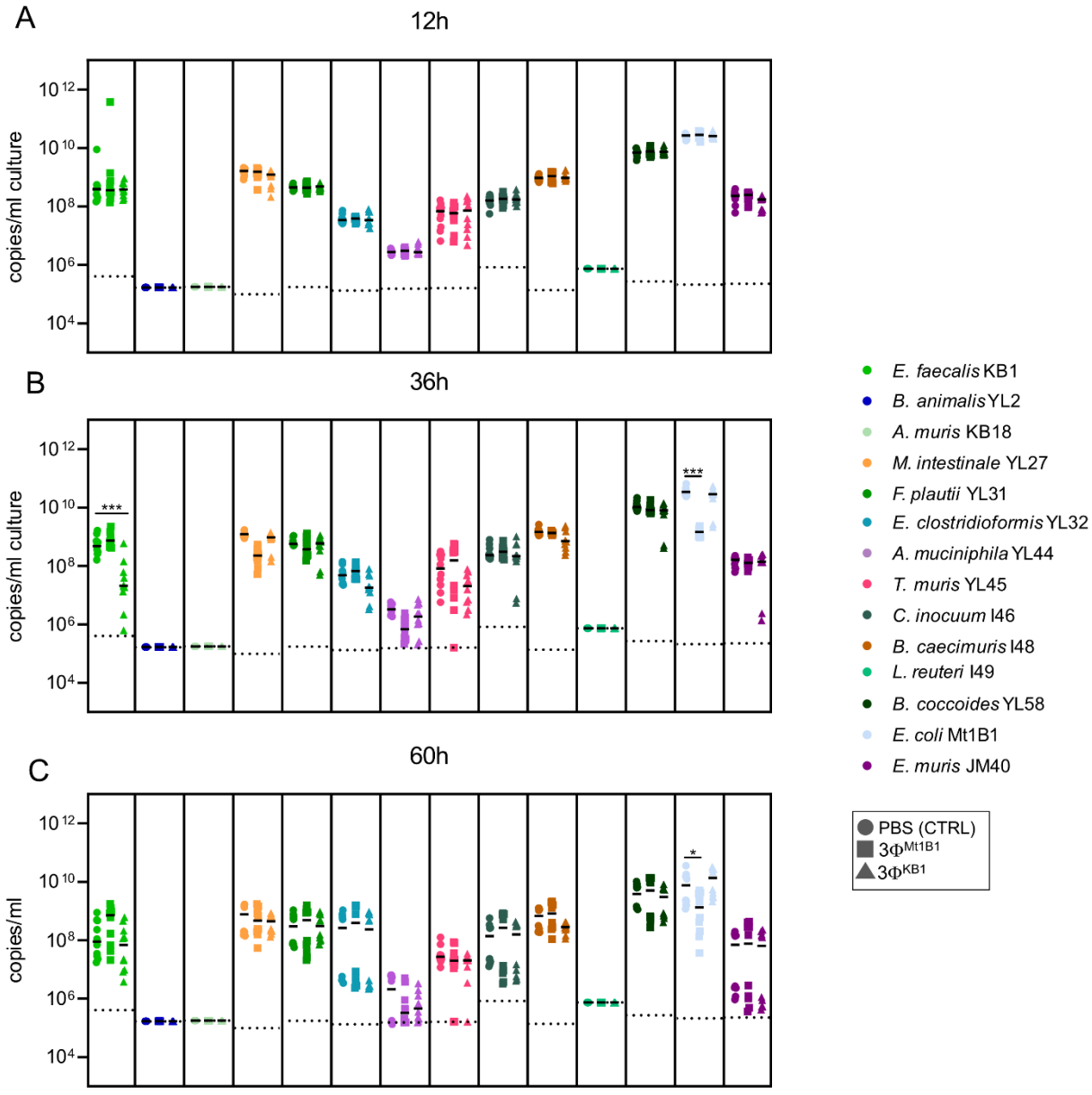

Fig. 19: Phages specifically target their hosts without changing the overall community composition

Community composition 12 h (A), 36h (B) and 60h (C) after phage addition from experiment shown in Fig.18, determined via strain-specific qPCR and absolute abundances plotted as 16S rRNA copy numbers per ml culture. Statistical analysis was performed using the Mann-Whitney Test comparing the treatment groups (N=10) against the control group (N=10) (* $p<0.05$, ** $p<0.01$, *** $p<0.001$). Each dot represents one well, black lines indicate median, dotted lines indicate detection limit (DTL)..

Figure and figure legend modified from von Strempel et al., 2023.

4.3.2 Phages specifically target their host strains *E. clostridioformis* and *C. innocuum* in a batch culture setup without interfering the community composition

After investigating the effect of the two phage cocktails targeting *E. coli* and *E. faecalis*, I also wanted to test the efficiency of the two phages vB_cin and vB_ccl on targeting their hosts in a bacterial *in vitro* community. The setup was the same as for the previous batch culture experiment. First, all 14 community members (OMM^{14}) were added at equal ratios (OD_{600}) to anaerobic media (AF medium, (Weiss et al., 2022)) and diluted (1:100) every 24 h in batch culture for three days. 12 h after dilution, phages were added to the batch culture as undiluted phage lysates (10^6 phages in 10 µl) and incubation was prolonged for three days with dilution every 24 h (**Fig 20A).** 12h after phage addition, *E. clostridioformis* shows a significant drop in abundance in the phage treatment group compared to the control group (**Fig 20B**). This drop in bacterial loads recovers within 24h and after 36h, the bacterial loads showed no significant change between the treatment groups anymore. *C. innocuum* did not show any changes in abundance in any of the treatment groups (**Fig 20C**). Nevertheless, phage vB_cin is able to stay present in the batch culture until the end of the experiment, showing that it is still able to amplify without decreasing its hosts abundance. Also, phage vB_ccl is detected via qPCR in stable loads until 60h after addition to the batch culture (**Fig 20D**).

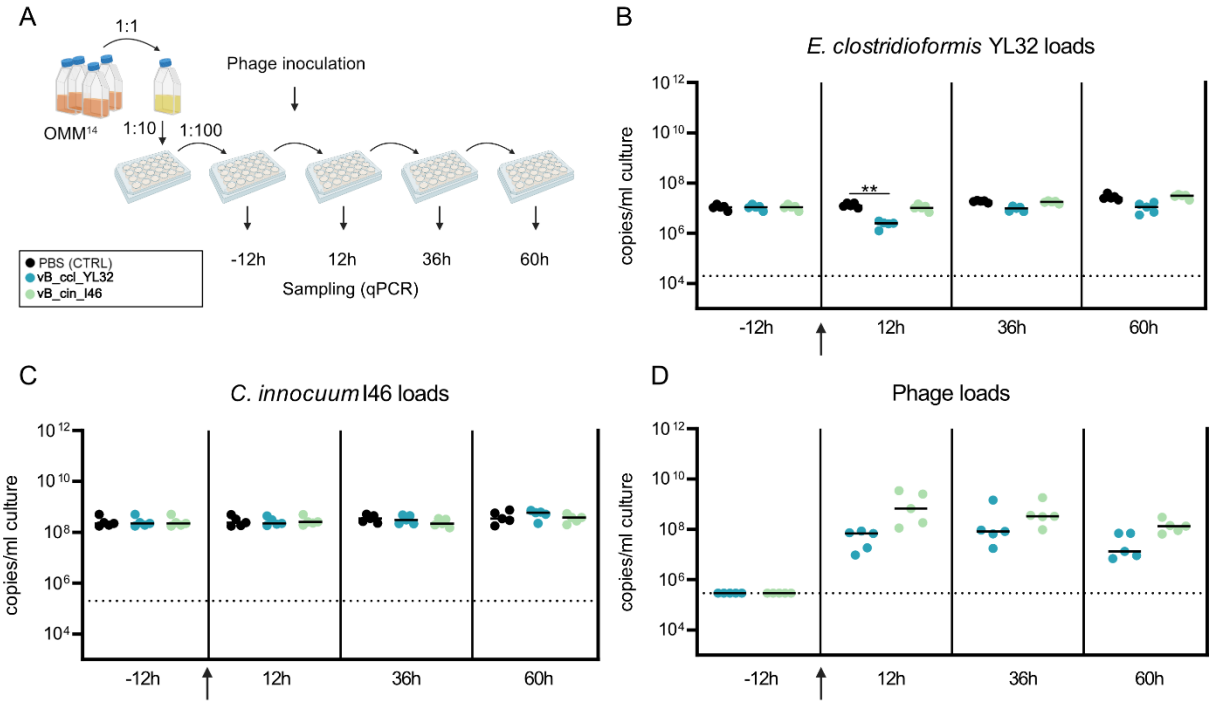

Fig. 20: Phages specifically target their hosts within a bacterial community *in vitro*

A) Experimental setup for the batch culture. The OMM[14] strains were grown in monoculture, mixed at the same OD600 ratio and diluted every day 1:100 in AF medium. 12 hours after the third dilution, phages vB_cin and vB_ccl were added to each well. Samples were taken for plating and qPCR before dilutions. Scheme made with Biorender. (B) *E. clostridioformis* YL32 and (C) *C. innocuum* I46 loads determined by qPCR (Log10 copies/ml). (D) Phage loads were determined via qPCR (log10 copies/ml) .Statistical analysis was performed using the Mann-Whitney Test comparing the treatment groups (N=5) against the control group (N=10) (* $p<0.05$, ** $p<0.01$, *** $p<0.001$). Each dot represents one well, black lines indicate median, dotted lines indicate detection limit (DTL). The experiment was conducted in two biological replicates with five technical replicates in total.

Figure legend modified from von Strempel et al., 2023.

The community composition was monitored by strain specific qPCR on three time points as in the previous batch culture experiment to see, if the phages influence the general community structure. A seen bevor, the overall community composition remained stable over 3 days and between the treatment groups. meaning that also these phages target their hosts and replicate within the community without disturbing the overall community composition (**Fig 21**).

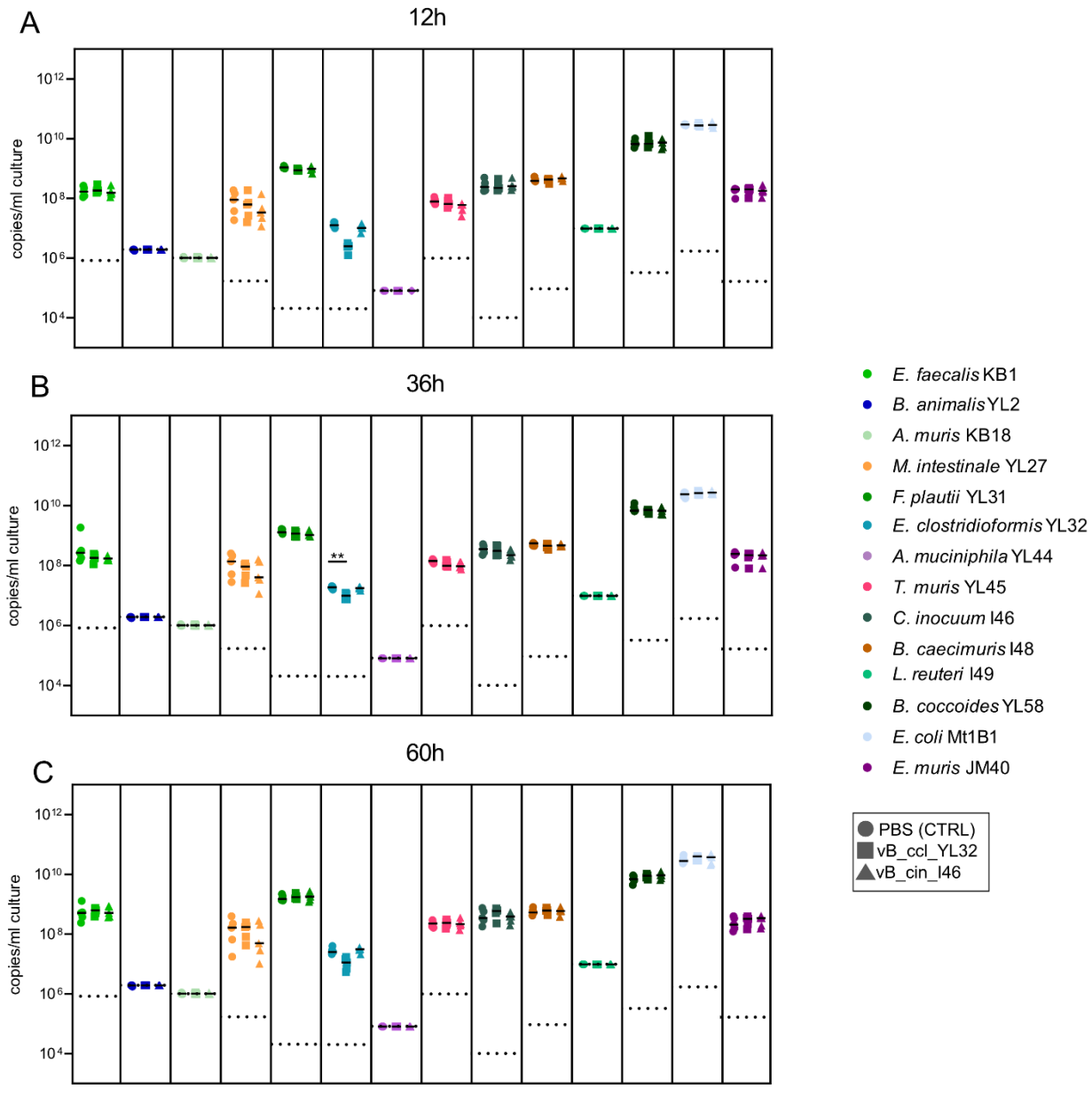

Fig 21: Phages specifically target their hosts without changing the overall community composition

Community composition 12 h (A), 36h (B) and 60h (C) after phage addition from experiment shown in Fig. 20, absolute abundance of each strain was determined using a strain-specific qPCR and plotted as 16S rRNA copy numbers per ml culture. Statistical analysis was performed using the Mann-Whitney Test comparing the treatment groups (N=5) against the control group (N=10) (* $p<0.05$, ** $p<0.01$, *** $p<0.001$). Each dot represents one well, black lines indicate median, dotted lines indicate detection limit (DTL).

Figure legend modified from von Strempel et al., 2023.

4.4 Impact of phages on their hosts in a synthetic bacterial community *in vivo*

4.4.1 *E. coli* Mt1B1 and *E. faecalis* KB1 are specifically targeted by phage-cocktails in gnotobiotic OMM14 mice

Next, we conducted an experiment to examine the effects of the phage cocktails targeting *E. coli* and *E. faecalis* ($3\Phi^{Mt1B1}$ and $3\Phi^{KB1}$) on their host bacteria *in vivo*. For this purpose, we established a stable colony of gnotobiotic OMM^{14} mice. Adult germfree mice kept in a sterile isolator were inoculated twice with live bacterial cultures of all 14 bacteria orally and rectally (50 µl each). Successful colonization was checked via qPCR and the mice were used for breeding. Offspring of the colonized mice showed a stable colonization over several generations of twelve out of the 14 bacteria (**Fig 22**). *B. longum* subsp. *animalis* YL2 and *A. muris* KB18 were not detected, consistent with previous findings in OMM^{12} mice (Afrizal Afrizal, 2022; Eberl et al., 2019); these strains either do not colonize or, much rather, fecal levels are below the detection limit of the qPCR since these bacteria were initially isolated from mice.

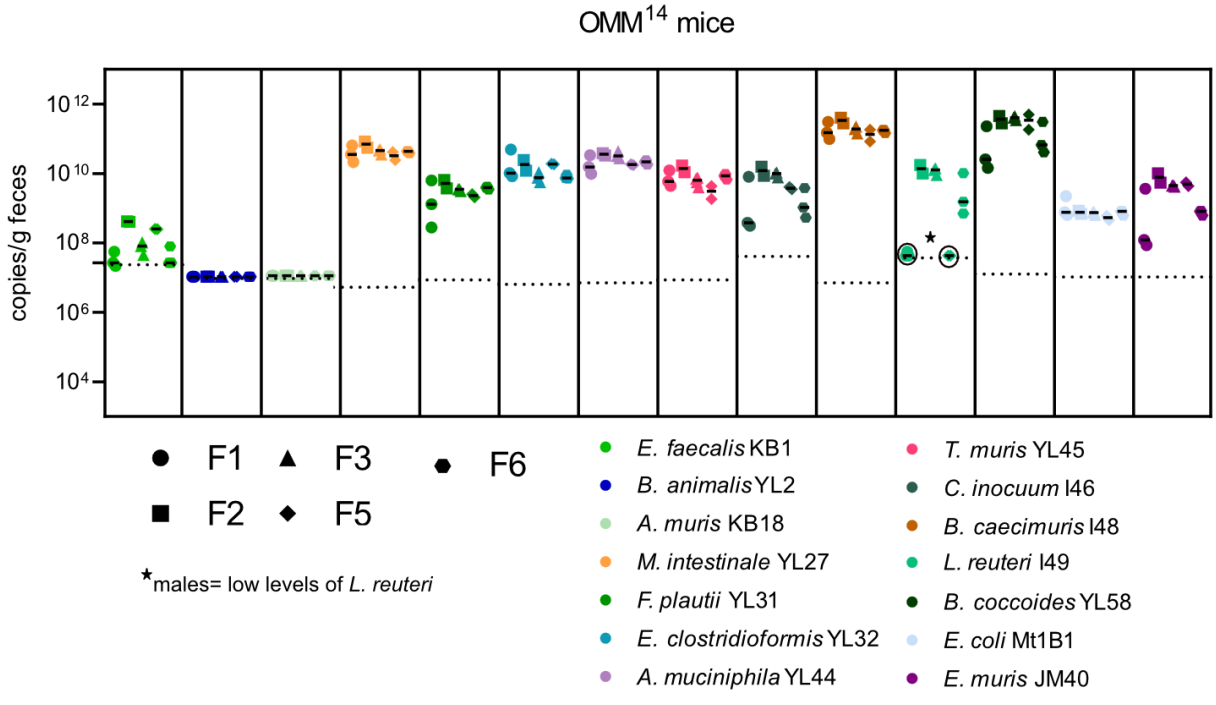

Fig. 22: The OMM^{14} colonize mice in a stable manner over several generations

Absolute abundance of all 14 bacteria across multiple breeding generations (F1, F2, F3, F5 and F6, displayed by different shapes), assessed via strain-specific qPCR in 16S rRNA copies per gram feces. Each dot represents one mouse, black line indicates median, dotted lines indicate DTL.

Figure and figure legend modified from von Strempel et al., 2023.

Using the OMM^{14} mouse model, we studied changes in the microbial community composition and the targeted bacteria following a single oral challenge of 3Φ^{Mt1B1} or 3Φ^{KB1} (1 x 10^7 PFU of each phage in 100µl PBS or only PBS as control without phages, n = 4-6, **Fig 23A**). Absolute abundances of the targeted bacteria and their phages in the feces was monitored from day 0 (before phage challenge) throughout 4 and day 7 post phage challenge (p.c.) via strain- and phage-specific qPCR. As a first result I showed, that the treatment with 3Φ^{Mt1B1} significantly reduced *E. coli* Mt1B1 loads on day 1-4, followed by a recovery of the bacterial populations which reached basal levels again by day 7 as seen as16S rRNA gene copy numbers (**Fig 23C**). The reduction of *E. faecalis* KB1 loads was more pronounced at day 2 after treatment with 3Φ^{KB1}, showing a decrease in absolute numbers of almost 2 orders of magnitude, but the population also recovered by day 7 p.c. (**Fig 23D**). Treatment with the respective other phage did not change absolute abundance of these bacteria (von Strempel et al., 2023).

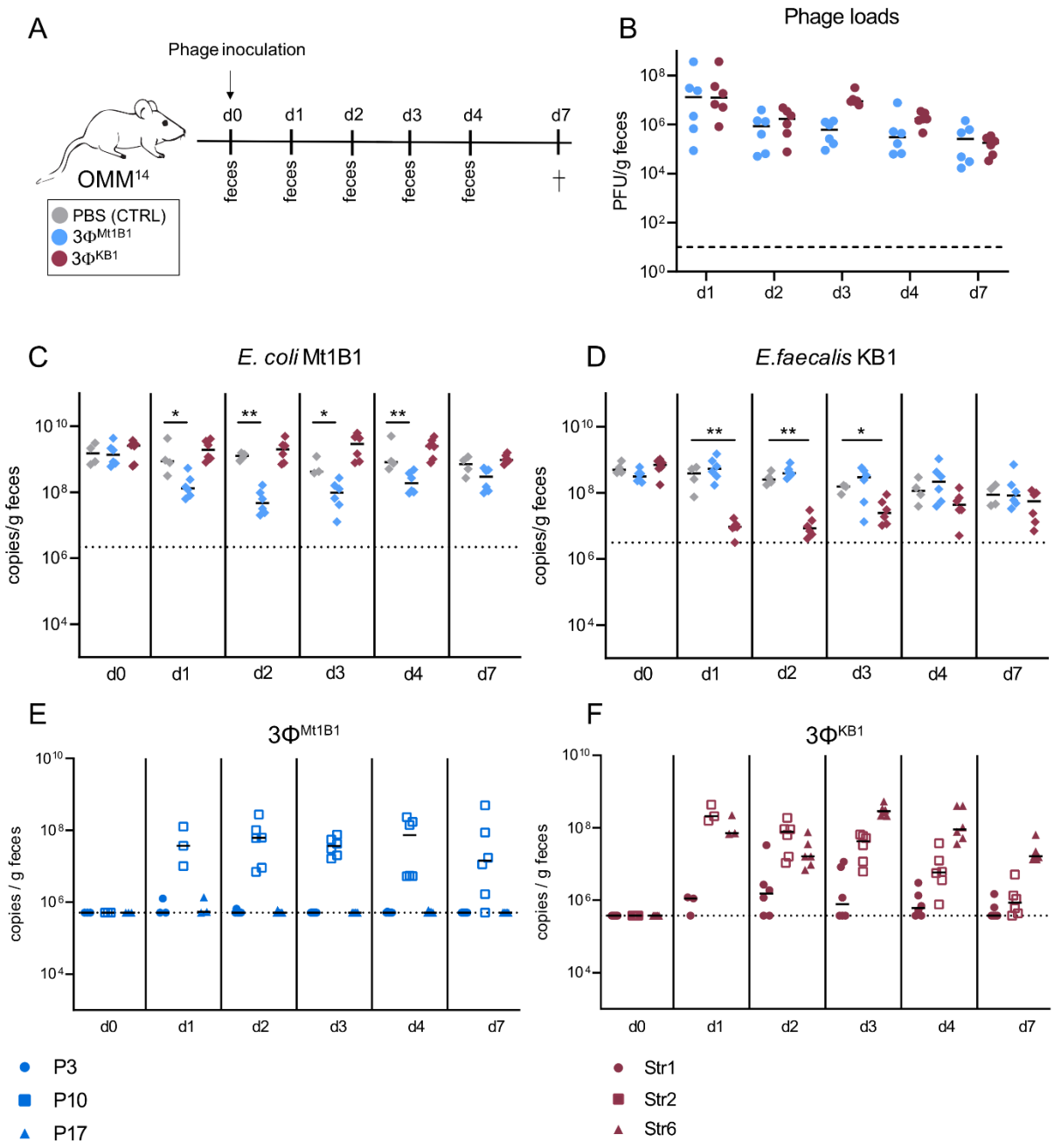

Fig. 23: *E. coli* Mt1B1 and *E. faecalis* KB1 can be specifically targeted by phages in OMM^{14} mice

(A) Experimental setup, stably colonized OMM^{14} mice were challenged with phage cocktails 3Φ^{Mt1B1} or 3Φ^{KB1} or PBS as control (10^7 PFU per phage) orally. Feces were collected every day. Mice were sacrificed on day 7 via cervical dislocation. (B) Phage loads (PFU/g feces) were determined via spot assays. (C) *E. coli* Mt1B1 and (D) *E. faecalis* KB1 loads were determined by qPCR in fecal samples at different time points p.c.. (B) Abundances of the single phages in the phage cocktails 3Φ^{Mt1B1} and (C) 3Φ^{KB1}, determined by specific qPCR. Different shapes show different phages. Statistical analysis was performed using the Mann-Whitney Test comparing the treatment groups (N=6) against the control group (N=4) (* $p<0.05$, ** $p<0.01$, *** $p<0.001$). Each dot represents one mouse, black lines indicate median, dotted lines indicate limit of detection.

Figure and figure legend modified from von Strempel et al., 2023.

Total phage levels (PFU/g feces) which were determined via spot assays were comparable between the phage cocktails $3\Phi^{Mt1B1}$ and $3\Phi^{KB1}$, reaching a maximum on day 1 p.c. with approximately 10^7 PFU/g feces, followed by stable levels between 10^5 PFU/g feces -10^6 PFU/g feces until day 7 p.c. (**Fig 23B**). Interestingly, in contrast to the results from the batch culture, qPCR revealed that only one of the three *E. coli* phages, namely phage P10, was detectable at high levels in the feces (**Fig 23E**). Levels of this phage remained stable over time at approximately 10^8 copies/g feces, whereas the other two phages showed much lower abundances as in the batch culture. Phage P3 was only detectable on day 1 and 2 p.c. and then decreased below the detection limit of the qPCR. Phage P17 was only detectable at early time points (day 1 and day 2) in half of the mice (3 out of 6) at very low abundances (10^5 copies/g feces - 10^6 copies/g feces) which is close to the detection limit of the qPCR. On the other hand, the phages in the cocktail targeting *E. faecalis* displayed a different outcome. All three phages were detectable in feces via qPCR until day 7 of the experiment in relatively high numbers (**Fig 23F**). Str2 and Str6 were highly abundant (10^7 copies/g feces - 10^9 copies/g feces) and only showed a slight decrease in numbers at day 4 and day 7, whilst abundances of Str1 was lower but still above the detection limit in most of the mice during the whole experiment (von Strempel et al., 2023).

Furthermore, the absolute abundance of the whole community was also monitored via qPCR over time (**Fig 24A-C**). Despite the significant drop of *E. coli* and *E. faecalis* in the respective phage treatment groups on day 2 (**Fig 24B**), no changes could be observed between the treatment groups for the other bacteria, showing that the phages only specifically target their hosts also *in vivo* (von Strempel et al., 2023*)*.

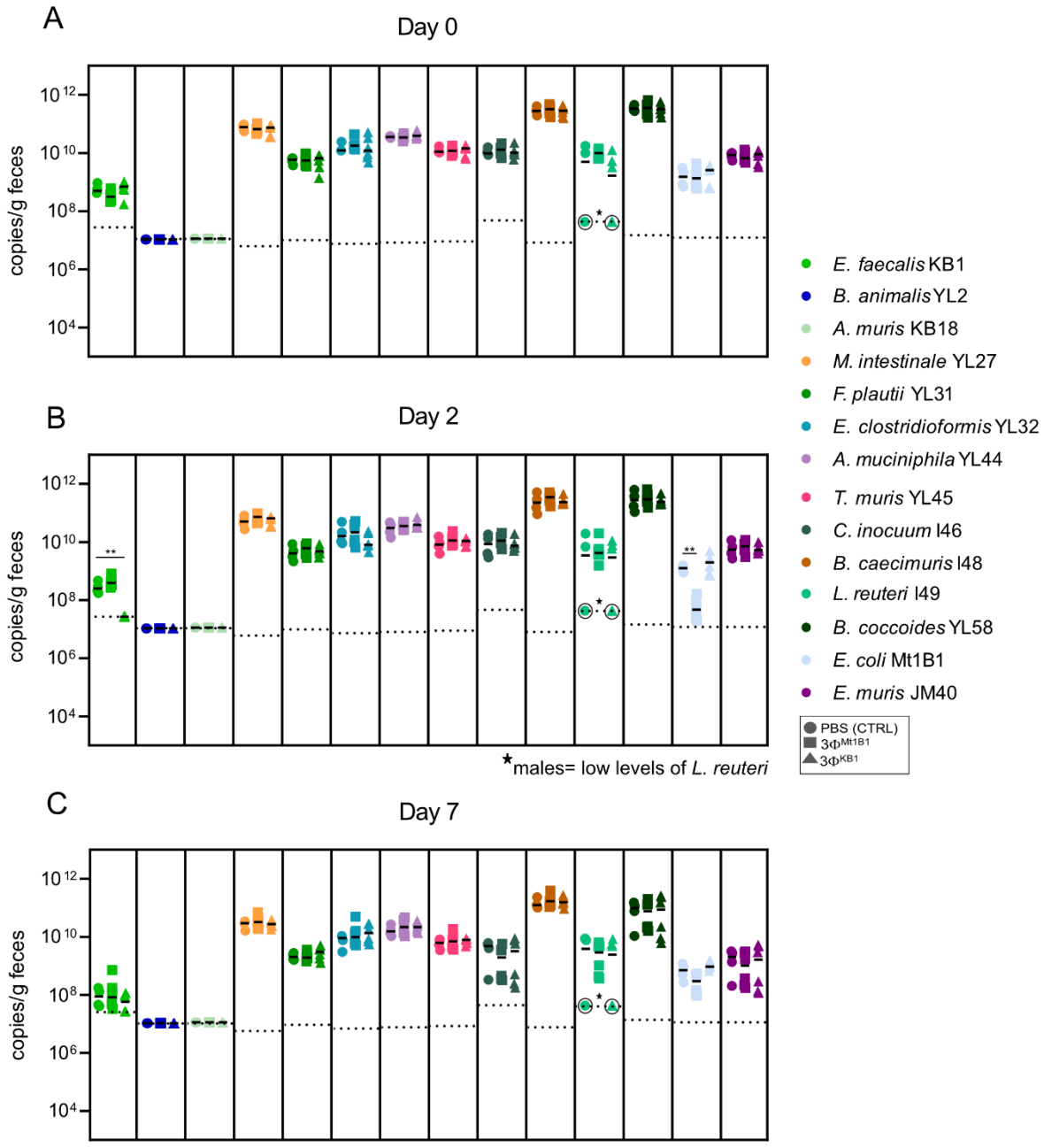

Fig. 24: Community composition in feces

Absolute abundances of the OMM[14] community from the experiment shown in Fig. 23, determined by strain-specific qPCR on day 0 (A), on day 2 p. c. (B) and day 7 p.c. (C). Each color represents one bacterial strain, different shapes represent different experimental groups. Each dot represents one mouse, black line indicates median, dotted lines indicate DTL. Statistical analysis was performed using the Mann-Whitney Test comparing the treatment groups against the control group (* $p<0.05$, ** $p<0.01$, *** $p<0.001$). Each dot represents one mouse, black lines indicate median, dotted lines indicate limit of detection.

Figure and figure legend modified from von Strempel et al., 2023.

4.4.2 Administration of phage cocktails targeting *E. coli* and *E. faecalis* leads to decreased colonization resistance of OMM^{14} mice against *S.* Tm

From former studies in our lab, it was already known that *E. coli* and *E. faecalis* next to others are important in mediating colonization resistance in OMM^{12} mice (Eberl et al., 2021). These experiments were conducted in drop out mice, where the respective bacteria were missing from the mice from the start of colonization. Since the phage cocktails used in this study only reduced and not depleted their host, I wanted to investigate if this effect is enough to have a functional impact on the colonization resistance against *Salmonella*. In order to evaluate this, an avirulent *Salmonella enterica* serovar Typhimurium strain (*S.* Tm^{avir}) was used, which colonizes the gut but does not induce inflammation due to the lack of functional type III secretion systems 1 and 2 (Brugiroux et al., 2016). OMM^{14} mice (n = 6-8) were orally infected with *S.* Tm^{avir} (1x10^7 CFU) and immediately thereafter received either the 3Φ^{Mt1B1} or 3Φ^{KB1} phage cocktail (1x10^7 PFU of each phage in PBS) or PBS control without phage (**Fig 25A**). Fecal samples were collected on day one and two post infection (p. i.) with *S.* Tm and total bacterial loads were scored by plating the feces on agar plates containing selective antibiotics. As observed in the previous experiment, *E. coli* Mt1B1 and *E. faecalis* KB1 loads significantly decreased at day one p.c. by about one (*E. coli*) and two (*E. faecalis*) orders of magnitude (**Fig 25BC**). Phages were detectable in the gut for two days via spot assays, with total loads ranging between 4.2x10^4 PFU/g feces and 7.07x10^7 PFU/g feces which was also seen in the previous experiment. (**Fig 25D)** which showed the reproducibility of the effect of the phages (von Strempel et al., 2023**)**.

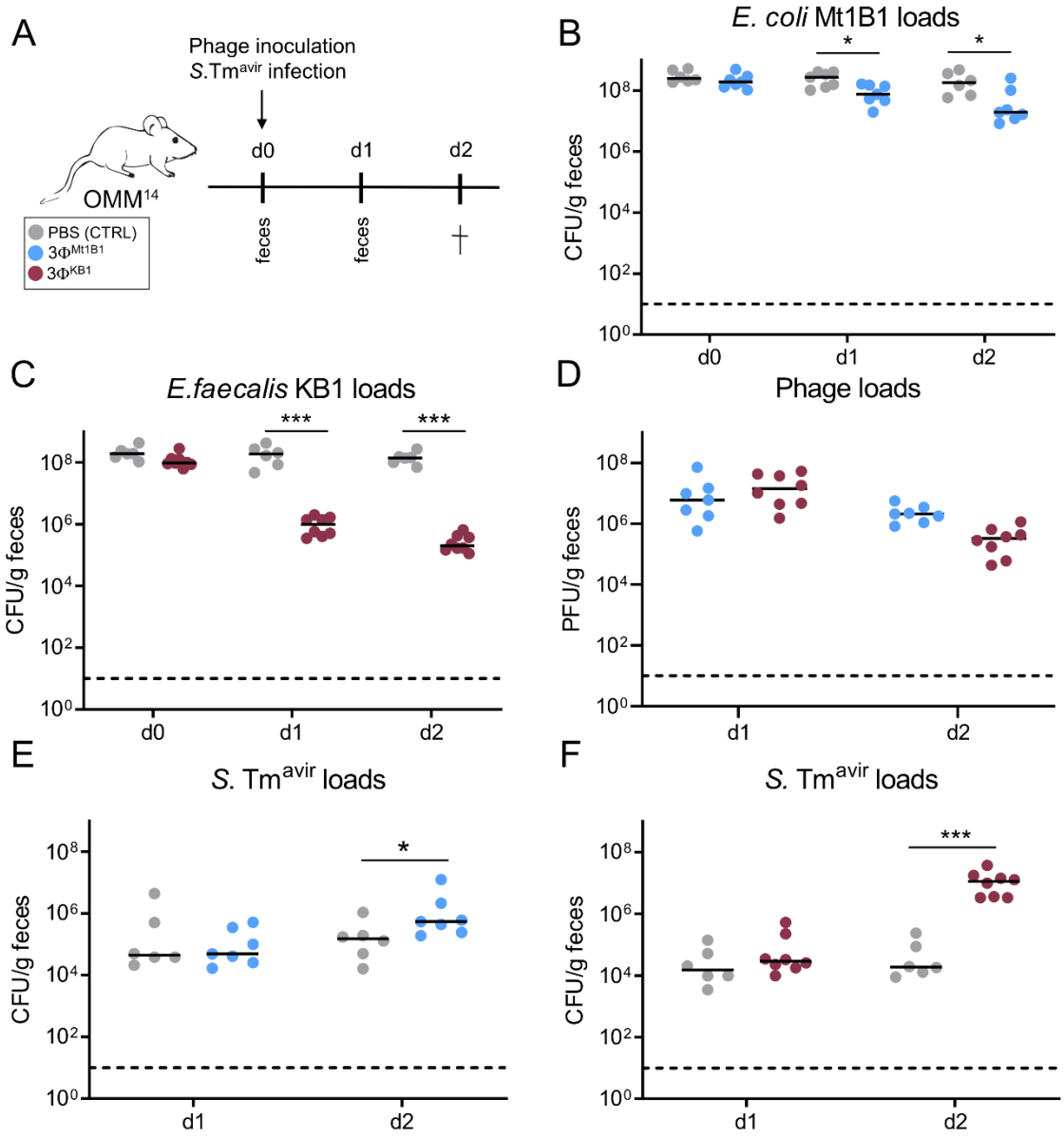

Fig. 25: Decrease of *E. coli* and *E. faecalis* by treatment with specific phages leads to increased S. Tm loads after infection of OMM^{14} mice

(A)) Experimental setup, stably colonized OMM^{14} mice were challenged with phage cocktails 3Φ^{Mt1B1} or 3Φ^{KB1} or PBS as control (10^7 PFU per phage) orally. Feces were collected every day. Mice were sacrificed on day 2 via cervical dislocation. (B) *E. coli* Mt1B1 and (C) *E. faecalis* KB1 loads (CFU/g feces) were determined in feces by plating on agar containing selective antibiotics. (D) Phage loads (PFU/g feces) were determined by spot assays. (E, F) *S.* Tm^{avir} loads at day 1 and 2 after phage challenge (= day 1 and 2 post infection (p.i.)). Statistical analysis was performed using the Mann-Whitney Test (* $p<0.05$, ** $p<0.01$, *** $p<0.001$, N=6-8). Each dot represents one mouse, black lines indicate median, dotted lines indicate limit of detection.

Figure and figure legend modified from von Strempel et al., 2023.

One day post infection, there was no difference in *S.* Tm loads between the control groups (median: 4.4x10^4 CFU/g (**Fig 25E**), median: 1.5 x10^4 (**Fig 25F**)) and any of the phage treatment groups (median: 4.9 x10^4 CFU/g (**Fig 25E**), median: 2.9 x10^4 CFU/g (**Fig 25F)**) although loads of *E. coli* and *E. faecalis* were already significantly decreased. Strikingly, at day two p. i., *S.* Tm loads were significantly increased in mice challenged with either of the phage cocktails (median: 5.5x10^5 CFU/g (**Fig 25E**), median: 1.1 x10^7 (**Fig 25F**)) compared to the control groups (median: 1.5x10^5 CFU/g (**Fig 25E**), median: 1.8 x10^4 (**Fig 25F)).** This effect was particularly pronounced in the case of mice treated with 3Φ^{KB1}, where the presence of the *E. faecalis* specific phages led to a two-order-of-magnitude increase in *S.* Tm loads (**Fig 25F**).

Furthermore, we confirmed via qPCR that also the infection of *S.* Tm^{avir} and addition of phages together does not affect the absolute abundance of the other bacteria two days p.i. (**Fig 26**). The members of the OMM^{14} community did not show any changes in between the treatment groups on day two (von Strempel et al., 2023).

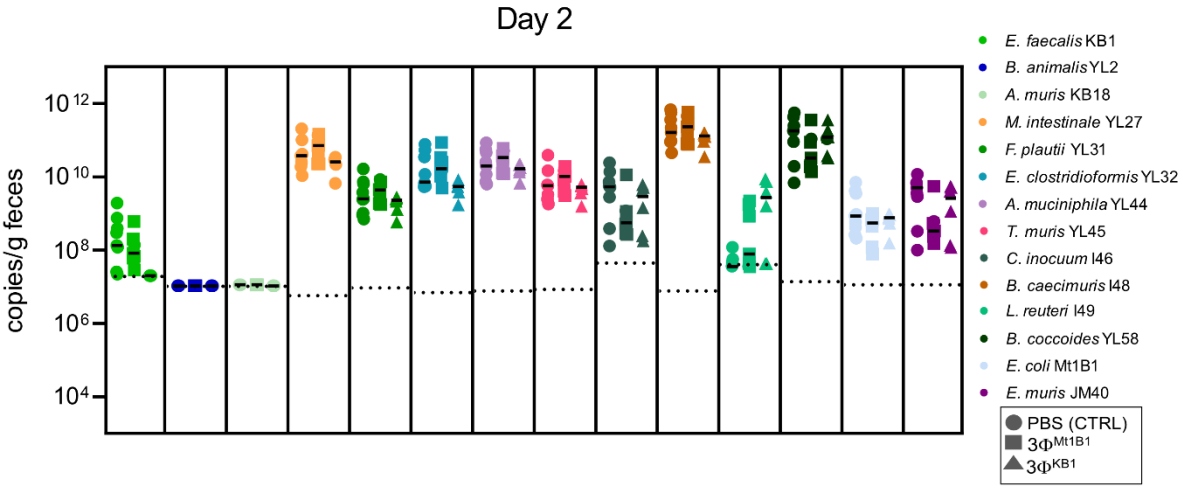

Fig. 26: Abundance of OMM^{14} community member in feces

Absolute abundances measured with strain-specific qPCR on day 2 p.i. in feces of all 14 bacteria shown in Fig. 25. Each color represents one bacterial strain, different shapes represent different experimental groups. Each dot represents one mouse, black line indicates median, dotted lines indicate DTL.

Figure and figure legend modified from von Strempel et al., 2023

Next, we wanted to test if both phage cocktails applied at the same time cause an additive effect on colonization resistance. For this, we orally infected OMM^{14} mice (n=5) with *S.* Tm^{avir} (1x10^{7} CFU), directly followed by all phages together (3Φ^{Mt1B1} and 3Φ^{KB1}, 1x10^{7} PFU of each phage in PBS) or PBS control (**Fig 27A**). The significant declines in *E. coli* Mt1B1 and *E. faecalis* KB1 levels on day one and day two p. c. (**Fig 27BC**) were similar to the outcomes observed with phage cocktails targeting individual bacteria (**Fig 25**). ahe measured phage loads in fecal spot assays ranged between 10^{6} and 10^{8} PFU/g feces, which were also comparable (**Fig 27E**). Intriguingly, *S.* Tm loads on day 1 p.i. already are significantly elevated (median: 2.4x10^{6} CFU/g versus control median: 1.1x10^{5} CFU/g, **Fig 27D**), a phenomenon which was not observed with treatment with the single phage cocktails (**Fig 25**) (von Strempel et al., 2023).

On day 2 p. i., *S.* Tm loads in the phage treatment group exhibited further upgrowth (median: 6.3x10^{7} CFU/g versus control median: 1.7x10^{6} CFU/g, **Fig 27D**). However, in contrast to treatment with the single phage cocktail, the overall loads and the discrepancy from the control group were not notably more pronounced, suggesting a lack of clear additive effect from the two phage cocktails..

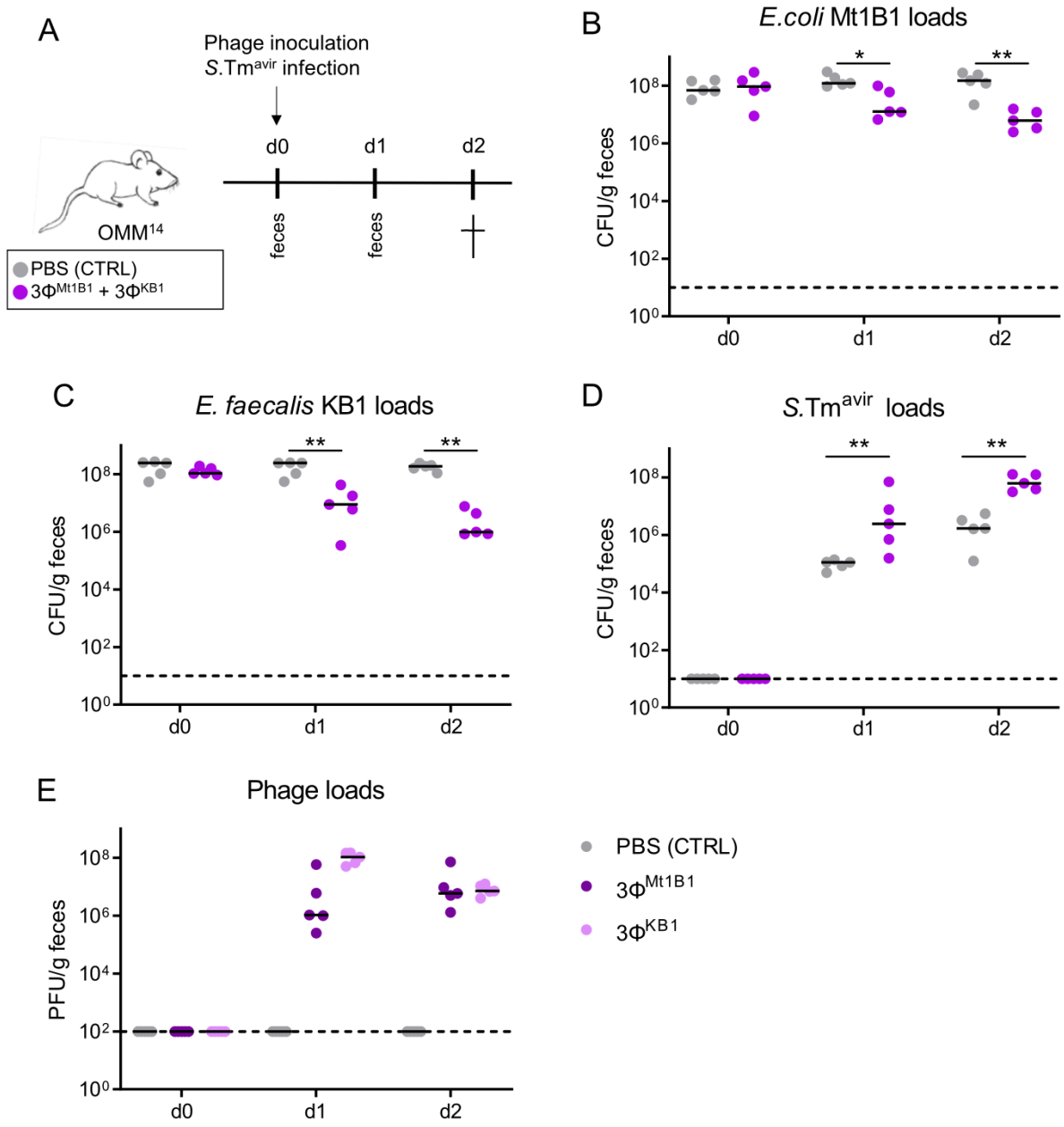

Fig. 27: Treatment with both phage cocktails together doesn't show an additive effect on the impairment of the colonization resistance

(A) Experimental setup: OMM^{14} mice were infected with S. Tm^{avir} (5x107 CFU) and directly after orally challenged with phage cocktails (3Φ^{Mt1B1} and 3Φ^{KB1}, 1x10^{7} PFU of each phage in PBS) or PBS as control (n=5). Feces were taken at day one and two p.c. and mice were sacrificed at day two p.c.. (B) *E. coli* Mt1B1 and (C) *E. faecalis* KB1 loads (CFU/g feces) were determined in feces by plating. (D) *S.* Tm^{avir} loads at day 1 and 2 after phage challenge (= day 1 and 2 post infection (p.i.)). (E) Phage loads (PFU/g feces) were determined by spot assays. Statistical analysis was performed using the Mann-Whitney Test (* $p<0.05$, ** $p<0.01$, *** $p<0.001$, N=5). Each dot represents one mouse, black lines indicate median, dotted lines indicate limit of detection.

Figure and figure legend modified from von Strempel et al., 2023

Again, the community composition was monitored via strain specific qPCR. In contrast to our previous results, a significant change in several bacteria was observed. Four bacteria (*C. innocuum* I46, *L. reuteri* I49, *B. coccoides* YL58, *E. muris* JM40) showed a significant increase in total abundance in mice treated with both phage cocktails at the same time (**Fig 28**) which was not observed when the cocktails were added separate. This suggests, that adding phages that target more than one bacterium in a community might lead to disturbance of the general community composition (von Strempel et al., 2023).

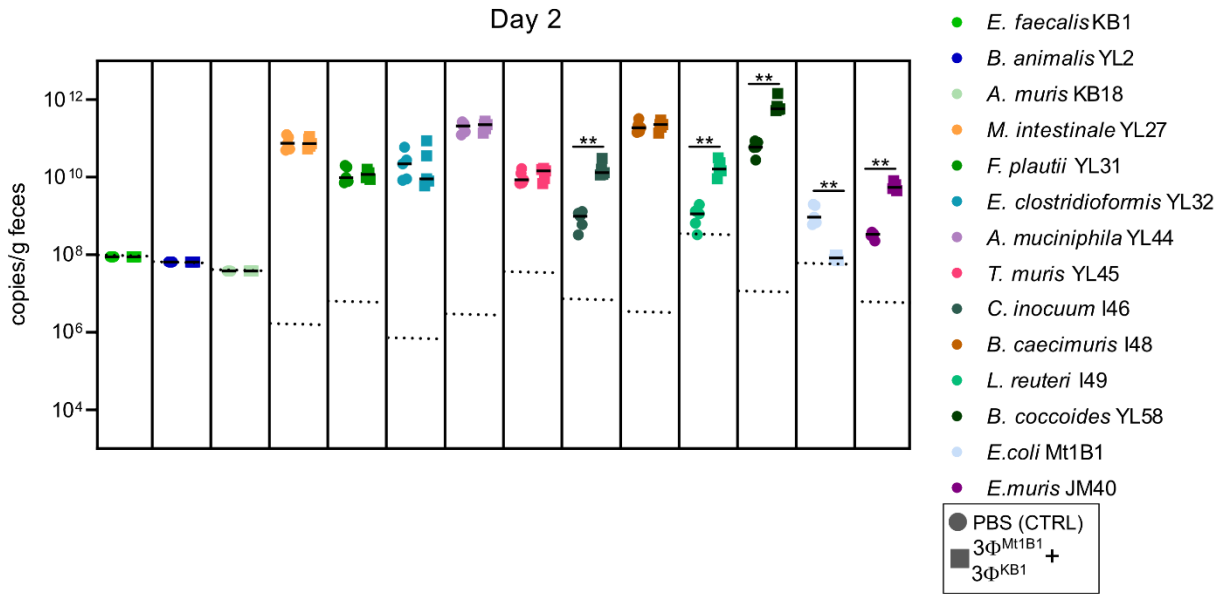

Fig. 28: Abundance of OMM^{14} community member in feces

Absolute abundances in feces of all 14 bacteria from the experiment shown in Fig. 27, determined by strain-specific qPCR on day 2 p. c.. Each color represents one bacterial strain, different shapes represent different experimental groups. Each dot represents one mouse, black line indicates median, dotted lines indicate DTL.

Figure and figure legend modified from von Strempel et al., 2023

4.4.3 Phage treatment impairs colonization resistance independently of the abundance of protective bacteria

Since the phages targeting *E. coli* and *E. faecalis* were able to stay in the gut for 7 days and coexist with their hosts, I aimed to investigate whether phages also have an impact on colonization resistance during co-existence. For this, OMM^{14} mice were inoculated with either $3\Phi^{Mt1B1}$ or $3\Phi^{KB1}$ (or PBS control) on day 0, followed by an infection with *S.* Tm^{avir} ($1x10^7$ CFU) on day seven p.c. (**Fig 29A**). On this timepoint, no significant differences in *E. coli* Mt1B1 or *E. faecalis* KB1 loads were observed between the treatment groups anymore (**Fig 29BC**), but spot assays revealed that the phages were still present at steady numbers in the feces (**Fig 29D**). Furthermore, the overall OMM^{14} composition shows no difference between the groups and the timepoints (**Fig 30AB**). Fecal samples were collected on day one and two post infection (p. i.) to determine the *Salmonella* loads. Strikingly, *S.* Tm^{avir} loads at day 8 and 9 p.c. (corresponding to day one and two p.i.) were significantly elevated in both phage-treated groups compared to the control group (**Fig 29E**). For $3\Phi^{KB1}$, this effect is not as pronounced as on day 2 p.c. (**Fig 25F**), but still significantly different to the control group. This suggests that phages can also impair colonization resistance without detectable impact on the abundance of their target bacteria or overall composition of the microbiota. The community composition shows no differences between day 0 and day 7 of the experiment and between the treatment groups (**Fig 30AB**), showing that this effect is solely dependent on the addition of the phages (von Strempel et al., 2023).

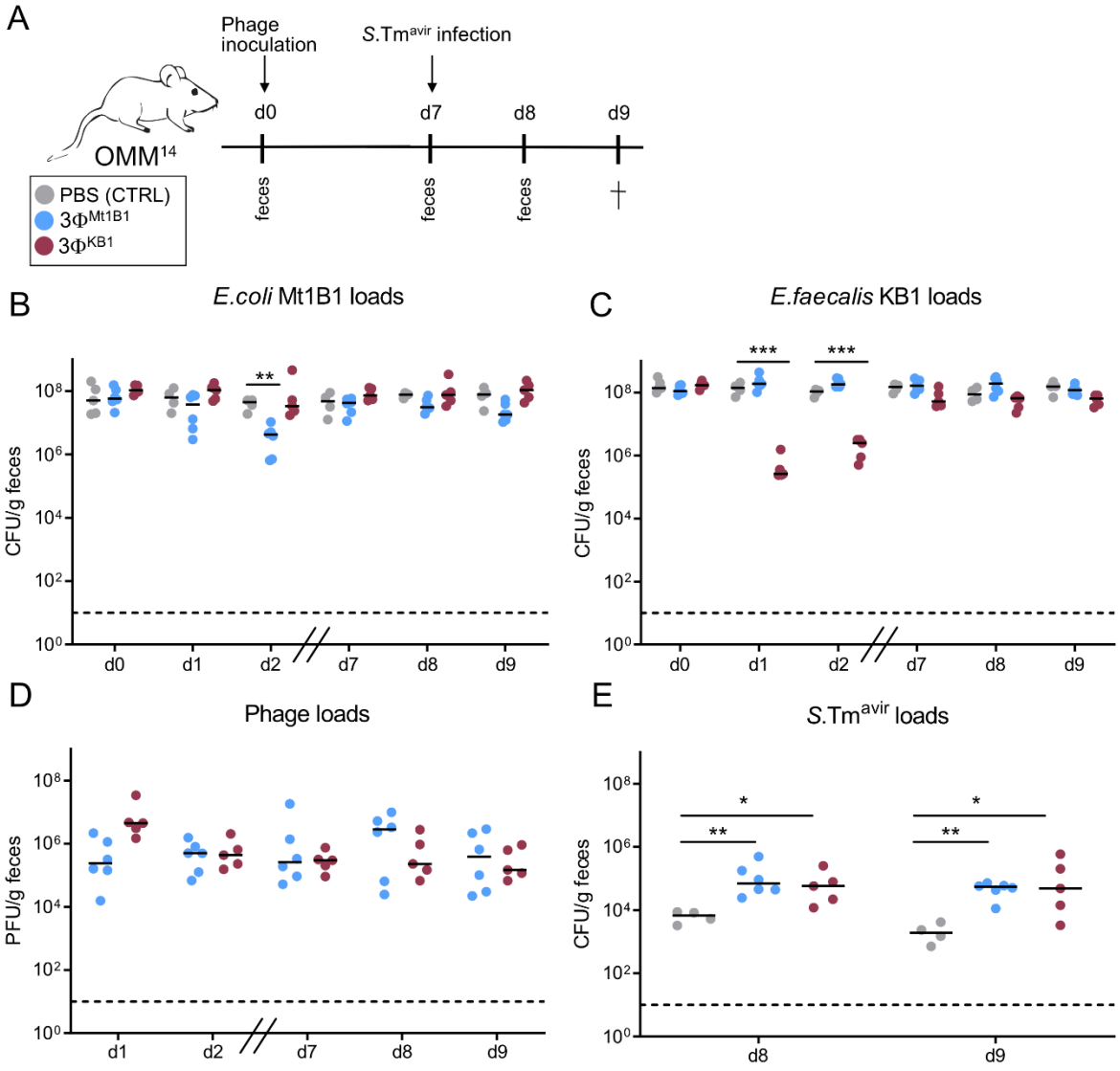

Fig. 29: Phages impair colonization resistance at late time points independently of changing abundance of protective bacteria

(A) Experimental setup, OMM^{14} mice were challenged with phage cocktails (3Φ^{Mt1B1} and 3Φ^{KB1}, 1x10^{7} PFU of each phage in PBS) or PBS as control and infected with *S.* Tm^{avir} (5x10^{7} CFU) at day 7 p.c.. Feces were taken at day 1, 2, 7, 8 and 9 p.c. and mice were sacrificed at day 9 p.c. (corresponding to day two p.i.). (B) *E. coli* Mt1B1 and (C) *E. faecalis* KB1 loads (CFU/g) were determined in feces by plating. (D) Phage loads (PFU/g feces) of 3Φ^{Mt1B1} and 3Φ^{KB1}were determined by spot assays in fecal samples at different time points p.c.. (E) *S.* Tm^{avir} loads at day 8 and 9 p.c. (= day 1 and 2 p.i.). Statistical analysis was performed using the Mann-Whitney Test (* $p<0.05$, ** $p<0.01$, *** $p<0.001$, N=4-6). Each dot represents one mouse, black lines indicate median, dotted lines indicate limit of detection.

Figure and figure legend modified from von Strempel et al., 2023.

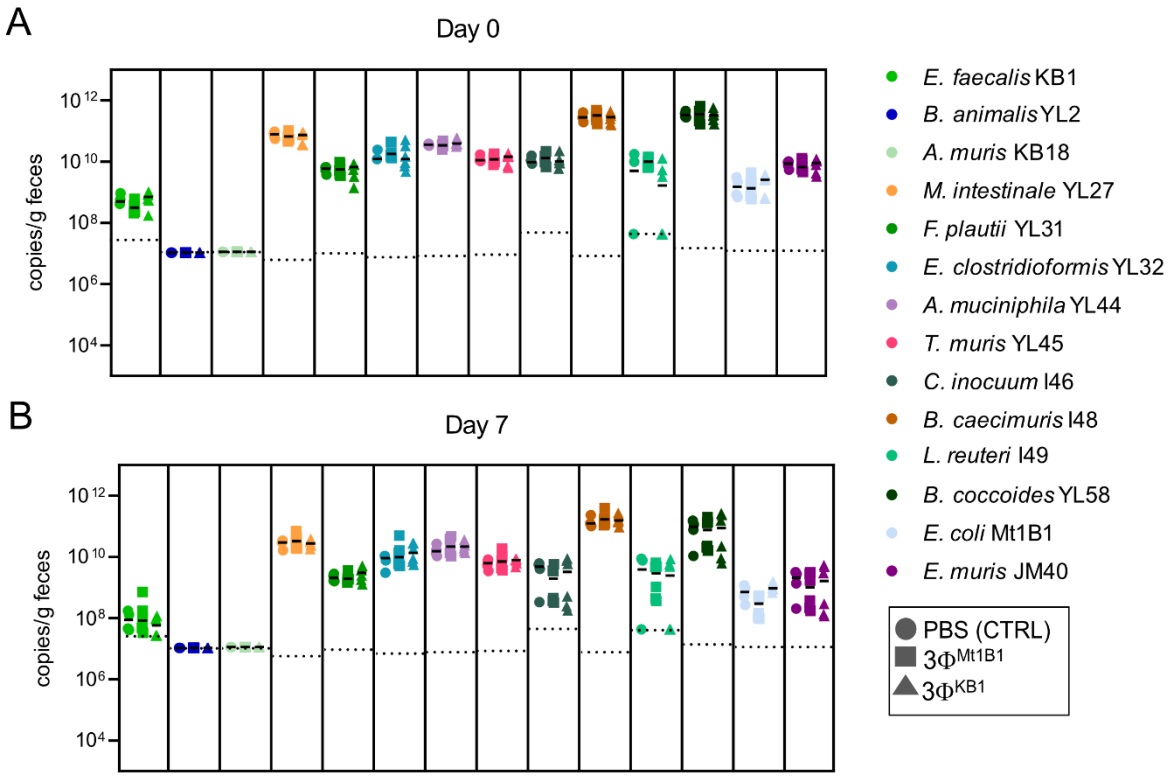

Fig. 30: Abundance of OMM^{14} community member in feces

Absolute abundances of all 14 bacteria from the experiment shown in Fig. 29, assessed via strain-specific qPCR on day 0 (A) and day 7 p. c. (B). Each color represents one bacterial strain, different shapes represent different experimental groups. Each dot represents one mouse, black line indicates median, dotted lines indicate DTL.

Figure and figure legend modified from von Strempel et al., 2023.

4.4.4 Treatment with a phagecocktail targeting *E. faecalis* KB1 in OMM^{14} mice facilitates development of *S.* Tm-induced colitis

As a next step we wanted to test, whether phage-mediated disruption of colonization resistance in OMM^{14} mice would also enhance the severe symptoms of a *S.* Tm-induced colitis. In all previous experiments, mice did not have colitis symptoms, since the *S.* Tm strain used was avirulent. Therefore, OMM^{14} mice were infected with *S.* Tm^{wt} (1x10^{7} CFU) and with either 3Φ^{Mt1B1} or 3Φ^{KB1} phage cocktail immediately after (1x10^{7} PFU of each phage in PBS or PBS control; **Fig 31A**). Fecal samples were collected from day 0 until day 4 post infection (p. i.) and mice were sacrificed on day 4. After sacrifice, also the spleen, liver and mesenteric lymph nodes were sampled to determine *S.* Tm loads. In this experiment, loads of *E. coli* Mt1B1 significantly decreased only at day one p. c. and then showed an increase in abundance, supposedly as a

reaction to the inflamed conditions in the gut. *E. faecalis* KB1 loads were significantly decreased at day 1- 4 p. c. (**Fig 31BC**) as observed in previous experiments.

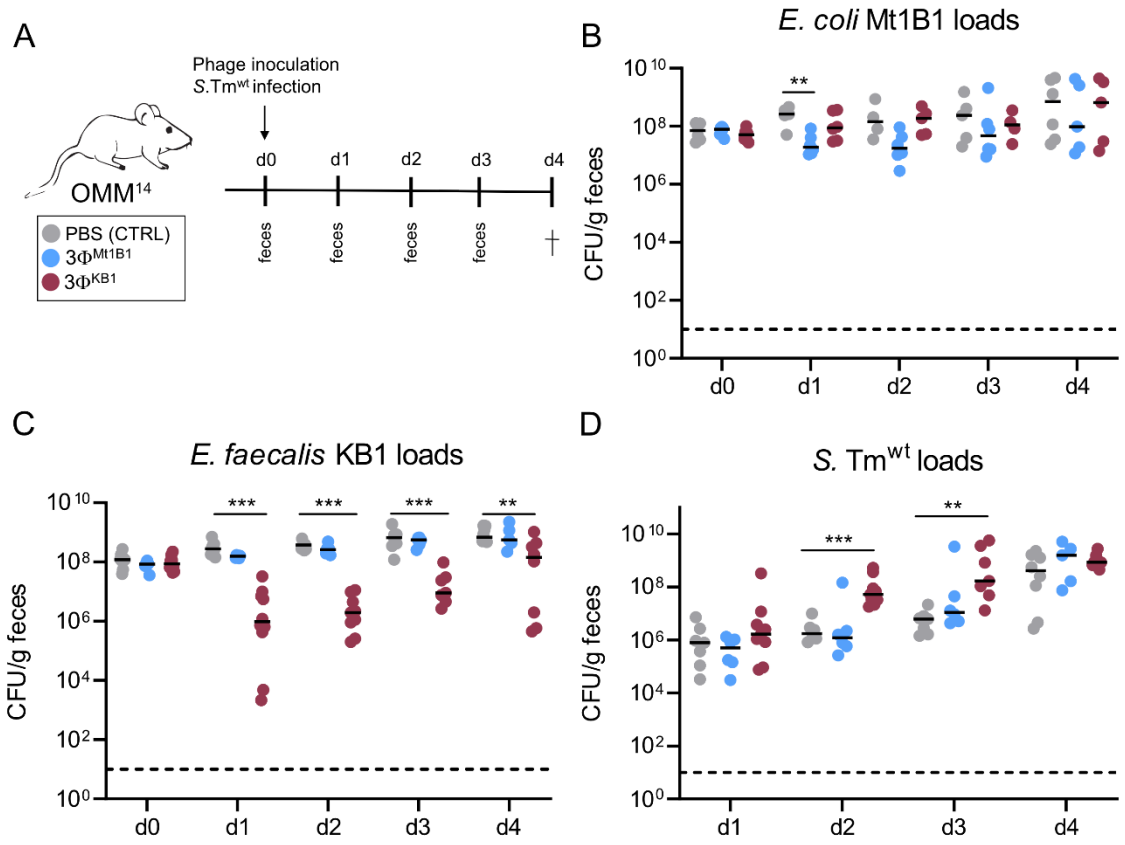

Fig. 31: Treatment with phage cocktail targeting *E. faecalis* impairs colonization resistance against *S.* Tm^{wt}

(A) Experimental setup, OMM^{14} mice were challenged orally with phage cocktails 3Φ^{Mt1B1} or 3Φ^{KB1} or PBS as control (10^7 PFU per phage) and infected with *S.* Tm^{wt} ($5x10^7$ CFU). Feces were taken at day 1-3 p.c. and mice were sacrificed at day 4 p.c. (B) *E. coli* Mt1B1, (C) *E. faecalis* KB1 and (D) *S.* Tm^{wt} loads (CFU/g) were determined in feces by plating. Statistical analysis was performed using the Mann-Whitney Test (* $p<0.05$, ** $p<0.01$, *** $p<0.001$, N=6-8). Each dot represents one mouse, black lines indicate median, dotted lines indicate limit of detection.

Figure and figure legend modified from von Strempel et al., 2023

Furthermore, *S.* Tm^{wt} loads showed a significant increase on day two and three p. c. only in the group treated with *E. faecalis* 3Φ^{KB1} phage cocktail compared to the control group (**Fig 32D**) but not in the group treated with 3Φ^{Mt1B1}, which was not observed in previous experiments.

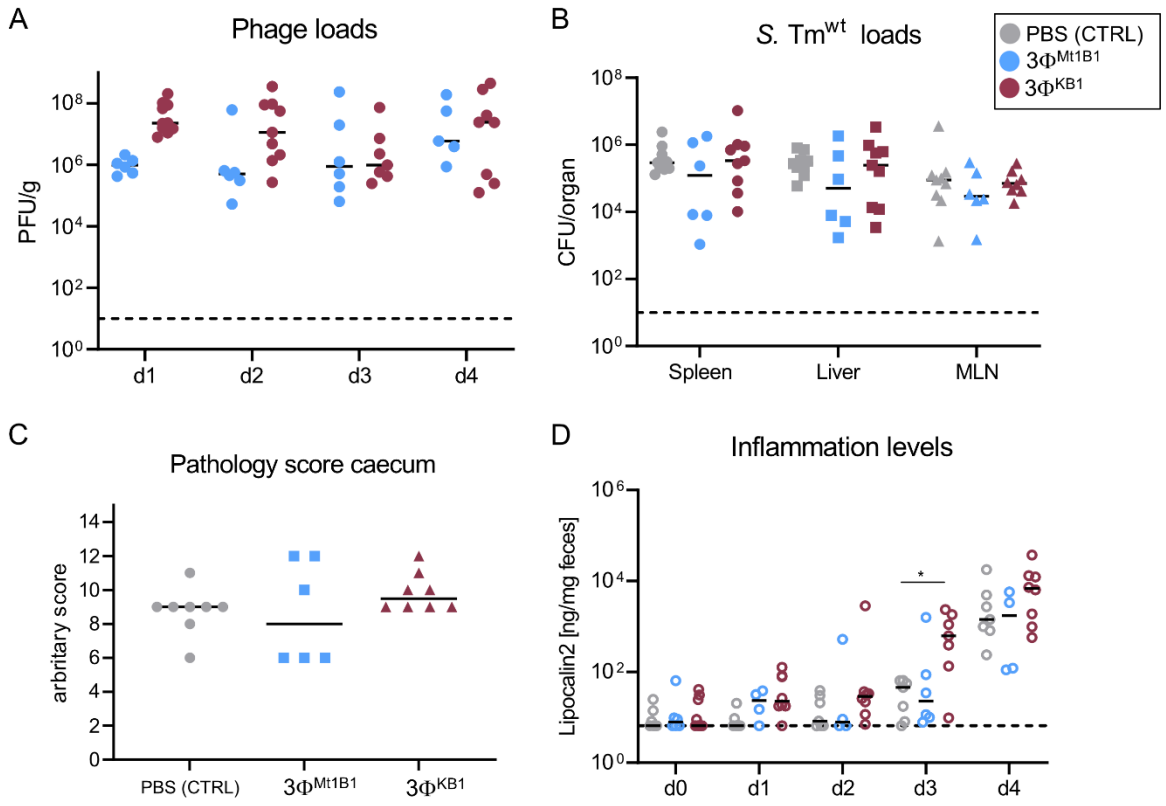

Fig. 32: Treatment with phage cocktail targeting *E. faecalis* facilitates *S.* Tm induced colitis in OMM^{14} mice

(A) Phage loads in feces from experiment shown in Fig. 31, determined by spot assays. (B) *S.* Tm^{wt} loads in spleen, liver and mesenteric lymph nodes (MLN), determined by plating on agar plates with selective antibiotic. (C) Histopathological score of the cecum at day 4. (D) Inflammation levels were determined by measuring the Lipocalin-2 (ng/mg feces) levels in the feces, utilizing a specific ELISA. Each dot represents one mouse, black line indicates median, dotted lines indicate DTL.

Figure and figure legend modified from von Strempel et al., 2023

Strikingly, in the group which was treated with phages targeting *E. faecalis*, *S.* Tm inflammation was enhanced as determined by increased fecal lipocalin-2 levels at day 3 p. i. (**Fig 32D**). This effect was only visible on day 3, marking a faster onset of the inflammation in this treatment group. No difference was found anymore at day 4 p. i. both in lipocalin-2 levels and cecal histology (**Fig 32CD**). Phage levels were comparable to the previous *in vivo* experiments and stayed stable until day four p. c. despite the strong inflammation in the gut (**Fig 32A**) and the presence of the wildtype *S.* Tm. In the group treated with *E. coli* 3Φ^{Mt1B1} phage cocktail, no significant difference in *S.* Tm inflammation or *S.* Tm loads was observed compared to the

control group. Also, the *S.* Tm loads in the organs (spleen, liver and mesenteric lymph nodes) did not show any differences between the treatment groups on day 4 **(Fig 32B**) but display high loads independent from the treatment (von Strempel et al., 2023).

The absolute abundances of all members of the OMM^{14} consortium was determined by qPCR (**Fig 33**). In general, overall bacterial levels were stable on day 0 (**Fig 33A**), followed by a strong variation in abundance in all treatment groups on day four (**Fig 33B**) which was not seen in the experiments with the avirulent *S.* Tm. This effect is likely due to the severe *S.* Tm-induced gut inflammation.

In conclusion, I could show that phage treatment targeting *E. faecalis* accelerates not only pathogen invasion but also disease onset in case of the 3Φ^{KB1} phage cocktail (von Strempel et al., 2023).

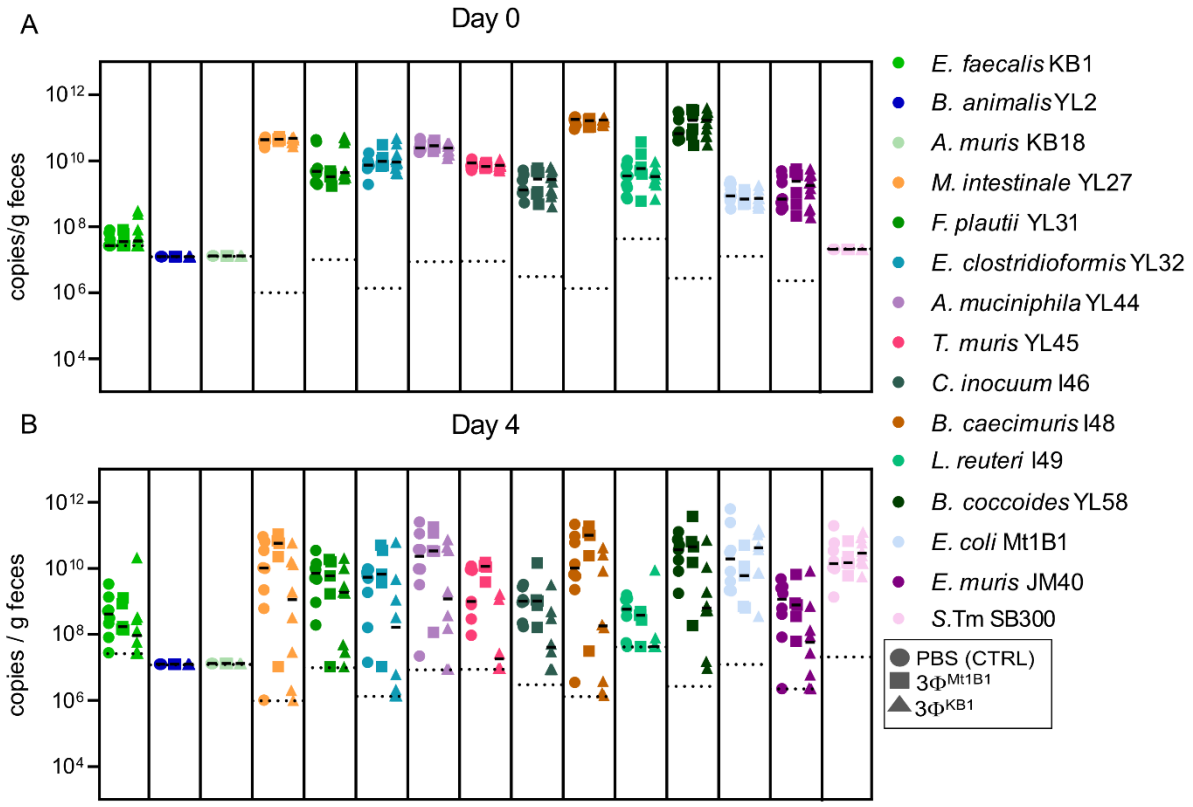

Fig. 33: Abundance of OMM^{14} community member in feces

Absolute abundances of all 14 bacteria shown in Fig. 31 and 32, determined by strain-specific qPCR on day 0 (A) and day 4 p. c. (B). Each color represents one bacterial strain, different shapes represent different experimental groups. Each dot represents one mouse, black line indicates median, dotted lines indicate DTL.

Figure and figure legend modified from von Strempel et al., 2023

4.4.5 Treatment with a phage targeting no member of the community does not impair the colonization resistance against *Salmonella*

To make sure, that the introduction of phages alone is not the cause for the impaired colonization resistance, we conducted experiments to determine whether a phage, unable to amplify in OMM^{14} mice due to the absence of its host strain *S. aureus* would influence the susceptibility to *S.* Tm infection. OMM^{14} mice were orally administered either a single phage strain (vB_SauP_EBHT, 1x10^{7} PFU in 100µL PBS), targeting *Staphylococcus aureus* (strain EMRSA-15) or 100µL PBS and infected them with *S.* Tm^{avir} **(Fig 34A**). Previously, spot assays confirmed that vB_SauP_EBHT did not target any of the OMM^{14} strains *in vitro* (von Strempel et al., 2023).

The results revealed no significant difference in *S.* Tm^{avir} loads between the control group ($p = 0.42$) and those treated with phage vB_SauP_EBHT **(Fig 34B**), indicating that the phage treatment alone did not modify susceptibility to *S.* Tm colonization. Also, loads of *E. coli* Mt1B1 and *E. faecalis* KB1 determined by plating remained unaffected by the addition of the phage (**Fig 34CD**). Phage loads were determined via spot assays on *S. aureus*, but were only detectable in low numbers at day 1 p.c. **(Fig 34E),** confirming the expectation that the phage was not able to replicate in absence of its originate host bacterium (von Strempel et al., 2023).

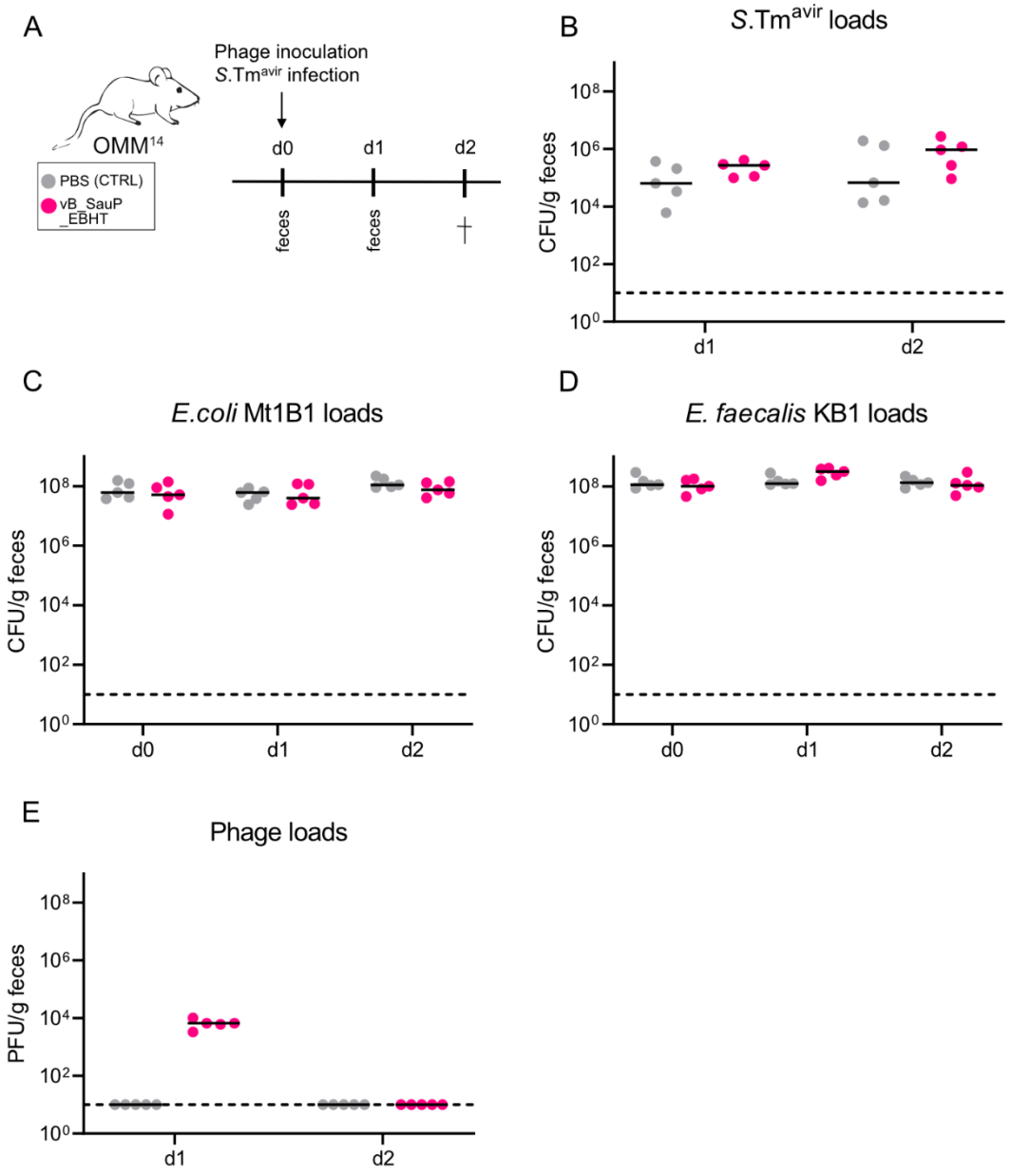

Fig. 34: Treatment with an unspecific phage does not impair the colonization resistance against S. Tm^{avir}

(A) Experimental setup: OMM^{14} mice were challenged orally with phage vB_SauP_EBHT (10^7 PFU) or PBS as a control and at the same time challenged with S. Tm^{avir} ($5x10^7$ CFU). Feces were taken every day and mice were sacrificed on day 2 p. i.. (B) S. Tm^{avir} loads, (C) *E. coli* Mt1B1 loads and (D) *E. faecalis* KB1 loads were monitored via plating. (E) phage loads were determined via spot assays on *S. aureus*. Each dot represents one mouse, black line indicates median, dotted lines indicate DTL**.**

Figure and figure legend modified from von Strempel et al., 2023.

4.4.6 Phages targeting strictly anaerobic members of the OMM^{14} also show an effect on their hosts *in vivo* without disturbing the community

We next wanted to characterize the other two phages I isolated on two members of the OMM^{14} *in vivo* regarding their ability to target their host bacteria and their impact on the overall community. For this, I took mice that are stably colonized with the OMM^{14} and gavaged them with a single phage (vB_ccl_YL32, targeting *E. clostridioformis* YL32 or vB_cin_I46, targeting *C. innocuum* I46, 1x10^{7} PFU in 100µL PBS) or 100µL PBS (**Fig 35A**). Feces for qPCR were taken on day 1-4 p.c. and mice were sacrificed on day 7. *E. clostridioformis* is present in high numbers in the mouse gut. When phage vB_ccl was added, no effect was detectable until day 2 p.c.. On day 3, a slight but significant drop in the phage treatment group can be detected, which is not observed at day 7 anymore. Although the effect on the bacterial host is not as pronounced as for the other phages tested in this study, strain specific qPCR showed that phage vB_ccl was present in the gut in high numbers for the time of the experiment (**Fig 35D**). For *C. innocuum,* no significant effect of the phage on the bacterial loads could be detected in the feces (**Fig 35C**). Surprisingly, qPCR data revealed, that the corresponding phage was still able to replicate in the gut and was detectable for the time of the experiment **(Fig 35D**). Furthermore, the addition of the respective other phage did not affect the abundance of neither of the two strains.

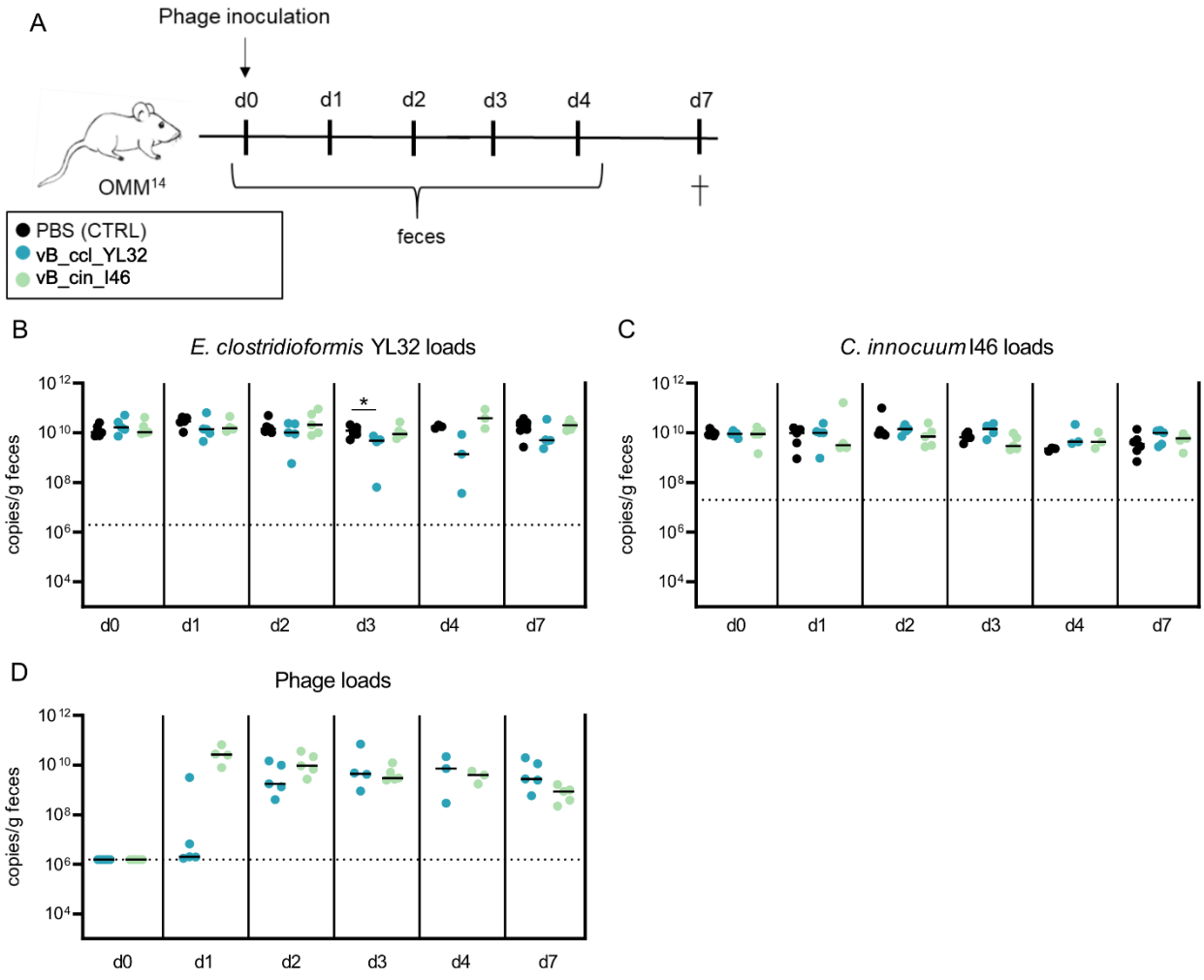

Fig. 35: Phages vB_cin and vB_ccl are able to amplify in the gut

(A) Experimental setup, OMM^{14} mice were challenged orally with phage vB_ccl or vB_cin or PBS as control (10^7 PFU per phage) and feces were collected every day. On day 7 post phage challenge (p.c.), the mice were sacrificed. (B) *E. clostridioformis* loads, (C) *C. innocuum* and (D) phage loads were determined by qPCR in fecal samples at different time points p.c.. Statistical analysis was performed using the Mann-Whitney Test comparing the treatment groups (N=5) against the control group (N=5) (* $p<0.05$, ** $p<0.01$, *** $p<0.001$). Each dot represents one mouse, black lines indicate median, dotted lines indicate limit of detection.

Figure legend modified from von Strempel et al., 2023.

The absolute abundance of the other members of the OMM^{14} community showed no significant changes in the treatment groups compared to the control. qPCR data showed, that already on day 0 some fluctuations can be detected within the treatment groups, which is to be expected in mice (**Fig 27A**) but this did not change with time or with treatment (**Fig 27BC**).

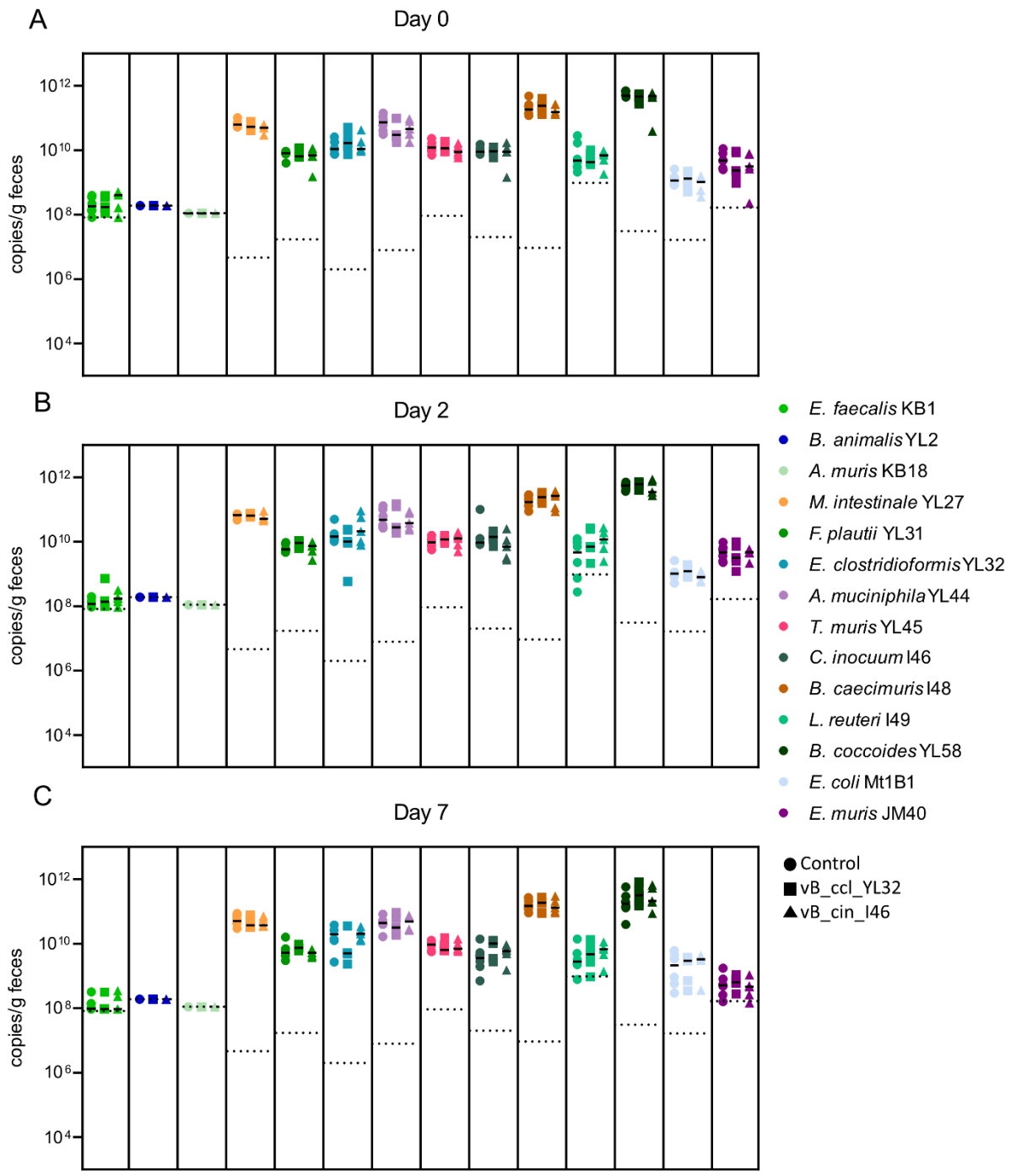

Fig. 36: Abundance of OMM[14] community member in feces

Absolute abundances of all 14 bacteria from the experiment shown in Fig. 35, determined by strain-specific qPCR on day 0 (A), 2 (B) and day 7 p. c. (C). Each color represents one bacterial strain, different shapes represent different experimental groups. Each dot represents one mouse, black line indicates median, dotted lines indicate DTL.

Figure legend modified from von Strempel et al., 2023.

5. Discussion

Phages are the predominant entity in the gut microbiome (Breitbart et al., 2008; Guerin & Hill, 2020) and get taken up continuously via the ingestion of food and drinks. Most of the phages in the gut follow a lysogenic lifestyle, but also virulent phages stably co-exist with their bacterial hosts over long periods of time and thereby play an important role in shaping bacterial communities (De Sordi, Khanna, & Debarbieux, 2017; Marbouty, Thierry, Millot, & Koszul, 2021). Most of our knowledge on phages in the gut stems from large metagenomic data sets, but there are only few experimental studies addressing the functional role of phages in managing bacterial populations, impacting the host and overall microbiome functionality.

In my thesis, I generated experimental tools and a model system to study the impact of virulent phages on a synthetic bacterial gut community. Therefore, I isolated phages for bacterial members of the Oligo Mouse Microbiota (OMM) syncom and characterized them with respect to their phylogeny, morphology and impact on bacterial growth. Further, I developed methods for specific absolute quantification to validate the abundance of the single phages and their target bacteria within a bacterial community in different setups.

Using this system, I showed, that virulent phages exhibit very different plaque morphologies, genomic features and lysis behaviors. Via specific absolute quantification I saw, that not all phages amplify equally well in the gut. Further, I showed that virulent phages transiently reduce their bacterial target population, followed by co-existence over longer times. This first drop in abundance generated niches in the gut that alleviated colonization resistance (CR) and allowed invasion of pathogens. This effect could also be shown when phages and their host bacteria stably co-exist.

Overall, my work established a novel toolbox to target and manipulate the microbiome and to allow experimental testing of hypothesis derived from metagenomics data. I showed the functional importance of phages in generating transient invasion niches in the microbiome which impacts colonization resistance.

5.1 Diversity and phylogeny of the isolated phages

5.1.1 Characterization *In vitro*

Characterization *in vitro* revealed, that the three phages targeting *E. coli* and *E. faecalis* respectively showed very different qualities regarding their plaque morphology, genomic features, the effect on growth of their bacterial hosts and their host range. This shows, in accordance to recent publications (Dion, Oechslin, & Moineau, 2020; Sausset, Petit, Gaboriau-Routhiau, & De Paepe, 2020), that phages can exhibit variable characteristics although isolated on the same bacterial host.

Phages targeting *E. faecalis* have been isolated and characterized before since this bacterium can cause health threads in food and become pathogenic in humans. Therefore, phages have already been considered promising tools to specifically target harmful *Enterococci* since most of them are considered harmless commensals (Rodriguez-Lucas & Ladero, 2023). Phage therapy was already successful in some studies, for example in removing *E. faecalis* biofilm on the surface from chicken meat (Jin et al., 2023). Nevertheless, functional studies on how *E. faecalis* phages behave in the gut are still missing.

For *E. coli*, there are also many phages already isolated and characterized with bacteriophage T4 being one of the model phages for research (Barry & Alberts, 1994). While many *E. coli* strains are part of the normal flora of the intestine, some strains can cause disease in humans and animals and the idea to treat these infections with phages was made already quite early. Several studies could already successfully show that especially *E. coli* induced urinary tract infections can be treated with phages (Bhargava et al., 2023).

While many virulent phages could be isolated for *E. coli* and *E. faecalis*, only two virulent phages could be isolated for the remaining OMM members, namely *C. inocuum* and *E. clostridioformis* respectively, from sewage water. Reasons for that can be the anaerobic metabolism of the bacteria (Hernandez & Vives, 2020) and low density of phages targeting these bacteria in the sewage water. In general, only little phages targeting obligate anaerobic gut bacteria have been isolated and described.

The vast majority of phages targeting anaerobic gut bacteria occurs in the genus *Clostridium*, especially in clinically important species as *C. perfringens* and *C. difficile* where phages are isolated to target and decrease pathogenic bacteria (Hargreaves & Clokie, 2015; Seal, 2013). Besides, several OMM strains encode one or more prophages, which show different activity *in*

vitro and *in vivo* (Lamy-Besnier et al., 2023). Prophages can protect their host from additional phage infections, which might further hinder the process of isolating virulent phages for these bacteria.

All of the phages targeting *E. coli*, *E. faecalis* and *E. clostridioformis* exhibited clear plaques, which is typical for virulent phages. Plaques formed by vB_cin were very small surrounded by a halo and therefore not clearly distinguishable if they were clear or rather turbid. Turbid plaques may indicate the ability to lysogenize the host cells (Jiang, Kellogg, & Paul, 1998). Phage P3 shows characteristics of a "bulls-eye" plaque morphology, forming plaques with greater turbidity towards the plaque peripheries. This might be a consequence of decreasing lytic efficiency caused by aging of the bacterial lawn (Jurczak-Kurek et al., 2016), which is consistent with our observations *in vivo*, where this phage shows the lowest abundance and therefore allegedly the lowest infection efficiency. Phage Str2 and P10 exhibited a halo (semi-transparent zone) around clear plaques. This could stem from phage-derived soluble enzymes which diffuse around the plaque and destroy the cell envelope from neighboring cells (Jurczak-Kurek et al., 2016). Further, plaque size is known to correlate with the head size of the phages, resulting in phages with bigger heads forming smaller plaques because they diffuse more slowly in the bacterial lawn (Jurczak-Kurek et al., 2016). Phage Str1 and vB_ccl exhibited small plaques, and the EM picture revealed structure of a siphoviridae with a big head for both phages, supporting this hypothesis. Further, phage Str2, which forms much bigger plaques, has a smaller head when imaged via EM. Unfortunately, no EM pictures could be obtained for the phages targeting *E. coli*, but phage P17, which formed the smallest plaques, showed the biggest genome with 150kb, which might lead to a bigger head, therefore also matching the hypothesis.

Next, the phages were characterized regarding their lysis behavior on their bacterial host in liquid culture. When added separately, the phages targeting *E. coli* did not exhibit extremely different lysis behaviors. Notably, the strongest effect on the growth was detected when the phages were added together. Nevertheless, *E. coli* showed fast adaption to the phage predation and exhibited growth after few hours, although the optical density did not resemble the control. This fast adaptation hints towards resistance mechanisms that the bacteria can acquire in an easy and fast way, like point mutations in genes encoding for surface receptors (Chapman-McQuiston & Wu, 2008), for example OmpC, which was characterized as a primary receptor during phage infection in *E. coli* before (Yu & Mizushima, 1982). Further, variation of receptor molecules (Porter et al., 2020) or other mechanisms including translational changes of proteins which are important for phage infection and attachment can lead to resistance. This is supported

by the fact, that the bacterial growth is still impaired by the phage and did not recover completely, indicating a fitness defect on cost of the phage resistance which was already seen before for *E. coli* (Mangalea & Duerkop, 2020). Nevertheless, more work would be needed to proof the emergence of these mutations and if they have an impact on the fitness of the bacteria. Further, the three phages exhibited differently broad host ranges when tested on a variety of *E. coli* isolates, indicating that although their lysis behavior seemed to be similar in the liquid culture, their infection mechanism might still vary a lot.

For the three phages targeting *E. faecalis*, similar results can be seen. In enterococci, the enterococcal polysaccharide antigen has been proposed as a phage receptor necessary for phage adsorption, and mutations in genes encoding for this antigen reduce phage adsorption and efficiency (Teng, Singh, Bourgogne, Zeng, & Murray, 2009), which might explain the fast adaption of *E. faecalis* to the phage predation in our experiments. When all three phages are added together, the lysis curve resembles very much the curve of phage Str1 alone. This phage exhibits the fastest and strongest lysis on its host, which might impose a strong selection on *E. faecalis* to develop phage resistance (Koonjan, Cardoso Palacios, & Nilsson, 2022), explaining the high up growth after almost complete depletion by the phage and the fact that the phage cocktail did not show a stronger impact on growth then the phage alone. Also, these phages exhibited different host ranges when tested on several *Enterococcus* isolates. Interestingly, phage Str1 only infected its host strain KB1, although it exhibited the strongest lysis of all three phages. Since we saw fast adaptation of *E. faecalis* in liquid culture, resistance against this phage might already be widespread in several *Enterococci*. Further investigation would be needed to evaluate this, like sequencing of the isolates to find specific phage-resistance related mutations.

Although vB_cin and vB_ccl exhibited clearly visible plaques on their hosts, their effect on growth in liquid culture was weak compared to the other phages isolated in this study. A typical lysis curve, as observed for the majority of virulent phages, could not be observed and growth in general was only slightly affected by addition of the phage. This might be due to slower growth rates of the host bacteria but also lysis and infection features of the phages. The genomes of these phages could only be poorly annotated, showing that there is still little known about phages targeting strictly anaerobic gut bacteria. Nevertheless, we were able to also establish a strain specific qPCR for these phages to be able to track them in the gut which is useful for further applications.

5.1.2 Characterization in batch culture and i*n vivo*

We divided phage infection in our experimental setups in two phases. First, the acute infection phase (1-4 days post challenge), where a transient reduction of the bacterial target population can be observed. The second phase is characterized by stable co-existence of phages and bacteria until day 7 p. c. in the gut.

While all phages targeting *E. coli* and *E. faecalis* could be detected using specific qPCR in the *in vitro* batch culture experiments, abundance of the three different phages in each cocktail differed vastly in the murine gut. In the phage cocktail targeting *E. coli*, phage P10 dominated at all time points whereas the loads of the other two phages rapidly decreased after inoculation. The abundance of the three phages targeting *E. faecalis* also differed between the batch culture *in vitro* and the mouse gut *in vivo*, but all phages could be detected with qPCR in the mouse gut until day 7 p. c.. Different abundances of the phages may be due to burst size, lysis efficiency and selection of phage-resistant mutants, showing the different abilities of the individual phages to infect and amplify and the differences between the simple environment *in vitro* and the complex gut, as well as the different evading mechanisms of the bacteria in different environments (Shkoporov & Hill, 2019). In an *in vitro* system, coevolution normally ends in the emergence of a resistant bacterial phenotype that the phages cannot overcome. Resistance in these laboratory environments emerges from *de novo* mutations most of the times, causing modifications of bacterial surface molecules that are targeted by the phage, therefore preventing phage attachment (Dennehy, 2012). In complex environments like soil or the gut, previous studies showed, that neither the bacteria nor the phage become more resistant or infective over time. One explanation is, that resistance in complex environments is more costly and would lead to a decreased fitness of the bacterium, leading to fluctuating dynamics and co-existence rather than depletion of the bacteria or the phages (Gomez & Buckling, 2013) which explains the different abundances of the single phages in our setups. To further look into the interactions of the phages and their respective bacteria in our system, more experiments need to be conducted, as for example evaluating the emergence of resistance in the targeted bacterial population and fitness of these strains. Furthermore, the differences between the experimental setups show, that it might not be enough to characterize phages only on their lysis behaviors *in vitro*, since the abundances and effect on their hosts differ between the diverse environments. Before using phages as tools for targeted microbiome manipulation, this needs to be further evaluated.

5.1.3 Phage-bacteria co-existence

Although absolute abundances of the single phages in the phage cocktails varied, I observed stable coexistence of phage P10, Str1, Str2 and Str6 with their host strains *E. coli* and *E. faecalis* respectively in the mouse gut for 9 days. Phages vB_cin and vB_ccl showed no strong effect on their hosts when added to mice colonized with the OMM^{14} as already seen *in vitro*, only a slight decrease of *E. clostridioformis* YL32 can be detected on day 2 p.c.. Nevertheless, via qPCR I could show, that the phages are still able to amplify and persist in the gut for 7 days, also co-existing with their bacterial hosts.

Stable co-existence of phages and their host bacteria in the gut can be mediated by several different mechanisms, one being that the mucus layer can serve as a spatial refuge for part of the host bacterial population by harboring phage-inaccessible sites (Lourenco et al., 2020). Another mechanism is, that bacterial populations can differentially regulate their gene expression to escape phage predation in the gut, which can lead to coexistence (Lourenco et al., 2022) by allowing part of the population to become infected and killed by the virus, while the other part stays uninfected. Further, phages can adapt to the mucosal environment via de novo mutations, which can facilitate phage adherence to the mucus, providing a fitness advantage against the non-mutated phage, also supporting phage-bacteria co-existence (Chin et al., 2022). Our observations, an immediate decrease in bacterial abundance followed by a co-existence, might be the result of coevolution of the phages and their respective bacteria, as a result of phage adaptation to the bacterial population and the environment in the gut and bacterial response to phage-mediated selection. In the gut, this can promote high levels of population diversity in terms of bacterial resistance and phage infectivity and therefore foster co-existence (Koskella & Brockhurst, 2014).

All in all, these results show the importance to functionally characterize phages to understand their role on the microbiome. *In vitro* studies might reveal certain characteristics and lysis behaviors, but more complex setups are needed to fully understand the interaction with phages and their hosts within a bacterial community. Before using phages as therapeutic agents to target specific bacteria in the gut, it is important to evaluate their ability to infect their host in a complex system and the lysis behavior when added together with other phages in a cocktail. Moreover, bacterial response to phage predation needs to be further evaluated *in vivo*, with respect to evading mechanisms that lead to co-existence and resistance development.

5.2 Role of phages in alleviating colonization resistance

5.2.1 Influence on colonization resistance in the acute infection phase

We found, that phage-treatment impaired colonization resistance against *S.* Tm both, in the acute phase but also the stable co-existence phase. CR in the OMM^{12} model has been recently studied in detail and is mediated by competition for substrates including C5/C6 sugars, oxygen and electron acceptors for anaerobic respiration (Eberl et al., 2021). As shown in a previous study, OMM^{11} mice lacking *S.* Tm competitors *E. coli* Mt1B1 or *E. faecalis* KB1 exhibit strongly reduced CR (Eberl et al., 2021). Thus, that transient reduction of these two species in the acute phase of phage infection might lead to a short-term increase in substrate availability opening a nutrient niche for pathogen invasion. The concept of this theory is, that the nutrient landscape determines whether an organism can successfully colonize and persist in the gut. An invading organism can only stay in an existing and evolved community if it is able to utilize one or a few limiting nutrients more efficiently than its competitors. If that is not possible, a nutrient niche needs to be opened to enable establishment of an invading organism in the community (Pereira & Berry, 2017). In support of the idea, the degree of reduction of the target population in this study correlates indirectly with increase in pathogen loads, again supporting the nutrient-niche theory. Further, the absolute abundance of the other OMM^{14} members did not change in the mouse gut after addition of $3\Phi^{Mt1B1}$ and $3\Phi^{KB1}$, showing that the impaired colonization resistance is only dependent on the decrease of the targeted bacteria *E. coli* and *E. faecalis*.

Of note, the simultaneous application of both phage cocktails let to a reduction of both *E. coli* Mt1B1 and *E. faecalis* KB1 as observed previously but this only resulted in slight elevation of *S.* Tm loads at day 1 p.i. and did not strongly affect loads at day 2 p.i. compared to the treatment with the single phage cocktails. Overall, this suggested that the effect of phage cocktails on colonization resistance is not additive in our employed system. One explanation might be, that *S.* Tm only uses the free nutrients that can be utilized most efficiently, even if more free nutrients are available. Further, in this experimental setup, several OMM^{14} members showed higher abundances in the phage treatment group which might lead to less free nutrients in the mouse gut which counteracts the up growth of *S.* Tm.

Besides phage-induced changes in the microbiota, there are several other factors that can impact colonization resistance. Antibiotic-mediated disruption of the microbiota for example leads to transiently increases levels of free sugars which can be exploited by pathogens (Ng et al., 2013)

and a high-fat diet causing bile acid release and microbiota dysbiosis can also facilitate pathogen invasion (Wotzka et al., 2019). However, this can be excluded as factors influencing colonization resistance in this study, since all experiments are conducted in a controlled environment.

For a wildtype *S.* Tm strain which was previously shown to trigger gut inflammation within 3 days of infection in gnotobiotic mice (Eberl et al., 2021), we observed a faster onset of gut inflammation in case of treatment with the *E. faecalis* cocktail $3\Phi^{KB1}$ but not $3\Phi^{Mt1B1}$. The varying impact of phages on an avirulent versus wildtype *S.* Tm infections could be attributed to the utilization of different niches by both *S.* Tm and *E. coli* in the healthy versus inflamed intestine. In general, the invasion of *S.* Tm in the gut stimulates a complex cascade of immune responses in the host (Wotzka, Nguyen, & Hardt, 2017), which efficiently reduces *S.* Tm tissue loads, but the intestinal environment is drastically changed by the resulting inflammation which leads to dysbiosis and blooming of *Enterobacteriaceae* (Stecher, 2015; Stecher et al., 2007), which explains why the effect of the phage cocktail on *E. coli* is not as efficient under inflamed conditions. In addition, a general increase in *E. coli* abundance corresponding to the increase in inflammation can be seen in this setup, supporting this theory. Moreover, the respiratory growth facilitates *S.* Tm to metabolize otherwise unfavored carbon sources such as ethanolamine, propanediol, and succinate (Thiennimitr, Winter, & Baumler, 2012) which might influence the nutritional competition of *S.* Tm with the OMM^{14} community and therefore explain the differences in colonization resistance under normal versus inflamed conditions.

5.2.2 Influence on colonization resistance during co-existence

Surprisingly, at day 7 post phage challenge, mice demonstrated impaired colonization resistance even when the phages and their target strains co-existed steadily in the gut and no effect on bacterial loads was detected anymore. This suggest mechanisms to be involved that also act independently on the reduction of the loads of competing bacteria. Phages may decrease the target population locally and not evenly throughout the gut (Hoyles et al., 2014), allowing *S.* Tm to invade despite no apparent differences in overall bacterial levels are visible anymore. Furthermore, the presence of phages might induce transcriptional changes in the host strains, resulting in increased resistance against the phages but decreased overall fitness. These might include expression of like anti-phage systems or reconditioning of bacterial metabolism (De Smet et al., 2016) and phage receptors (Lourenco et al., 2022) which might directly or indirectly

affect CR against *S.* Tm. Expansion of bacteriophages is linked to exacerbated colitis by stimulating TLR signaling (Gogokhia et al., 2019), which might also alter bacterial stress or defense responses and impair CR. Also, it is known, that phages can modulate the gut metabolome, which leads to changing metabolite levels (Hsu et al., 2019) and therefore might facilitate *S.* Tm growth even during co-existence.

Taken together, the ingestion of phages in conjunction with pathogen contaminated food or water sources could promote pathogen invasion and consequently, could serve as risk factors for human *Salmonella* infection. Coliphage content in water varies, ranging from $8x10^4$ PFU/100mL in wastewater to 30 PFU/100mL for river source waters (Nappier, Hong, Ichida, Goldstone, & Eftim, 2019), which might be sufficient to target protective bacteria in the gut.

Subsequently, further research will be necessary to elucidate whether the therapeutic application of phage cocktails against multidrug-resistant *E. coli* or *E. faecalis* strains might also facilitate pathogen invasion in the human host. As such, applications should be approached with caution and further evaluation will be needed.

In summary, this work elucidated the role of virulent phages on their bacterial hosts and important community functions in the gut. The results indicate, that phages are effectively influencing the abundance of their host bacteria in the gut which is a great basis for further research aiming to evaluate the future use of phages to specifically target and manipulate the microbiome.

5.3 Future perspectives

To further characterize virulent phages and their role on bacterial communities in the gut, it is important to elucidate the mechanism underlying stable co-existence. This can be done by investigating how part of the bacterial population escapes phage predation, if resistance is arising and how phages evolve to persist in the gut. This might then help to disentangle the factors which impair colonization resistance not only during acute infection phase but also during co-existence and further helps to disentangle factors influencing *Salmonella* infection.

Moreover, using phages to facilitate invasion of novel, potentially beneficial bacteria might be a great tool for microbiome engineering. Establishing new strains in a complex community is often prevented as nutrient niches are already occupied by autochthonous bacteria. In this work

I could show, that phages could be a promising tool to mediate strain invasion which might be exploited to mediate introduction of beneficial bacteria in the microbiome.

Further, isolating and characterizing more phages targeting anaerobic gut bacteria might help to understand more of the general interactions of phages and bacteria in the gut and help to disentangle how phages influence and shape bacterial communities.

6. References

Ackermann, H. W. (1992). Frequency of morphological phage descriptions. *Arch Virol, 124*(3-4), 201-209. doi:10.1007/BF01309802

Ackermann, H. W. (2001). Frequency of morphological phage descriptions in the year 2000. Brief review. *Arch Virol, 146*(5), 843-857. doi:10.1007/s007050170120

Afrizal Afrizal, S. A. V. J., Thomas C. A. Hitch, Thomas Riedel, Marijana Basic, Atscharah Panyot, Nicole Treichel, Fabian T. Hager, Ramona Brück, Erin Oi-Yan Wong, Alexandra von Strempel, Claudia Eberl, Eva M. Buhl, Birte Abt, André Bleich, René Tolba, William W. Navarre, View ORCID ProfileFabian Kiessling, Hans-Peter Horz, Natalia Torow, Vuk Cerovic, Bärbel Stecher, Till Strowig, Jörg Overmann, Thomas Clavel. (2022). Enhanced cultured diversity of the mouse gut microbiota enables custom-made synthetic communities. *Cell Host Microbe*. doi:10.1016/j.chom.2022.09.011

Alavi, S., Mitchell, J. D., Cho, J. Y., Liu, R., Macbeth, J. C., & Hsiao, A. (2020). Interpersonal Gut Microbiome Variation Drives Susceptibility and Resistance to Cholera Infection. *Cell, 181*(7), 1533-1546 e1513. doi:10.1016/j.cell.2020.05.036

Almeida, G. M. F., Laanto, E., Ashrafi, R., & Sundberg, L. R. (2019). Bacteriophage Adherence to Mucus Mediates Preventive Protection against Pathogenic Bacteria. *mBio, 10*(6). doi:10.1128/mBio.01984-19

Antimicrobial Resistance, C. (2022). Global burden of bacterial antimicrobial resistance in 2019: a systematic analysis. *Lancet, 399*(10325), 629-655. doi:10.1016/S0140-6736(21)02724-0

Appleton, J. (2018). The Gut-Brain Axis: Influence of Microbiota on Mood and Mental Health. *Integr Med (Encinitas), 17*(4), 28-32. Retrieved from https://www.ncbi.nlm.nih.gov/pubmed/31043907

Asnicar, F., Thomas, A. M., Beghini, F., Mengoni, C., Manara, S., Manghi, P., . . . Segata, N. (2020). Precise phylogenetic analysis of microbial isolates and genomes from metagenomes using PhyloPhlAn 3.0. *Nat Commun, 11*(1), 2500. doi:10.1038/s41467-020-16366-7

Bankevich, A., Nurk, S., Antipov, D., Gurevich, A. A., Dvorkin, M., Kulikov, A. S., . . . Pevzner, P. A. (2012). SPAdes: a new genome assembly algorithm and its applications to single-cell sequencing. *J Comput Biol, 19*(5), 455-477. doi:10.1089/cmb.2012.0021

Barry, J., & Alberts, B. (1994). A role for two DNA helicases in the replication of T4 bacteriophage DNA. *J Biol Chem, 269*(52), 33063-33068. Retrieved from https://www.ncbi.nlm.nih.gov/pubmed/7806534

Bhargava, K., Nath, G., Dhameja, N., Kumar, R., Aseri, G. K., & Jain, N. (2023). Bacteriophage therapy for Escherichia coli-induced urinary tract infection in rats. *Future Microbiol, 18*, 323-334. doi:10.2217/fmb-2022-0107

Bolger, A. M., Lohse, M., & Usadel, B. (2014). Trimmomatic: a flexible trimmer for Illumina sequence data. *Bioinformatics, 30*(15), 2114-2120. doi:10.1093/bioinformatics/btu170

Boling, L., Cuevas, D. A., Grasis, J. A., Kang, H. S., Knowles, B., Levi, K., . . . Rohwer, F. (2020). Dietary prophage inducers and antimicrobials: toward landscaping the human gut microbiome. *Gut Microbes, 11*(4), 721-734. doi:10.1080/19490976.2019.1701353

Bolsega, S., Bleich, A., & Basic, M. (2021). Synthetic Microbiomes on the Rise-Application in Deciphering the Role of Microbes in Host Health and Disease. *Nutrients, 13*(11). doi:10.3390/nu13114173

Bouras, G., Nepal, R., Houtak, G., Psaltis, A. J., Wormald, P. J., & Vreugde, S. (2023). Pharokka: a fast scalable bacteriophage annotation tool. *Bioinformatics, 39*(1). doi:10.1093/bioinformatics/btac776

Breitbart, M., Haynes, M., Kelley, S., Angly, F., Edwards, R. A., Felts, B., . . . Rohwer, F. (2008). Viral diversity and dynamics in an infant gut. *Res Microbiol, 159*(5), 367-373. doi:10.1016/j.resmic.2008.04.006

Brugiroux, S., Beutler, M., Pfann, C., Garzetti, D., Ruscheweyh, H. J., Ring, D., . . . Stecher, B. (2016). Genome-guided design of a defined mouse microbiota that confers colonization resistance against Salmonella enterica serovar Typhimurium. *Nat Microbiol, 2*, 16215. doi:10.1038/nmicrobiol.2016.215

Buffie, C. G., & Pamer, E. G. (2013). Microbiota-mediated colonization resistance against intestinal pathogens. *Nat Rev Immunol, 13*(11), 790-801. doi:10.1038/nri3535

Camarillo-Guerrero, L. F., Almeida, A., Rangel-Pineros, G., Finn, R. D., & Lawley, T. D. (2021). Massive expansion of human gut bacteriophage diversity. *Cell, 184*(4), 1098-1109 e1099. doi:10.1016/j.cell.2021.01.029

Chapman-McQuiston, E., & Wu, X. L. (2008). Stochastic receptor expression allows sensitive bacteria to evade phage attack. Part I: experiments. *Biophys J, 94*(11), 4525-4536. doi:10.1529/biophysj.107.120212

Chevallereau, A., Pons, B. J., van Houte, S., & Westra, E. R. (2022). Interactions between bacterial and phage communities in natural environments. *Nat Rev Microbiol, 20*(1), 49-62. doi:10.1038/s41579-021-00602-y

Chin, W. H., Kett, C., Cooper, O., Museler, D., Zhang, Y., Bamert, R. S., . . . Barr, J. J. (2022). Bacteriophages evolve enhanced persistence to a mucosal surface. *Proc Natl Acad Sci U S A, 119*(27), e2116197119. doi:10.1073/pnas.2116197119

Clavel, T., Gomes-Neto, J. C., Lagkouvardos, I., & Ramer-Tait, A. E. (2017). Deciphering interactions between the gut microbiota and the immune system via microbial cultivation and minimal microbiomes. *Immunol Rev, 279*(1), 8-22. doi:10.1111/imr.12578

Clavel, T., Lagkouvardos, I., Blaut, M., & Stecher, B. (2016). The mouse gut microbiome revisited: From complex diversity to model ecosystems. *Int J Med Microbiol, 306*(5), 316-327. doi:10.1016/j.ijmm.2016.03.002

Clooney, A. G., Sutton, T. D. S., Shkoporov, A. N., Holohan, R. K., Daly, K. M., O'Regan, O., . . . Hill, C. (2019). Whole-Virome Analysis Sheds Light on Viral Dark Matter in Inflammatory Bowel Disease. *Cell Host Microbe, 26*(6), 764-778 e765. doi:10.1016/j.chom.2019.10.009

Coburn, B., Grassl, G. A., & Finlay, B. B. (2007). Salmonella, the host and disease: a brief review. *Immunol Cell Biol, 85*(2), 112-118. doi:10.1038/sj.icb.7100007

Collaborators, G. B. D. A. R. (2022). Global mortality associated with 33 bacterial pathogens in 2019: a systematic analysis for the Global Burden of Disease Study 2019. *Lancet, 400*(10369), 2221-2248. doi:10.1016/S0140-6736(22)02185-7

D'Herelle, F. (2007). On an invisible microbe antagonistic toward dysenteric bacilli: brief note by Mr. F. D'Herelle, presented by Mr. Roux. 1917. *Res Microbiol, 158*(7), 553-554. doi:10.1016/j.resmic.2007.07.005

Dash, P. K., Gorantla, S., Poluektova, L., Hasan, M., Waight, E., Zhang, C., . . . Gendelman, H. E. (2021). Humanized Mice for Infectious and Neurodegenerative disorders. *Retrovirology, 18*(1), 13. doi:10.1186/s12977-021-00557-1

David, L. A., Maurice, C. F., Carmody, R. N., Gootenberg, D. B., Button, J. E., Wolfe, B. E., . . . Turnbaugh, P. J. (2014). Diet rapidly and reproducibly alters the human gut microbiome. *Nature, 505*(7484), 559-563. doi:10.1038/nature12820

De Smet, J., Zimmermann, M., Kogadeeva, M., Ceyssens, P. J., Vermaelen, W., Blasdel, B., . . . Lavigne, R. (2016). High coverage metabolomics analysis reveals phage-specific alterations to Pseudomonas aeruginosa physiology during infection. *ISME J, 10*(8), 1823-1835. doi:10.1038/ismej.2016.3

De Sordi, L., Khanna, V., & Debarbieux, L. (2017). The Gut Microbiota Facilitates Drifts in the Genetic Diversity and Infectivity of Bacterial Viruses. *Cell Host Microbe, 22*(6), 801-808 e803. doi:10.1016/j.chom.2017.10.010

Dedrick, R. M., Guerrero-Bustamante, C. A., Garlena, R. A., Russell, D. A., Ford, K., Harris, K., . . . Spencer, H. (2019). Engineered bacteriophages for treatment of a patient with a disseminated drug-resistant Mycobacterium abscessus. *Nat Med, 25*(5), 730-733. doi:10.1038/s41591-019-0437-z

Dennehy, J. J. (2012). What Can Phages Tell Us about Host-Pathogen Coevolution? *Int J Evol Biol, 2012*, 396165. doi:10.1155/2012/396165

Dion, M. B., Oechslin, F., & Moineau, S. (2020). Phage diversity, genomics and phylogeny. *Nat Rev Microbiol, 18*(3), 125-138. doi:10.1038/s41579-019-0311-5

Dohnalova, L., Lundgren, P., Carty, J. R. E., Goldstein, N., Wenski, S. L., Nanudorn, P., . . . Thaiss, C. A. (2022). A microbiome-dependent gut-brain pathway regulates motivation for exercise. *Nature, 612*(7941), 739-747. doi:10.1038/s41586-022-05525-z

Dzunkova, M., Low, S. J., Daly, J. N., Deng, L., Rinke, C., & Hugenholtz, P. (2019). Defining the human gut host-phage network through single-cell viral tagging. *Nat Microbiol, 4*(12), 2192-2203. doi:10.1038/s41564-019-0526-2

Eberl, C., Ring, D., Munch, P. C., Beutler, M., Basic, M., Slack, E. C., . . . Stecher, B. (2019). Reproducible Colonization of Germ-Free Mice With the Oligo-Mouse-Microbiota in Different Animal Facilities. *Front Microbiol, 10*, 2999. doi:10.3389/fmicb.2019.02999

Eberl, C., Weiss, A. S., Jochum, L. M., Durai Raj, A. C., Ring, D., Hussain, S., . . . Stecher, B. (2021). E. coli enhance colonization resistance against Salmonella Typhimurium by competing for galactitol, a context-dependent limiting carbon source. *Cell Host Microbe, 29*(11), 1680-1692 e1687. doi:10.1016/j.chom.2021.09.004

European Food Safety, A., European Centre for Disease, P., & Control. (2022). The European Union One Health 2021 Zoonoses Report. *EFSA J, 20*(12), e07666. doi:10.2903/j.efsa.2022.7666

Fan, Y., & Pedersen, O. (2021). Gut microbiota in human metabolic health and disease. *Nat Rev Microbiol, 19*(1), 55-71. doi:10.1038/s41579-020-0433-9

Federici, S., Kredo-Russo, S., Valdes-Mas, R., Kviatcovsky, D., Weinstock, E., Matiuhin, Y., . . . Elinav, E. (2022). Targeted suppression of human IBD-associated gut microbiota commensals by phage consortia for treatment of intestinal inflammation. *Cell, 185*(16), 2879-2898 e2824. doi:10.1016/j.cell.2022.07.003

Feuerstein, R., Forde, A. J., Lohrmann, F., Kolter, J., Ramirez, N. J., Zimmermann, J., . . . Henneke, P. (2020). Resident macrophages acquire innate immune memory in staphylococcal skin infection. *Elife, 9*. doi:10.7554/eLife.55602

Fischer, F., Romero, R., Hellhund, A., Linne, U., Bertrams, W., Pinkenburg, O., . . . Steinhoff, U. (2020). Dietary cellulose induces anti-inflammatory immunity and transcriptional programs via maturation of the intestinal microbiota. *Gut Microbes, 12*(1), 1-17. doi:10.1080/19490976.2020.1829962

Forslund, K., Hildebrand, F., Nielsen, T., Falony, G., Le Chatelier, E., Sunagawa, S., . . . Pedersen, O. (2015). Disentangling type 2 diabetes and metformin treatment signatures in the human gut microbiota. *Nature, 528*(7581), 262-266. doi:10.1038/nature15766

Freedberg, D. E., Toussaint, N. C., Chen, S. P., Ratner, A. J., Whittier, S., Wang, T. C., . . . Abrams, J. A. (2015). Proton Pump Inhibitors Alter Specific Taxa in the Human Gastrointestinal Microbiome: A Crossover Trial. *Gastroenterology, 149*(4), 883-885 e889. doi:10.1053/j.gastro.2015.06.043

Garzetti, D., Brugiroux, S., Bunk, B., Pukall, R., McCoy, K. D., Macpherson, A. J., & Stecher, B. (2017). High-Quality Whole-Genome Sequences of the Oligo-Mouse-Microbiota Bacterial Community. *Genome Announc, 5*(42). doi:10.1128/genomeA.00758-17

Goehler, L. E., Gaykema, R. P., Opitz, N., Reddaway, R., Badr, N., & Lyte, M. (2005). Activation in vagal afferents and central autonomic pathways: early responses to intestinal infection with Campylobacter jejuni. *Brain Behav Immun, 19*(4), 334-344. doi:10.1016/j.bbi.2004.09.002

Gogokhia, L., Buhrke, K., Bell, R., Hoffman, B., Brown, D. G., Hanke-Gogokhia, C., . . . Round, J. L. (2019). Expansion of Bacteriophages Is Linked to Aggravated Intestinal Inflammation and Colitis. *Cell Host Microbe, 25*(2), 285-299 e288. doi:10.1016/j.chom.2019.01.008

Gomez, P., & Buckling, A. (2013). Coevolution with phages does not influence the evolution of bacterial mutation rates in soil. *ISME J, 7*(11), 2242-2244. doi:10.1038/ismej.2013.105

Gregory, A. C., Zablocki, O., Zayed, A. A., Howell, A., Bolduc, B., & Sullivan, M. B. (2020). The Gut Virome Database Reveals Age-Dependent Patterns of Virome Diversity in the Human Gut. *Cell Host Microbe, 28*(5), 724-740 e728. doi:10.1016/j.chom.2020.08.003

Guerin, E., & Hill, C. (2020). Shining Light on Human Gut Bacteriophages. *Front Cell Infect Microbiol, 10*, 481. doi:10.3389/fcimb.2020.00481

Guerrero, L. D., Perez, M. V., Orellana, E., Piuri, M., Quiroga, C., & Erijman, L. (2021). Long-run bacteria-phage coexistence dynamics under natural habitat conditions in an environmental biotechnology system. *ISME J, 15*(3), 636-648. doi:10.1038/s41396-020-00802-z

Guigoz, Y., Dore, J., & Schiffrin, E. J. (2008). The inflammatory status of old age can be nurtured from the intestinal environment. *Curr Opin Clin Nutr Metab Care, 11*(1), 13-20. doi:10.1097/MCO.0b013e3282f2bfdf

Hargreaves, K. R., & Clokie, M. R. (2015). A Taxonomic Review of Clostridium difficile Phages and Proposal of a Novel Genus, "Phimmp04likevirus". *Viruses, 7*(5), 2534-2541. doi:10.3390/v7052534

Heilmann, S., Sneppen, K., & Krishna, S. (2012). Coexistence of phage and bacteria on the boundary of self-organized refuges. *Proc Natl Acad Sci U S A, 109*(31), 12828-12833. doi:10.1073/pnas.1200771109

Hernandez, S., & Vives, M. J. (2020). Phages in Anaerobic Systems. *Viruses, 12*(10). doi:10.3390/v12101091

Herp, S., Brugiroux, S., Garzetti, D., Ring, D., Jochum, L. M., Beutler, M., . . . Stecher, B. (2019). Mucispirillum schaedleri Antagonizes Salmonella Virulence to Protect Mice against Colitis. *Cell Host Microbe, 25*(5), 681-694 e688. doi:10.1016/j.chom.2019.03.004

Hoffmann, C., Dollive, S., Grunberg, S., Chen, J., Li, H., Wu, G. D., . . . Bushman, F. D. (2013). Archaea and fungi of the human gut microbiome: correlations with diet and bacterial residents. *PLoS One, 8*(6), e66019. doi:10.1371/journal.pone.0066019

Hoiseth, S. K., & Stocker, B. A. (1981). Aromatic-dependent Salmonella typhimurium are non-virulent and effective as live vaccines. *Nature, 291*(5812), 238-239. doi:10.1038/291238a0

Hou, K., Wu, Z. X., Chen, X. Y., Wang, J. Q., Zhang, D., Xiao, C., . . . Chen, Z. S. (2022). Microbiota in health and diseases. *Signal Transduct Target Ther, 7*(1), 135. doi:10.1038/s41392-022-00974-4

Howe, A., Ringus, D. L., Williams, R. J., Choo, Z. N., Greenwald, S. M., Owens, S. M., . . . Chang, E. B. (2016). Divergent responses of viral and bacterial communities in the gut microbiome to dietary disturbances in mice. *ISME J, 10*(5), 1217-1227. doi:10.1038/ismej.2015.183

Hoyles, L., McCartney, A. L., Neve, H., Gibson, G. R., Sanderson, J. D., Heller, K. J., & van Sinderen, D. (2014). Characterization of virus-like particles associated with the human faecal and caecal microbiota. *Res Microbiol, 165*(10), 803-812. doi:10.1016/j.resmic.2014.10.006

Hsu, B. B., Gibson, T. E., Yeliseyev, V., Liu, Q., Lyon, L., Bry, L., . . . Gerber, G. K. (2019). Dynamic Modulation of the Gut Microbiota and Metabolome by Bacteriophages in a Mouse Model. *Cell Host Microbe, 25*(6), 803-814 e805. doi:10.1016/j.chom.2019.05.001

Human Microbiome Project, C. (2012). Structure, function and diversity of the healthy human microbiome. *Nature, 486*(7402), 207-214. doi:10.1038/nature11234

Hyatt, D., Chen, G. L., Locascio, P. F., Land, M. L., Larimer, F. W., & Hauser, L. J. (2010). Prodigal: prokaryotic gene recognition and translation initiation site identification. *BMC Bioinformatics, 11*, 119. doi:10.1186/1471-2105-11-119

Jiang, S. C., Kellogg, C. A., & Paul, J. H. (1998). Characterization of marine temperate phage-host systems isolated from Mamala Bay, Oahu, Hawaii. *Appl Environ Microbiol, 64*(2), 535-542. doi:10.1128/AEM.64.2.535-542.1998

Jin, X., Sun, X., Wang, Z., Dou, J., Lin, Z., Lu, Q., . . . Luo, Q. (2023). Virulent Phage vB_EfaS_WH1 Removes Enterococcus faecalis Biofilm and Inhibits Its Growth on the Surface of Chicken Meat. *Viruses, 15*(5). doi:10.3390/v15051208

Johnson, L. S., Eddy, S. R., & Portugaly, E. (2010). Hidden Markov model speed heuristic and iterative HMM search procedure. *BMC Bioinformatics, 11*, 431. doi:10.1186/1471-2105-11-431

Jurczak-Kurek, A., Gasior, T., Nejman-Falenczyk, B., Bloch, S., Dydecka, A., Topka, G., . . . Wegrzyn, A. (2016). Biodiversity of bacteriophages: morphological and biological properties of a large group of phages isolated from urban sewage. *Sci Rep, 6*, 34338. doi:10.1038/srep34338

Kim, S., Covington, A., & Pamer, E. G. (2017). The intestinal microbiota: Antibiotics, colonization resistance, and enteric pathogens. *Immunol Rev, 279*(1), 90-105. doi:10.1111/imr.12563

Kohler, T., Luscher, A., Falconnet, L., Resch, G., McBride, R., Mai, Q. A., . . . van Delden, C. (2023). Personalized aerosolised bacteriophage treatment of a chronic lung infection due to multidrug-resistant Pseudomonas aeruginosa. *Nat Commun, 14*(1), 3629. doi:10.1038/s41467-023-39370-z

Koonjan, S., Cardoso Palacios, C., & Nilsson, A. S. (2022). Population Dynamics of a Two Phages-One Host Infection System Using Escherichia coli Strain ECOR57 and Phages vB_EcoP_SU10 and vB_EcoD_SU57. *Pharmaceuticals (Basel), 15*(3). doi:10.3390/ph15030268

Korf, I. H. E., Meier-Kolthoff, J. P., Adriaenssens, E. M., Kropinski, A. M., Nimtz, M., Rohde, M., . . . Wittmann, J. (2019). Still Something to Discover: Novel Insights intoEscherichia coli Phage Diversity and Taxonomy. *Viruses, 11*(5). doi:10.3390/v11050454

Koskella, B., & Brockhurst, M. A. (2014). Bacteria-phage coevolution as a driver of ecological and evolutionary processes in microbial communities. *FEMS Microbiol Rev, 38*(5), 916-931. doi:10.1111/1574-6976.12072

Kreuzer, M., & Hardt, W. D. (2020). How Food Affects Colonization Resistance Against Enteropathogenic Bacteria. *Annu Rev Microbiol, 74*, 787-813. doi:10.1146/annurev-micro-020420-013457

Lagkouvardos, I., Pukall, R., Abt, B., Foesel, B. U., Meier-Kolthoff, J. P., Kumar, N., . . . Clavel, T. (2016). The Mouse Intestinal Bacterial Collection (miBC) provides host-specific insight into cultured diversity and functional potential of the gut microbiota. *Nat Microbiol, 1*(10), 16131. doi:10.1038/nmicrobiol.2016.131

Lamy-Besnier, Q., Bignaud, A., Garneau, J. R., Titecat, M., Conti, D. E., Von Strempel, A., . . . Marbouty, M. (2023). Chromosome folding and prophage activation reveal specific genomic architecture for intestinal bacteria. *Microbiome, 11*(1), 111. doi:10.1186/s40168-023-01541-x

Lamy-Besnier, Q., Koszul, R., Debarbieux, L., & Marbouty, M. (2021). Closed and High-Quality Bacterial Genome Sequences of the Oligo-Mouse-Microbiota Community. *Microbiol Resour Announc, 10*(17). doi:10.1128/MRA.01396-20

Letunic, I., & Bork, P. (2007). Interactive Tree Of Life (iTOL): an online tool for phylogenetic tree display and annotation. *Bioinformatics, 23*(1), 127-128. doi:10.1093/bioinformatics/btl529

Loc-Carrillo, C., & Abedon, S. T. (2011). Pros and cons of phage therapy. *Bacteriophage, 1*(2), 111-114. doi:10.4161/bact.1.2.14590

Lourenco, M., Chaffringeon, L., Lamy-Besnier, Q., Pedron, T., Campagne, P., Eberl, C., . . . De Sordi, L. (2020). The Spatial Heterogeneity of the Gut Limits Predation and Fosters Coexistence of Bacteria and Bacteriophages. *Cell Host Microbe, 28*(3), 390-401 e395. doi:10.1016/j.chom.2020.06.002

Lourenco, M., Chaffringeon, L., Lamy-Besnier, Q., Titecat, M., Pedron, T., Sismeiro, O., . . . Debarbieux, L. (2022). The gut environment regulates bacterial gene expression which modulates susceptibility to bacteriophage infection. *Cell Host Microbe, 30*(4), 556-569 e555. doi:10.1016/j.chom.2022.03.014

Maier, L., Vyas, R., Cordova, C. D., Lindsay, H., Schmidt, T. S., Brugiroux, S., . . . Hardt, W. D. (2013). Microbiota-derived hydrogen fuels Salmonella typhimurium invasion of the gut ecosystem. *Cell Host Microbe, 14*(6), 641-651. doi:10.1016/j.chom.2013.11.002

Mallott, E. K., & Amato, K. R. (2021). Host specificity of the gut microbiome. *Nat Rev Microbiol, 19*(10), 639-653. doi:10.1038/s41579-021-00562-3

Mangalea, M. R., & Duerkop, B. A. (2020). Fitness Trade-Offs Resulting from Bacteriophage Resistance Potentiate Synergistic Antibacterial Strategies. *Infect Immun, 88*(7). doi:10.1128/IAI.00926-19

Marbouty, M., Thierry, A., Millot, G. A., & Koszul, R. (2021). MetaHiC phage-bacteria infection network reveals active cycling phages of the healthy human gut. *Elife, 10*. doi:10.7554/eLife.60608

Meier-Kolthoff, J. P., & Goker, M. (2017). VICTOR: genome-based phylogeny and classification of prokaryotic viruses. *Bioinformatics, 33*(21), 3396-3404. doi:10.1093/bioinformatics/btx440

Minot, S., Bryson, A., Chehoud, C., Wu, G. D., Lewis, J. D., & Bushman, F. D. (2013). Rapid evolution of the human gut virome. *Proc Natl Acad Sci U S A, 110*(30), 12450-12455. doi:10.1073/pnas.1300833110

Munch, P. C., Eberl, C., Woelfel, S., Ring, D., Fritz, A., Herp, S., . . . Stecher, B. (2023). Pulsed antibiotic treatments of gnotobiotic mice manifest in complex bacterial community dynamics and resistance effects. *Cell Host Microbe, 31*(6), 1007-1020 e1004. doi:10.1016/j.chom.2023.05.013

Nappier, S. P., Hong, T., Ichida, A., Goldstone, A., & Eftim, S. E. (2019). Occurrence of coliphage in raw wastewater and in ambient water: A meta-analysis. *Water Res, 153*, 263-273. doi:10.1016/j.watres.2018.12.058

Nasser, A., Azizian, R., Tabasi, M., Khezerloo, J. K., Heravi, F. S., Kalani, M. T., . . . Jalilian, F. A. (2019). Specification of Bacteriophage Isolated Against Clinical Methicillin-Resistant Staphylococcus Aureus. *Osong Public Health Res Perspect, 10*(1), 20-24. doi:10.24171/j.phrp.2019.10.1.05

Naureen Z, Dautaj A, Anpilogov K, Camilleri G, Dhuli K, Tanzi B, Maltese PE, Cristofoli F, De Antoni L, Beccari T, Dundar M, Bertelli M. Bacteriophages presence in nature and their role in the natural selection of bacterial populations. Acta Biomed. 2020 Nov 9;91(13-S):e2020024. doi: 10.23750/abm.v91i13-S.10819. PMID: 33170167; PMCID: PMC8023132.

Nayfach, S., Camargo, A. P., Schulz, F., Eloe-Fadrosh, E., Roux, S., & Kyrpides, N. C. (2021). CheckV assesses the quality and completeness of metagenome-assembled viral genomes. *Nat Biotechnol, 39*(5), 578-585. doi:10.1038/s41587-020-00774-7

Ng, K. M., Ferreyra, J. A., Higginbottom, S. K., Lynch, J. B., Kashyap, P. C., Gopinath, S., . . . Sonnenburg, J. L. (2013). Microbiota-liberated host sugars facilitate post-antibiotic expansion of enteric pathogens. *Nature, 502*(7469), 96-99. doi:10.1038/nature12503

Nilsson, A. S. (2014). Phage therapy--constraints and possibilities. *Ups J Med Sci, 119*(2), 192-198. doi:10.3109/03009734.2014.902878

Nishimura, Y., Yoshida, T., Kuronishi, M., Uehara, H., Ogata, H., & Goto, S. (2017). ViPTree: the viral proteomic tree server. *Bioinformatics, 33*(15), 2379-2380. doi:10.1093/bioinformatics/btx157

Oh, J. H., Alexander, L. M., Pan, M., Schueler, K. L., Keller, M. P., Attie, A. D., . . . van Pijkeren, J. P. (2019). Dietary Fructose and Microbiota-Derived Short-Chain Fatty Acids Promote Bacteriophage Production in the Gut Symbiont Lactobacillus reuteri. *Cell Host Microbe, 25*(2), 273-284 e276. doi:10.1016/j.chom.2018.11.016

Oren, A., & Garrity, G. M. (2021). Valid publication of the names of forty-two phyla of prokaryotes. *Int J Syst Evol Microbiol, 71*(10). doi:10.1099/ijsem.0.005056

Osbelt, L., Wende, M., Almasi, E., Derksen, E., Muthukumarasamy, U., Lesker, T. R., . . . Strowig, T. (2021). Klebsiella oxytoca causes colonization resistance against multidrug-resistant K. pneumoniae in the gut via cooperative carbohydrate competition. *Cell Host Microbe, 29*(11), 1663-1679 e1667. doi:10.1016/j.chom.2021.09.003

Pavel, F. M., Vesa, C. M., Gheorghe, G., Diaconu, C. C., Stoicescu, M., Munteanu, M. A., . . . Bungau, S. (2021). Highlighting the Relevance of Gut Microbiota Manipulation in Inflammatory Bowel Disease. *Diagnostics (Basel), 11*(6). doi:10.3390/diagnostics11061090

Pereira, F. C., & Berry, D. (2017). Microbial nutrient niches in the gut. *Environ Microbiol, 19*(4), 1366-1378. doi:10.1111/1462-2920.13659

Porter, N. T., Hryckowian, A. J., Merrill, B. D., Fuentes, J. J., Gardner, J. O., Glowacki, R. W. P., . . . Martens, E. C. (2020). Phase-variable capsular polysaccharides and lipoproteins modify bacteriophage susceptibility in Bacteroides thetaiotaomicron. *Nat Microbiol, 5*(9), 1170-1181. doi:10.1038/s41564-020-0746-5

Pruesse, E., Peplies, J., & Glockner, F. O. (2012). SINA: accurate high-throughput multiple sequence alignment of ribosomal RNA genes. *Bioinformatics, 28*(14), 1823-1829. doi:10.1093/bioinformatics/bts252

Rakhuba, D. V., Kolomiets, E. I., Dey, E. S., & Novik, G. I. (2010). Bacteriophage receptors, mechanisms of phage adsorption and penetration into host cell. *Pol J Microbiol, 59*(3), 145-155. Retrieved from https://www.ncbi.nlm.nih.gov/pubmed/21033576

Rashed, R., Valcheva, R., & Dieleman, L. A. (2022). Manipulation of Gut Microbiota as a Key Target for Crohn's Disease. *Front Med (Lausanne), 9*, 887044. doi:10.3389/fmed.2022.887044

Reardon, S. (2014). Phage therapy gets revitalized. *Nature, 510*(7503), 15-16. doi:10.1038/510015a

Revell, L. (2012). phytools: an R package for phylogenetic comparative biology (and other things). *Methods in Ecology and Evolution*, https://doi.org/10.1111/j.2041-1210X.2011.00169.x.

Reyes, A., Semenkovich, N. P., Whiteson, K., Rohwer, F., & Gordon, J. I. (2012). Going viral: next-generation sequencing applied to phage populations in the human gut. *Nat Rev Microbiol, 10*(9), 607-617. doi:10.1038/nrmicro2853

Rodriguez-Lucas, C., & Ladero, V. (2023). Enterococcal Phages: Food and Health Applications. *Antibiotics (Basel), 12*(5). doi:10.3390/antibiotics12050842

Rogers, A. W. L., Tsolis, R. M., & Baumler, A. J. (2021). Salmonella versus the Microbiome. *Microbiol Mol Biol Rev, 85*(1). doi:10.1128/MMBR.00027-19

Rosen, G. L., Reichenberger, E. R., & Rosenfeld, A. M. (2011). NBC: the Naive Bayes Classification tool webserver for taxonomic classification of metagenomic reads. *Bioinformatics, 27*(1), 127-129. doi:10.1093/bioinformatics/btq619

Sausset, R., Petit, M. A., Gaboriau-Routhiau, V., & De Paepe, M. (2020). New insights into intestinal phages. *Mucosal Immunol, 13*(2), 205-215. doi:10.1038/s41385-019-0250-5

Schaedler, R. W., Dubs, R., & Costello, R. (1965). Association of Germfree Mice with Bacteria Isolated from Normal Mice. *J Exp Med, 122*(1), 77-82. doi:10.1084/jem.122.1.77

Seal, B. S. (2013). Characterization of bacteriophages virulent for Clostridium perfringens and identification of phage lytic enzymes as alternatives to antibiotics for potential control of the bacterium. *Poult Sci, 92*(2), 526-533. doi:10.3382/ps.2012-02708

Seeman, T. (2014). Prokka: rapid prokaryotic genome annotation. *Bioinformatics*, https://doi.org/10.1093/bioinformatics/btu1153.

Seemann, T. (2014). Prokka: rapid prokaryotic genome annotation. *Bioinformatics, 30*(14), 2068-2069. doi:10.1093/bioinformatics/btu153

Sender, R., Fuchs, S., & Milo, R. (2016). Revised Estimates for the Number of Human and Bacteria Cells in the Body. *PLoS Biol, 14*(8), e1002533. doi:10.1371/journal.pbio.1002533

Shkoporov, A. N., Clooney, A. G., Sutton, T. D. S., Ryan, F. J., Daly, K. M., Nolan, J. A., . . . Hill, C. (2019). The Human Gut Virome Is Highly Diverse, Stable, and Individual Specific. *Cell Host Microbe, 26*(4), 527-541 e525. doi:10.1016/j.chom.2019.09.009

Shkoporov, A. N., & Hill, C. (2019). Bacteriophages of the Human Gut: The "Known Unknown" of the Microbiome. *Cell Host Microbe, 25*(2), 195-209. doi:10.1016/j.chom.2019.01.017

Simmons, E. L., Bond, M. C., Koskella, B., Drescher, K., Bucci, V., & Nadell, C. D. (2020). Biofilm Structure Promotes Coexistence of Phage-Resistant and Phage-Susceptible Bacteria. *mSystems, 5*(3). doi:10.1128/mSystems.00877-19

Simonsen, J., Molbak, K., Falkenhorst, G., Krogfelt, K. A., Linneberg, A., & Teunis, P. F. (2009). Estimation of incidences of infectious diseases based on antibody measurements. *Stat Med, 28*(14), 1882-1895. doi:10.1002/sim.3592

Stecher, B. (2015). The Roles of Inflammation, Nutrient Availability and the Commensal Microbiota in Enteric Pathogen Infection. *Microbiol Spectr, 3*(3). doi:10.1128/microbiolspec.MBP-0008-2014

Stecher, B. (2021). Establishing causality in Salmonella-microbiota-host interaction: The use of gnotobiotic mouse models and synthetic microbial communities. *Int J Med Microbiol, 311*(3), 151484. doi:10.1016/j.ijmm.2021.151484

Stecher, B., Robbiani, R., Walker, A. W., Westendorf, A. M., Barthel, M., Kremer, M., . . . Hardt, W. D. (2007). Salmonella enterica serovar typhimurium exploits inflammation to compete with the intestinal microbiota. *PLoS Biol, 5*(10), 2177-2189. doi:10.1371/journal.pbio.0050244

Streidl, T., Karkossa, I., Segura Munoz, R. R., Eberl, C., Zaufel, A., Plagge, J., . . . Clavel, T. (2021). The gut bacterium Extibacter muris produces secondary bile acids and influences liver physiology in gnotobiotic mice. *Gut Microbes, 13*(1), 1-21. doi:10.1080/19490976.2020.1854008

Studer, N., Desharnais, L., Beutler, M., Brugiroux, S., Terrazos, M. A., Menin, L., . . . Hapfelmeier, S. (2016). Functional Intestinal Bile Acid 7alpha-Dehydroxylation by Clostridium scindens Associated with Protection from Clostridium difficile Infection in a Gnotobiotic Mouse Model. *Front Cell Infect Microbiol, 6*, 191. doi:10.3389/fcimb.2016.00191

Teng, F., Singh, K. V., Bourgogne, A., Zeng, J., & Murray, B. E. (2009). Further characterization of the epa gene cluster and Epa polysaccharides of Enterococcus faecalis. *Infect Immun, 77*(9), 3759-3767. doi:10.1128/IAI.00149-09

Thiennimitr, P., Winter, S. E., & Baumler, A. J. (2012). Salmonella, the host and its microbiota. *Curr Opin Microbiol, 15*(1), 108-114. doi:10.1016/j.mib.2011.10.002

Turnbaugh, P. J., Ley, R. E., Mahowald, M. A., Magrini, V., Mardis, E. R., & Gordon, J. I. (2006). An obesity-associated gut microbiome with increased capacity for energy harvest. *Nature, 444*(7122), 1027-1031. doi:10.1038/nature05414

Turnbaugh, P. J., Ridaura, V. K., Faith, J. J., Rey, F. E., Knight, R., & Gordon, J. I. (2009). The effect of diet on the human gut microbiome: a metagenomic analysis in humanized gnotobiotic mice. *Sci Transl Med, 1*(6), 6ra14. doi:10.1126/scitranslmed.3000322

Turner, D., Kropinski, A. M., & Adriaenssens, E. M. (2021). A Roadmap for Genome-Based Phage Taxonomy. *Viruses, 13*(3). doi:10.3390/v13030506

Visconti, A., Le Roy, C. I., Rosa, F., Rossi, N., Martin, T. C., Mohney, R. P., . . . Falchi, M. (2019). Interplay between the human gut microbiome and host metabolism. *Nat Commun, 10*(1), 4505. doi:10.1038/s41467-019-12476-z

von Strempel, A., Weiss, A. S., Wittmann, J., Salvado Silva, M., Ring, D., Wortmann, E., . . . Stecher, B. (2023). Bacteriophages targeting protective commensals impair resistance against Salmonella Typhimurium infection in gnotobiotic mice. *PLoS Pathog, 19*(8), e1011600. doi:10.1371/journal.ppat.1011600

Waldor, M. K., & Mekalanos, J. J. (1996). Lysogenic conversion by a filamentous phage encoding cholera toxin. *Science, 272*(5270), 1910-1914. doi:10.1126/science.272.5270.1910

Weinbauer, M. G. (2004). Ecology of prokaryotic viruses. *FEMS Microbiol Rev, 28*(2), 127-181. doi:10.1016/j.femsre.2003.08.001

Weiss, A. S., Burrichter, A. G., Durai Raj, A. C., von Strempel, A., Meng, C., Kleigrewe, K., . . . Stecher, B. (2022). In vitro interaction network of a synthetic gut bacterial community. *ISME J, 16*(4), 1095-1109. doi:10.1038/s41396-021-01153-z

Weiss, A. S., Niedermeier, L. S., von Strempel, A., Burrichter, A. G., Ring, D., Meng, C., . . . Stecher, B. (2023). Nutritional and host environments determine community ecology and keystone species in a synthetic gut bacterial community. *Nat Commun, 14*(1), 4780. doi:10.1038/s41467-023-40372-0

Willy, C., Bugert, J. J., Classen, A. Y., Deng, L., Duchting, A., Gross, J., . . . Broecker, F. (2023). Phage Therapy in Germany-Update 2023. *Viruses, 15*(2). doi:10.3390/v15020588

Wotzka, S. Y., Kreuzer, M., Maier, L., Arnoldini, M., Nguyen, B. D., Brachmann, A. O., . . . Hardt, W. D. (2019). Escherichia coli limits Salmonella Typhimurium infections after diet shifts and fat-mediated microbiota perturbation in mice. *Nat Microbiol, 4*(12), 2164-2174. doi:10.1038/s41564-019-0568-5

Wotzka, S. Y., Nguyen, B. D., & Hardt, W. D. (2017). Salmonella Typhimurium Diarrhea Reveals Basic Principles of Enteropathogen Infection and Disease-Promoted DNA Exchange. *Cell Host Microbe, 21*(4), 443-454. doi:10.1016/j.chom.2017.03.009

Wyss, M., Brown, K., Thomson, C. A., Koegler, M., Terra, F., Fan, V., . . . McCoy, K. D. (2019). Using Precisely Defined in vivo Microbiotas to Understand Microbial Regulation of IgE. *Front Immunol, 10*, 3107. doi:10.3389/fimmu.2019.03107

Yu, F., & Mizushima, S. (1982). Roles of lipopolysaccharide and outer membrane protein OmpC of Escherichia coli K-12 in the receptor function for bacteriophage T4. *J Bacteriol, 151*(2), 718-722. doi:10.1128/jb.151.2.718-722.1982

Zhou, S., Liu, Z., Song, J., & Chen, Y. (2023). Disarm The Bacteria: What Temperate Phages Can Do. *Curr Issues Mol Biol, 45*(2), 1149-1167. doi:10.3390/cimb45020076

Danksagung

Zuallererst möchte ich mich bei **Prof. Dr. Bärbel Stecher** für die tolle Betreuung meiner Doktorarbeit bedanken. Vielen Dank, dass du immer ein offenes Ohr hattest und mit deiner Begeisterung für die Forschung auch mich immer wieder motiviert hast. Vielen Dank für dein Vertrauen in meine Ideen und in meine Arbeit und dass du es mir ermöglicht hast, auf vielen nationalen und internationalen Konferenzen und Meetings meine Forschungsergebnisse vorzustellen. Ich habe in den letzten Jahren unheimlich viel gelernt und konnte mich wissenschaftlich sehr weiterentwickeln und bin dir dafür mehr als dankbar.

Vielen Dank auch an **Diana Ring**, ohne die das Labor nicht das wäre was es ist, und die auch bei der hundertsten Frage immer eine nette Antwort parat hat. Vielen Dank für deine Unterstützung bei den zahlreichen Tierversuchen, Mittagspausen und Suchaktionen nach Dingen, die du auf rätselhafte Weise immer sofort gefunden hast selbst wenn man selber tagelang danach gesucht hat. Des Weiteren möchte ich allen anderen Mitgliedern der **AG Stecher** für die tolle Zeit bedanken! Es hat mir immer Spaß gemacht ins Labor zu kommen und mich gefreut, so tolle Arbeitskollegen zu haben. Außerdem ein herzlicher Dank an **Saib Hussain** und das **Tierhaus-Team** für eure tolle Arbeit und eure Unterstützung!

A very special thanks to my three friends **Benedikt**, **Marta** and especially **Anna**, and the whole **office room034**, I can not imagine doing this PhD without you guys! Thanks for having no boundaries in the office, you (and our coffe machine/snack corner) made every monday morning much better! Thanks for discussing everything starting from science to cooking recipes and always having an answer for every problem. Thanks for dealing with every emotional situation and for all the memories we made together, not only during work and work trips but also after work!

Mein ganz besonderer Dank geht an meine Familie, an meine Eltern **Archie** und **Sabine**, meine Brüder **Moritz** und **Henry** und an meine Großeltern **Irmi** und **Horst**, ohne euch und eure Unterstützung hätte ich meinen Weg so nicht gehen können. Danke dass ihr immer an mich geglaubt habt und mir die Freiheit gegeben habt, das machen zu können was mir Spaß macht.